Cell Reports

Article

IQGAP1 and NWASP promote human cancer cell dissemination and metastasis by regulating β1-integrin via FAK and MRTF/SRF

Graphical abstract

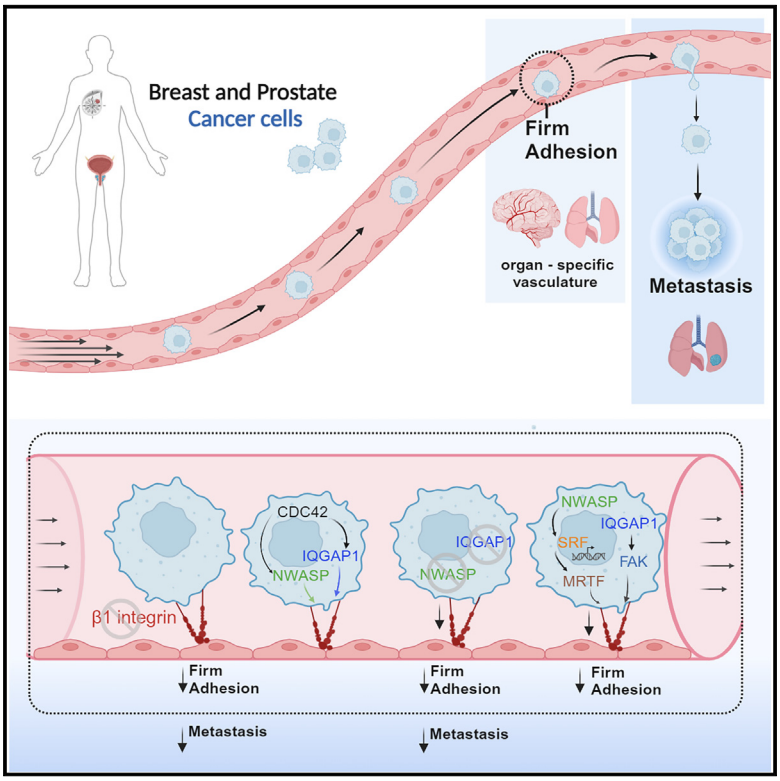

Highlights

- β1-integrin mediates attachment of cells to endothelial cells and metastatic colonization
- Cdc42 targets IQGAP1 and NWASP increase β1-integrin expression via FAK and the MRTF/SRF
- IQGAP1 and NWASP are required for cancer cell attachment to endothelial cells under flow
- IQGAP1 and NWASP contribute to metastatic colonization and nodule formation *in vivo*

Authors

Camilla Cerutti, Serena Lucotti, Sofia T. Menendez, ..., Ignacio A. Romero, Ruth Muschel, Anne J. Ridley

Correspondence

camilla.cerutti@brunel.ac.uk (C.C.), anne.ridley@bristol.ac.uk (A.J.R.)

In brief

Cerutti et al. show that the Cdc42 targets, NWASP and IQGAP1, mediate key early and late metastatic events by β1-integrin upregulation. NWASP and IQGAP1 increase β1-integrin expression via FAK and MRTF/SRF, suggesting that these proteins could be potential therapeutic targets to reduce breast and prostate cancer metastasis formation.

Cerutti et al., 2024, Cell Reports *43*, 113989
April 23, 2024
https://doi.org/10.1016/j.celrep.2024.113989

CellPress

Cell Reports

CellPress
OPEN ACCESS

Article

IQGAP1 and NWASP promote human cancer cell dissemination and metastasis by regulating β1-integrin via FAK and MRTF/SRF

Camilla Cerutti,[1,2,3,*] Serena Lucotti,[4,6] Sofia T. Menendez,[2,7] Nicolas Reymond,[2] Ritu Garg,[2] Ignacio A. Romero,[5] Ruth Muschel,[4] and Anne J. Ridley[1,2,8,*]

[1]School of Cellular and Molecular Medicine, University of Bristol, Bristol BS8 1TD, UK
[2]Randall Centre for Cell and Molecular Biophysics, King's College London, London SE1 U1L, UK
[3]Department of Life Sciences, Centre for Inflammation Research and Translational Medicine (CIRTM), Brunel University London, Uxbridge UB8 3PH, UK
[4]CRUK/MRC Oxford Institute for Radiation Oncology, University of Oxford, Oxford OX3 7DQ, UK
[5]School of Life, Health and Chemical Sciences, The Open University, Milton Keynes MK7 6AA, UK
[6]Present address: Department of Pediatrics, Weill Cornell Medicine, New York, NY, USA
[7]Present address: Instituto de Investigación Sanitaria del Principado de Asturias, Oviedo, Asturias, Spain
[8]Lead contact
*Correspondence: camilla.cerutti@brunel.ac.uk (C.C.), anne.ridley@bristol.ac.uk (A.J.R.)
https://doi.org/10.1016/j.celrep.2024.113989

SUMMARY

Attachment of circulating tumor cells to the endothelial cells (ECs) lining blood vessels is a critical step in cancer metastatic colonization, which leads to metastatic outgrowth. Breast and prostate cancers are common malignancies in women and men, respectively. Here, we observe that β1-integrin is required for human prostate and breast cancer cell adhesion to ECs under shear-stress conditions *in vitro* and to lung blood vessel ECs *in vivo*. We identify IQGAP1 and neural Wiskott-Aldrich syndrome protein (NWASP) as regulators of β1-integrin transcription and protein expression in prostate and breast cancer cells. IQGAP1 and NWASP depletion in cancer cells decreases adhesion to ECs *in vitro* and retention in the lung vasculature and metastatic lung nodule formation *in vivo*. Mechanistically, NWASP and IQGAP1 act downstream of Cdc42 to increase β1-integrin expression both via extracellular signal-regulated kinase (ERK)/focal adhesion kinase signaling at the protein level and by myocardin-related transcription factor/serum response factor (SRF) transcriptionally. Our results identify IQGAP1 and NWASP as potential therapeutic targets to reduce early metastatic dissemination.

INTRODUCTION

Cancer metastasis accounts for 90% of cancer-related deaths, but no metastasis-preventive treatment is available to date in clinical settings. For solid tumors such as prostate and breast cancer, metastasis involves invasion of the primary tumor cells into the surrounding tissue and then entry into local lymphatic and blood vessels, also called intravasation, leading to dissemination to lymph nodes and distant organs.[1] Attachment of circulating tumor cells (CTCs) to endothelial cells (ECs) lining blood vessels under hemodynamic conditions[2] is an important early step in metastatic colonization, which, together with cell extravasation, survival, and proliferation, leads to metastatic colonization and outgrowth.[3] Despite extensive research into the steps from dissemination to organ-specific metastatic colonization,[3,4] the mechanisms underlying this multi-step process remain largely unknown.

A variety of cell surface adhesion proteins are implicated in the multiple steps of metastasis, including integrins.[4–6] Integrins are transmembrane cell surface glycoproteins that can act as receptors on tumor cells or as counter receptors to other cells.[7] For example, β1-integrin is known to mediate invasion and metastasis in a variety of mouse cancer models.[5,8] We have previously shown that the Rho GTPase Cdc42 contributes to metastatic dissemination[9] in prostate cancer and breast cancer cells, acting via β1-integrin to regulate *trans*-endothelial migration *in vitro* and prostate cancer cell attachment to lung vascular ECs *in vivo*, which correlated with reduced formation of pulmonary metastases. β1-integrin is known to be involved in early metastatic colonization following extravasation,[5,10–13] but it is unclear whether it is also required for tumor cell attachment to ECs *in vivo* and *in vitro* under hemodynamic flow conditions.

Cdc42 cycles between an active GTP-bound and inactive GDP-bound conformation.[14] When bound to GTP, Cdc42 interacts with a variety of effector proteins, including protein kinases such as PAKs, actin polymerization inducers such as formins and Wiskott-Aldrich syndrome protein (WASP)/neural WASP (NWASP), and scaffold proteins such as IQGAPs.[15–17]

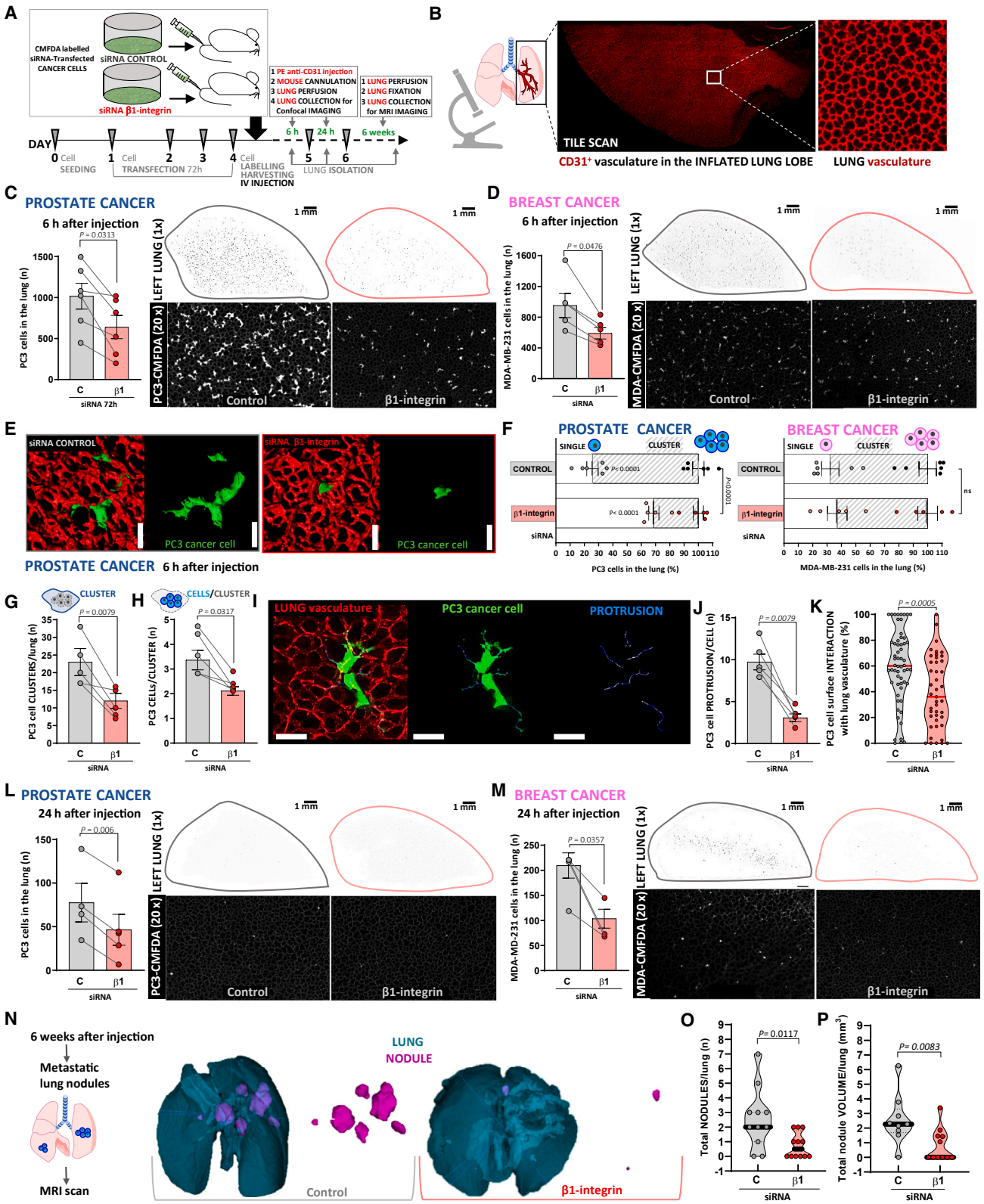

(legend on next page)

Several Cdc42 effectors are known to contribute to cancer progression,[18] but their roles in the attachment of tumor cells to ECs have not been investigated. In addition, whether and how any Cdc42 effectors alter β1-integrin expression is not known.

Here, we investigate the molecules linking Cdc42 to β1-integrin and metastasis dissemination. We demonstrate that β1-integrin mediates interaction of prostate and breast cancer cells with ECs *in vitro* under hemodynamic conditions and in the lung *in vivo*, a critical step for subsequent metastatic growth. We identify NWASP and IQGAP1 as key Cdc42 targets in cancer cells regulating β1-integrin expression via extracellular signal-regulated kinase (ERK)/focal adhesion kinase (FAK) signaling at the protein level, and by MRTF/serum response factor (SRF) transcriptionally, thereby mediating firm attachment to ECs and metastasis formation.

RESULTS

β1-integrin is required for cancer cell retention in the lung and metastatic nodule formation

To investigate the role of β1-integrin in cancer dissemination *in vivo*, we used an experimental model of lung metastasis coupled with whole-lung imaging.[9,19] We injected fluorescently labeled β1-integrin-depleted human cancer cells intravenously via the tail vein into mice and measured cancer cell retention and dissemination in the lung at 6 and 24 h (Figures 1A and S1A–S1C). Lung ECs were stained with PE-anti-CD31 antibody immediately before lung preparation and imaging (see STAR Methods for details; Figure 1B). The number of β1-integrin-depleted cancer cells retained in the lung vasculature was significantly reduced compared to control cells for both PC3 prostate cancer (Figure 1C) and MDA-MB-231 breast cancer (Figure 1D) cells. High-magnification 3D analysis revealed that cancer cells in blood vessels were found as either single cells or as clusters (Figure S1D; Video S1), similar to CTCs derived from patients with cancers,[20] in whom clustered tumor cells are more likely to contribute to metastasis.[21] Using cancer cell nucleus/volume ratio quantification (Figures S1E and S1F), we found that 70% of control PC3 cells were clustered, probably due to cell entrapment in the pulmonary capillaries, while 80% of β1-integrin-depleted PC3 cells were retained in the lung vasculature as single cells (Figures 1E and 1F). Further analysis showed that the clusters formed by β1-integrin-depleted PC3 cells were fewer and smaller in size compared to control cells (Figures 1G and 1H). We did not observe changes in MDA-MB-231 cell clustering (Figure 1F, right). Control cancer cells, either in clusters or as single cells, formed multiple protrusions in different directions within the vasculature (Figure 1I) that are associated with an invasive and pro-metastatic phenotype.[9,12,22] β1-integrin depletion in PC3 cells drastically reduced the number of cell protrusions (Figure 1J) and significantly reduced the cancer cell surface area interacting with ECs (Figure 1K; Video S2). No significant changes in MDA-MB-231 cell branching or EC interaction were observed (Figures S1G–S1J), possibly due to the difference in morphology and/or role of β1-integrin in these two cancer cell lines (Figures S1K and S1L). Of note, β1-integrin did not alter cancer cell volume or cell shape besides cell protrusion in the lung vasculature (Figures S1M and S1N).

We next evaluated the role of β1-integrin on cancer cell metastatic colonization in the lung. Based on previous results using this *in vivo* model,[19] disseminating cancer cells remain in the bloodstream for 1–4 days prior to extravasation. We tested cancer cell retention in the lung 24 h after tail injection (Figure 1A, 24 h). Significantly fewer β1-integrin-depleted cancer cells than control cells were retained in the lungs for both PC3 and MDA-MB-231 cells at 24 h post-injection (Figures 1L and 1M), suggesting reduced survival and/or attachment during their intravascular transit. We therefore tested the role of β1-integrin in experimental metastatic nodule formation in

Figure 1. β1-integrin contributes to cancer cell retention and nodule formation in the lung *in vivo*

(A) Schematic of the *in vivo* experiments used to study cancer cell retention, morphology, and metastatic nodule formation in the lung vasculature. siRNA-transfected and chloromethylfluorescein diacetate (CMFDA) fluorescently labeled cancer cells were injected into the tail vein. Lungs were isolated 6 h, 24 h, or 6 weeks after injection.

(B) CD31-PE was injected at 6 and 24 h to visualize the lung blood vessels. Confocal tile scan images of perfused and inflated whole left lobe lung vasculature (red) are shown. Lung vasculature enlarged view is used for quantification.

(C and D) Quantification of siRNA-control and -β1-integrin-transfected (C) prostate PC3 (n = 6 mice) and (D) breast MDA-MD-231 (n = 5 mice) cancer cell number in the left lung lobe. Scale bars, 1 mm. Representative left lobe tile scan with inverted look-up-table (LUT; top) and ×20 magnification (bottom) show CMFDA-labeled cancer cells (white).

(E) Representative 3D surface reconstruction of confocal z stacks of cancer cells (green) in the left lung lobe vasculature (endothelial cells, red). Scale bar (white), 30 μm.

(F) Quantification of grouped and single PC3 cells (control n = 6 mice, total 520 cells; β1-integrin n = 5 mice, total 380 cells) and MDA-MB-231 cells (control n = 5 mice, 1,120 cells; β1-integrin n = 5 mice, 688 cells).

(G) Number of cancer cell groups per lung, n = 5.

(H) Number of cancer cells per group per lung, n = 5.

(I) Representative confocal z-scans of cancer cells (CMFDA-green) in the lung vasculature (CD31-PE-red) and cell protrusions (blue). Scale bar (white), 30 μm.

(J) Number of cell protrusions per cancer cell per lung, n = 5.

(K) Percentage of cancer cell surface directly interacting with vasculature surface (n = 3 mice, 58 and 43 cells).

(L and M) Prostate (L) and breast cancer (M) cell numbers in the left lung lobe 24 h after injection and representative left lobe tile scan (top) and ×20 magnification (bottom) show CMFDA-labeled cancer cells (white). PC3 (control n = 4; β1-integrin n = 5 mice) and MDA-MB-231 (control n = 3 mice; β1-integrin n = 4).

(N) Representative MRI scans of whole lungs 6 weeks after intravenous (i.v.) injection are segmented by ITK-snap into lung (cyan) and metastatic nodules (magenta).

(O and P) Metastatic nodule number per lung (O) and total nodule volume per lung (P) (PC3 cells) (control n = 11 mice; β1-integrin n = 12).

Data are mean ± SEM. Statistical analysis of biological replicates by two-tailed paired t test (C, D, and L), two-way ANOVA (F), unpaired Mann-Whitney test (G–J, M, O, and P), or one-way ANOVA with Tukey's multiple comparison test (K).

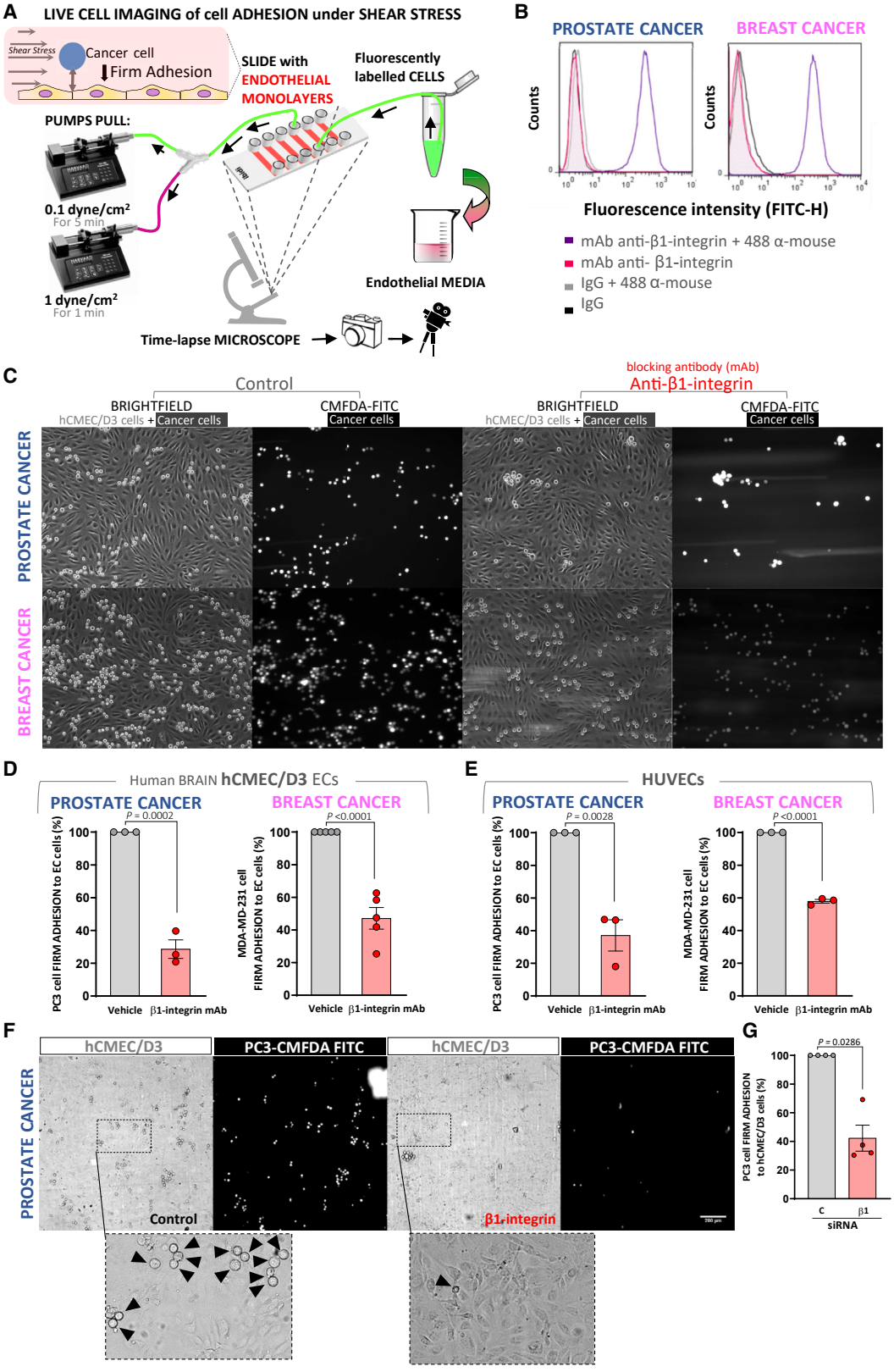

(legend on next page)

the PC3 cell model (Figure 1A, 6 weeks). Full lung MRI scans of fixed isolated lungs (Figure S1O) revealed that β1-integrin-depleted PC3 cells formed less metastatic nodules compared to control cells (Figures 1N and 1O). The volume of nodules formed by β1-integrin-depleted PC3 cells was also smaller compared to the control, resulting in a 50% reduction of the total metastatic volume per lung (Figure 1P). These results together show that β1-integrin is required for stable attachment and retention of prostate and breast cancer cells *in vivo*, correlating with increased metastatic nodule formation.

β1-integrin is required for attachment of cancer cells to ECs

The reduced pulmonary retention of β1-integrin-depleted cells within the lung vasculature led us to hypothesize that β1-integrin might be involved in cancer cell attachment to ECs. To test this, we assessed cancer cell adhesion to human ECs under flow in an *in vitro* model that mimics *in vivo* blood shear stress in human capillaries (Figure 2A).[2] We used primary human umbilical vein ECs (HUVECs)[9] and the brain microvascular hCMEC/D3 cell line as sources of ECs because breast and prostate cancer metastasize to different organs including the brain.[23] Cancer cell membrane β1-integrin was blocked via a monoclonal blocking antibody (mAb) that specifically recognized the native cell surface β1-integrin, as determined by flow cytometry (Figures 2B and S2A). Functional blockade was verified in Jurkat T cells, known to adhere to ECs via β1-integrins.[24] Their adhesion to brain hCMEC/D3 ECs was reduced by 80% by β1-integrin mAb treatment compared to either isotype control antibody or vehicle (Figures S2B and S2C; Video S3). β1-integrin mAb significantly reduced PC3 and MDA-MB-231 (50%–70%) cell shear-resistant firm adhesion to both hCMEC/D3 cells and HUVECs compared to vehicle control (Figures 2C–2E; PC3: Video S4; MDA-MB-231: Video S5). We confirmed these results via small interfering RNA (siRNA)-mediated β1-integrin depletion in PC3 cells (Figure S2D), which decreased firm adhesion of cancer cells to hCMEC/D3 cells by 60% (Figures 2F and 2G). Taken together, these data show that firm adhesion of PC3 and MDA-MB-231 cells to ECs under flow is β1-integrin mediated. The most characterized α subunit of β1-integrin is α4. The heterodimer α4β1-integrin (VLA-1) is involved in the adhesion of circulating melanoma cells[25] to endothelial VCAM-1 and fibronectin. MDA-MB-231 cells do not express α4 (Figure S2E, middle),[26] and PC3 cells express very low levels of α4 (Figure S2E, bottom), and it has been reported to be insufficient for EC adhesion.[23] Therefore, other β1-integrin heterodimers such as α3β1, α5β1, or α5β1 are likely to be involved in this process.[9,27,28] α5β1-integrin binds to the extracellular matrix protein fibronectin, while α6β1- and α3β1-integrins bind to laminin.[29] Both fibronectin and laminin were detected on the apical surface of HUVECs (Figure S2F, top) and hCMEC/D3 ECs (Figure S2F, bottom) grown on collagen; thus, they are very likely to contribute to cancer cell adhesion to ECs, as observed previously,[30,31] via β1-integrin. These results indicate that β1-integrin is important for stable binding of cancer cells to ECs, most likely through interaction with extracellular matrix proteins present on the apical surface of ECs.

IQGAP1 and NWASP contribute to β1-integrin expression in cancer cells

Cdc42 increases β1-integrin expression in PC3 cells through the transcription factor SRF,[9] but the Cdc42 targets that regulate β1-integrin downstream of Cdc42 are not known. We therefore performed a siRNA screen to identify which targets downstream of Cdc42 affect β1-integrin expression in PC3 cells (Figure 3A; key resources table). Cdc42 and β1-integrin siRNAs were used as positive controls. Depletion of IQGAP1, FMNL3, and NWASP had the strongest effects, reducing total β1-integrin protein levels by approximately 80%, 60%, and 50%, respectively (Figures 3A and S3A–S3E). IQGAP1 and NWASP depletion consistently reduced β1-integrin protein levels, but the effect of FMNL3 was not as marked. IQGAP3 silencing also slightly reduced β1-integrin protein levels but to a much lesser extent than IQGAP1 depletion (Figures S3F–S3H). Furthermore, we found that FMNL1 and FMNL3 siRNAs had opposite effects on total β1-integrin protein expression in PC3 cells: FMNL3 depletion reduced, whereas FMNL1 depletion increased, β1-integrin expression (Figures 3A and S3A). We then assessed whether NWASP, IQGAP1, and FMNL3 depletion reduced β1-integrin levels specifically on the cell surface. FMNL3 depletion did not significantly alter β1-integrin surface levels, although, interestingly, FMNL1 depletion increased surface levels (Figure S3I). By contrast, NWASP and IQGAP1 siRNA reduced active cell

Figure 2. β1-integrin contributes to shear-stress-resistant cancer cell adhesion to endothelial cells *in vitro*

(A) Schematic of the live imaging coupled with flow-based adhesion assay mimicking the *in vivo* microvasculature shear stress to study cancer cell adhesion to ECs.

(B) Representative flow cytometry histogram of PC3 and MDA-MD-231 cells treated for 20 min with mouse β1-integrin blocking antibody (mAb) and secondary anti-mouse (purple), mAb only (pink), immunoglobulin G (IgG) and secondary anti-mouse (negative control, gray), or IgG only (black) showing that the β1-integrin mAb binds to MDA-MB-231 and PC3 cells.

(C–E) β1-integrin blocking antibody reduces adhesion of cancer cells to ECs. Cancer cells were fluorescently labeled, harvested, and incubated with blocking β1-integrin antibody or vehicle (control) for 20 min. EC monolayers were exposed to 2×10^6 PC3 cells/mL at 0.1 dyn/cm^2 for 5 min followed by 1 dyn/cm^2 for 30 s. (C) Representative images of firmly adhered CMFDA-labeled PC3 (white, top) and CMFDA-labeled MDA-MD-231 (bottom) cells to human brain endothelial hCMEC/D3 cells (bright field) used for the quantification of shear-resistant cancer cells adhered to ECs in ten random different fields of view per channel/condition (1,204.4 × 1,615.9 μm). Percentage of prostate and breast cancer cells firmly adhered to (D) human brain ECs (hCMEC/D3) and (E) HUVECs. Data are mean ± SEM, PC3 (n = 3) and MDA-MB-231 (brain ECs n = 5; HUVECs n=3). Statistical analysis of biological replicates by two-tailed unpaired t test.

(F and G) β1-integrin-depleted prostate PC3 cells have decreased firm adhesion to hCMEC/D3 cells. PC3 cells were fluorescently labeled, harvested, and transfected with either β1-integrin or control siRNA. hCMEC/D3 cell monolayers were exposed to 2×10^6 PC3 cells/mL at 0.1 dyn/cm^2 for 5 min followed by 1 dyn/cm^2 for 30 s. (F) Representative images of firmly adhered CMFDA-labeled PC3 cells (white) and (G) percentage firmly adhered to hCMEC/D3 cells. Data are mean ± SEM (n = 4), two-tailed unpaired t test.

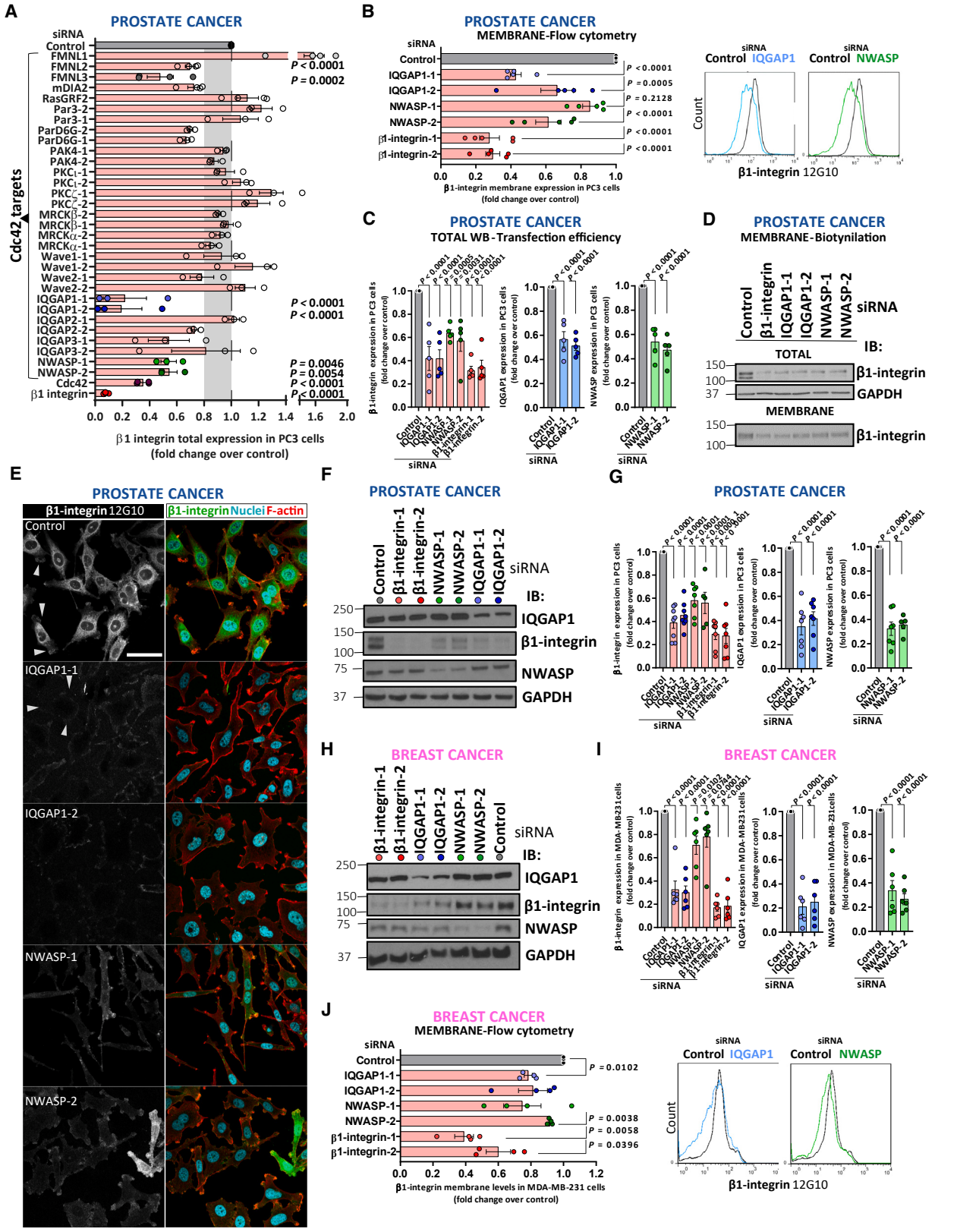

(legend on next page)

surface β1-integrin (clone 12G10) on PC3 cells as determined by flow cytometry (Figure 3B), immunoblotting (Figures 3C and S3I), a surface biotinylation assay (Figure 3D), and immunofluorescence (Figure 3E). Moreover, F-actin-rich cell protrusions containing active β1-integrin were noticeably reduced in number in IQGAP1-depleted cancer cells compared to control (Figure 3E, arrows, top two images). Similar to PC3 cells, NWASP- and IQGAP1-depleted MDA-MB-231 cells had reduced total β1-integrin expression (Figures 3F–3I) and active β1-integrin on the cell surface (Figure 3J). Additionally, we found that NWASP and IQGAP1 siRNAs in combination (Figure S3J) further reduced β1-integrin expression in both cell lines (Figures S3K–S3L) compared to either target individually. We did not observe a consistent and significant effect of NWASP and IQGAP1 downregulation (Figures S3M and S3N) on the expression at membrane level of β1-integrin α-chain binding partners (α 1–6) (Figures S3O and S3P).

Therefore, the Cdc42 targets IQGAP1 and NWASP together have the strongest effect on β1-integrin expression, both total and cell surface levels, with a similar phenotype to that of Cdc42.[9]

IQGAP1 and NWASP contribute to endothelial attachment and metastatic nodule formation

Given the roles of IQGAP1 and NWASP in regulating β1-integrin expression in prostate and breast cancer cells, we hypothesized that NWASP and IQGAP1 would affect cancer cell attachment to ECs. Indeed, IQGAP1 and NWASP depletion in PC3 cells (Figure S4A) reduced firm adhesion under shear stress to brain ECs (Figure S4B). To test whether NWASP and IQGAP1 regulate cancer cell retention in lung blood vessels, we used the experimental model of lung metastasis *in vivo* as described in Figure 1A. IQGAP1 depletion reduced PC3 cell retention in the lung vasculature 6 h post-injection (Figures 4A and S4C, top), consistent with our *in vitro* observations, whereas NWASP depletion (Figure S4D) did not affect cancer cell retention in the lung (Figure S4E), reflecting the stronger effect of IQGAP1 depletion on β1-integrin levels (Figure 3A). Similarly, reduction of IQGAP1 in MDA-MB-231 cells (Figure S4, bottom) decreased their retention in the lung (Figure 4B). In addition, IQGAP1 depletion strongly decreased the number of protrusions per cancer cell (Figures 4C–44E) and the contact area of cancer cells with EC surface (Figures 4F, 4G, and S4F) in both PC3 and MDA-MB-231 cells. In contrast to β1-integrin depletion (Figure 1F), IQGAP1 depletion did not alter the ability of cancer cells to form clusters (Figures S4G–S4I, PC3 cells, and S4L–S4N, MDA-MB-231 cells), implying that this phenotype requires a stronger reduction in β1-integrin levels than that induced by IQGAP1 depletion. IQGAP1 did not affect cancer cell volume or other shape parameters besides cell protrusions (Figures S4, S4J, and S4K, PC3 cells, and S4O and S4P, MDA-MB-231 cells). These data suggest that IQGAP1 contributes to cancer cell:EC interaction *in vitro* and *in vivo*.

Similar to our results at 6 h after injection, IQGAP1 depletion (Figure S4C) reduced PC3 cell number in the lung vasculature 24 h after injection (Figures 4H and 4I) and metastatic nodule formation 6 weeks after injection (Figures 4J and S4Q; Video S6). MRI of lungs revealed that both IQGAP1 and NWASP depletion by siRNAs strongly reduced metastatic nodules (Figure 4K) and nodule size, resulting in smaller metastatic mass per lung (Figure 4L). Collectively, these data show that IQGAP1 and NWASP contribute to different stages of cancer metastasis formation including cancer cell adhesion to EC, retention in the vasculature, and metastatic nodule formation.

Existing data (https://www.proteinatlas.org) show that both NWASP and IQGAP1 are prognostic markers and significantly associated with an unfavorable outcome for pancreatic cancer but a favorable one for renal cancer (RNA expression and survival analysis).[32,33] IQGAP1 and NWASP gene expression are significantly overexpressed in breast and prostate patient primary tumors compared to normal tissue[34,35] and, albeit with lower patient samples available, in metastatic tissue (breast cancer).[34] Survival analysis data by correlation between mRNA expression and 5-year survival[32,36] confirm high gene expression of IQGAP1 in patients with prostate cancer, while NWASP expression is mainly low (Figure 4M). In breast cancer, IQGAP1 was equally highly and lowly expressed, while NWASP was highly expressed (Figure 4N).

At the protein level, using data from prostate and breast cancer biopsy sections stained by immunohistochemistry[32] (1-mm tissue core samples from 216 patients), NWASP and IQGAP1 proteins were medium to highly expressed based on the staining intensity and fraction of stained cells (Figures 4O and 4P), although NWASP detection was dependent on the antibody used. Kaplan-Meier plots (https://kmplot.com/analysis/)[37,38] on breast cancer patient samples (Tang 2018 dataset[39]) showed that high NWASP (Figure S4R) and IQGAP1 (Figure S4S) protein expression correlated with shorter survival. Taken together,

Figure 3. Cdc42 targets IQGAP1 and NWASP regulate β1-integrin expression

(A) siRNA screening of Cdc42 targets for β1-integrin protein levels by immunoblotting. PC3 cells were transfected with either control siRNA or with the indicated Cdc42 target siRNAs and analyzed for β1-integrin expression after 72 h. β1-integrin siRNA was used as a positive control in all experiments. Mean ± SEM (n = 3 or 4 independent experiments), one-way ANOVA test.

(B) IQGAP1 and NWASP decrease active β1-integrin levels on the PC3 cell surface. (Left) Quantification by flow cytometry. Mean ± SEM; n = 5, one-way ANOVA test. (Right) Representative flow cytometry histograms.

(C) β1-integrin, IQGAP1, and NWASP protein levels in PC3 cells transfected with indicated siRNAs quantified from immunoblots. Mean ± SEM; n = 5, one-way ANOVA test.

(D) Representative biotinylation assay immunoblots for (top) total and (bottom) membrane levels of β1-integrin in PC3 cells transfected with the indicated siRNAs.

(E) Immunofluorescence analysis of active β1-integrin with 12G10 (left) and nuclei and F-actin (merge on right: green, cyan, red) of PC3 cells transfected with indicated siRNAs. Images acquired by confocal microscopy; actin-rich protrusions (white triangles). Scale bar, 50 μm.

(F–I) Representative immunoblots (F and H) and quantification (G and I) of total β1-integrin, IQGAP-1, and NWASP in PC3 cells (G) and MDA-MB-231 cells (I) transfected with the indicated siRNAs. Mean ± SEM; n = 5 to 7 independent experiments, one-way ANOVA test.

(J) Active β1-integrin levels at the cell surface in IQGAP1- and NWASP-depleted MDA-MB-231 cells determined by flow cytometry. (Left) Quantification; (right) representative histograms. Mean ± SEM; n = 4, one-way ANOVA.

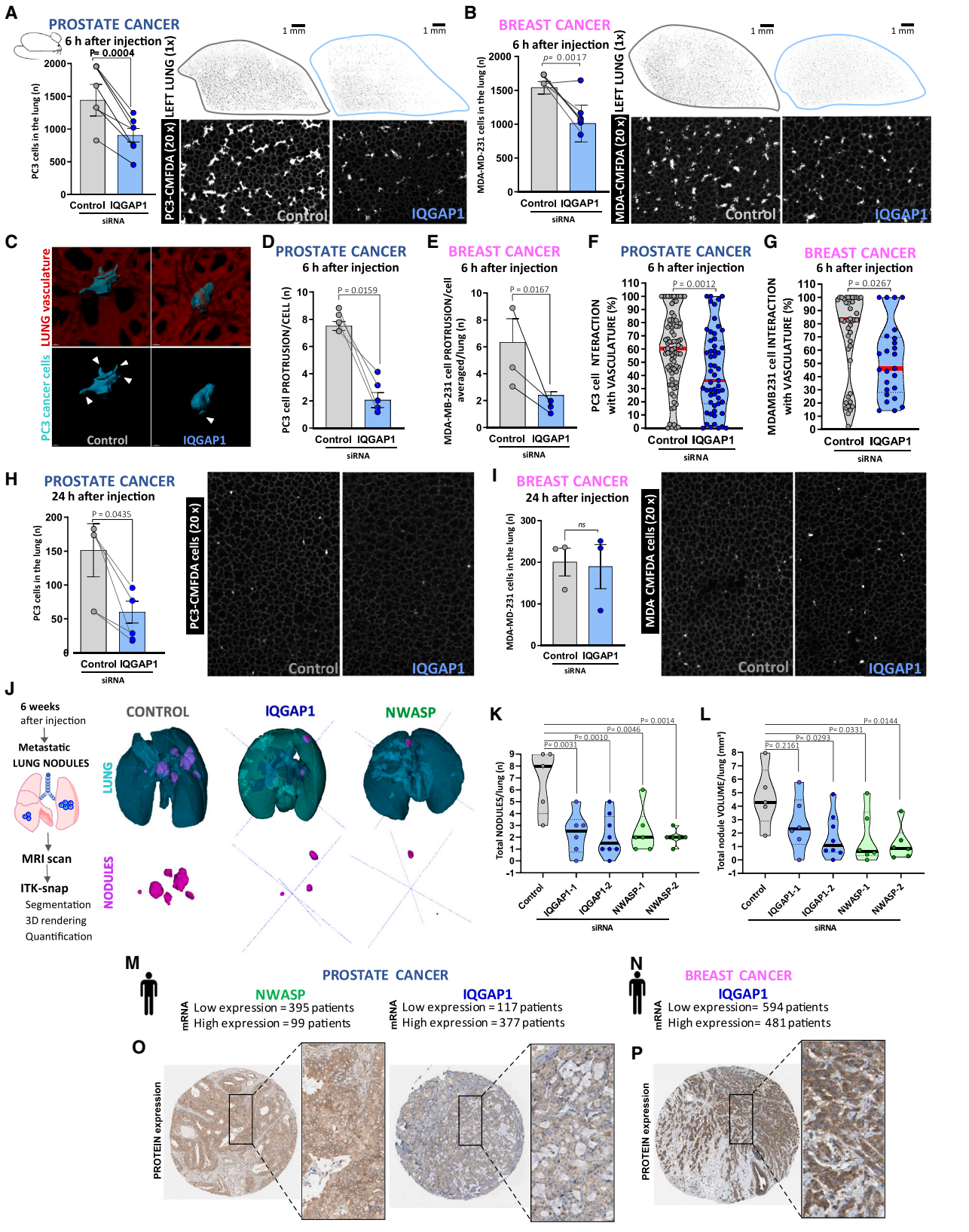

(legend on next page)

these results and analyses show that both IQGAP1 and NWASP contribute to prostate and breast cancer progression in human patients, correlating with our observations that they increase metastatic nodule formation in mouse lungs.

IQGAP1 and NWASP act through FAK and SRF/MRTF to induce β1-integrin expression

IQGAP1 and NWASP both contribute to β1-integrin expression (Figure 3A); therefore, we tested whether they could associate with endogenous β1-integrin,[40] which is known to have a large adhesome network.[41] Endogenous β1-integrin associated with endogenous IQGAP1 (Figures 5A and S5A), consistent with previous observations in fibroblasts,[42] but NWASP was not consistently detected. IQGAP1 is also reported to interact directly with NWASP,[43] and thus β1-integrin, IQGAP1, and NWASP could act together as part of a protein complex.

The prevention of cancer cell adhesion to the endothelium of distant organs remains an unmet clinical challenge. IQGAP1, NWASP, and their interacting proteins might be potential pharmacological targets to reduce this step of metastasis. We thus focused on understanding the signaling pathways downstream of IQGAP1 and NWASP that mediate their effects on β1-integrin expression. IQGAP1 serves as a scaffold for focal adhesion proteins such as FAK and paxillin (Figure S5B) in the context of cell migration[44] and metastasis.[45] FAK and paxillin are signaling links between actin cytoskeleton-related proteins and integrins. We therefore tested the roles of these proteins on β1-integrin expression levels. FAK is frequently upregulated in cancer: it is prognostic marker of breast cancer, and it is highly expressed in more than 50% of patients with prostate cancer. Treatment of PC3 cells with the FAK inhibitor (FAKi) 4548[46] (AZ13256675 FAKi) rapidly reduced total and active surface levels of β1-integrin (Figures 5B, S5C, and S5D). We confirmed that the FAKi reduced FAK Tyr397 phosphorylation (Figure 5B).[46] Strikingly, the FAKi strongly reduced firm adhesion of PC3 cells to brain ECs under shear stress (Figure 5C). By contrast, the FAKi did not significantly reduce β1-integrin expression in MDAMB231 cells or their firm adhesion to brain ECs under shear stress (Figures S5E–S5G), consistent with results shown *in vivo*.[47] In PC3, paxillin downregulation did not reduce β1-integrin expression (Figures S5H and S5I). These results indicate that FAK is a likely candidate for mediating early effects of IQGAP1 on β1-integrin. Both IQGAP1 and FAK associate with ERK1/2 mitogen-activated protein kinase pathway components; in particular, IQGAP1 binds to ERK1/2 and modulates its activity.[44,48–50] Treatment of PC3 cells with U0126 (MEKi), a selective inhibitor of ERK1/2 activation,[51] rapidly reduced total β1-integrin levels (Figure 5D), similar to the FAKi. MEKi also reduced FAK Tyr397 phosphorylation (Figure 5E). This suggests that downstream of IQGAP1, FAK and ERK1/2 could act together to induce rapid downregulation of β1-integrin. Indeed, IQGAP1 depletion in PC3 cells decreased FAK Tyr397 phosphorylation (Figure 5F) as observed in other cell types.[44,52]

In addition to this acute effect on β1-integrin expression, β1-integrin is known to be regulated more long term at the transcriptional level. For example, we have previously shown that Cdc42 increases β1-integrin expression through the transcription factor SRF.[9] Here, we confirm that SRF siRNA depletion decreases β1-integrin protein expression in PC3 cells (Figure 5G).[53] IQGAP1 and NWASP depletion reduced β1-integrin mRNA levels (Figures 5H and S5J), indicating that IQGAP1 and NWASP could mediate the effect of Cdc42 on β1-integrin transcription. Interestingly, NWASP and IQGAP1 depletion reduced SRF protein expression (Figure S5K), implying that their effect on β1-integrin mRNA regulation is due in part to a reduction in SRF.

SRF interacts with the G-actin-regulated myocardin-related transcription factors (MRTFs) to regulate transcription of genes involved in cytoskeletal dynamics, adhesion, and metastasis.[54–56] We therefore tested whether MRTFs altered β1-integrin expression. Two different MRTFis, CCG-1423[57,58] (MRTFi-1) and CCG-203971[59] (MRTFi-2), reduced total β1-integrin protein levels in PC3 cells (Figures 5I and 5J). MRTF-i-2 also reduced active

Figure 4. IQGAP1 and NWASP contribute to cancer adhesion to endothelial cells, retention in the lung vasculature, and metastatic nodule formation

(A and B) Quantification of siRNA-transfected (A) PC3 cells (control n = 4, IQGAP1 n = 5 mice) and (B) MDA-MB-231 cells (control n = 3, IQGAP1 n = 5 mice) retained in the lung (left lobe) vasculature 6 h post-tail vein injection. Mean ± SEM, two-tailed paired t test. (Top) Representative left lung lobe tile scan with inverted LUT and (bottom) ×20 magnification of CMFDA-labeled cells (white) in the lung.

(C) Fluorescent *in situ* image rendering (Imaris) of control and IQGAP1-depleted PC3 cells (cyan) in the lung vasculature (red). Arrows indicate PC3 cell protrusions. Scale bar, 5 μm.

(D and E) Number of cell protrusions, average mean per lung, for (D) PC3 cells (control n = 4, IQGAP1 n = 6) and (E) MDA-MB-231 cells (control n = 3, IQGAP1 n = 3). Mean ± SEM, two-tailed paired t test.

(F and G) Percentage of cancer cell surface directly interacting with lung vasculature surface for siRNA-transfected (F) PC3 cells (pooled samples: control, 56 cells from n = 4 lungs; IQGAP1, 54 cells from n = 5 lungs) and (G) MDA-MB-231 cells (pooled samples: control, 42 cells from n = 3 lungs; IQGAP1, 25 cells n = 3 lungs). Mann-Whitney test.

(H and I) (Left) Quantification of control and IQGAP-depleted PC3 (n = 5) (H) and MDA-MB-231 (n = 3) (I) cell numbers in left lung lobes 24 h after tail-vein injection. Mean ± SEM, two-tailed paired t test. (Right) Representative left lobe tile scans ×20 magnification with CMFDA-labeled cells (white).

(J) Schematic of the experimental metastasis study and representative images of whole-lung MRI scans 6 weeks after tail-vein injection segmented by ITK-snap: lung (cyan) and nodules (magenta). IQGAP1- (left) and (right) NWASP-depleted PC3 cell nodules are shown.

(K and L) Quantification of (K) PC3 cell metastatic nodules per lung and (L) total nodule volume per lung (mm^3) (control n = 5, IQGAP1-1 n = 6, IQGAP1-2 n = 7, NWASP-1 n = 6, NWASP-2 n = 6 mice), one-way ANOVA with Tukey's multiple comparison test. Data are mean ± SEM.

(M and N) Prostate (M, 494 patients) and breast (N, 1,075 patients) cancer IQGAP1 and NWASP mRNA expression analyzed by TCGA transcriptomic classified in low and high expression.

(O and P) Representative images of (O) prostate and (P) breast cancer patient tissue samples stained for NWASP and/or IQGAP1 proteins by immunohistochemistry (IHC).

(M)–(P) are from https://www.proteinatlas.org/pathology.[32]

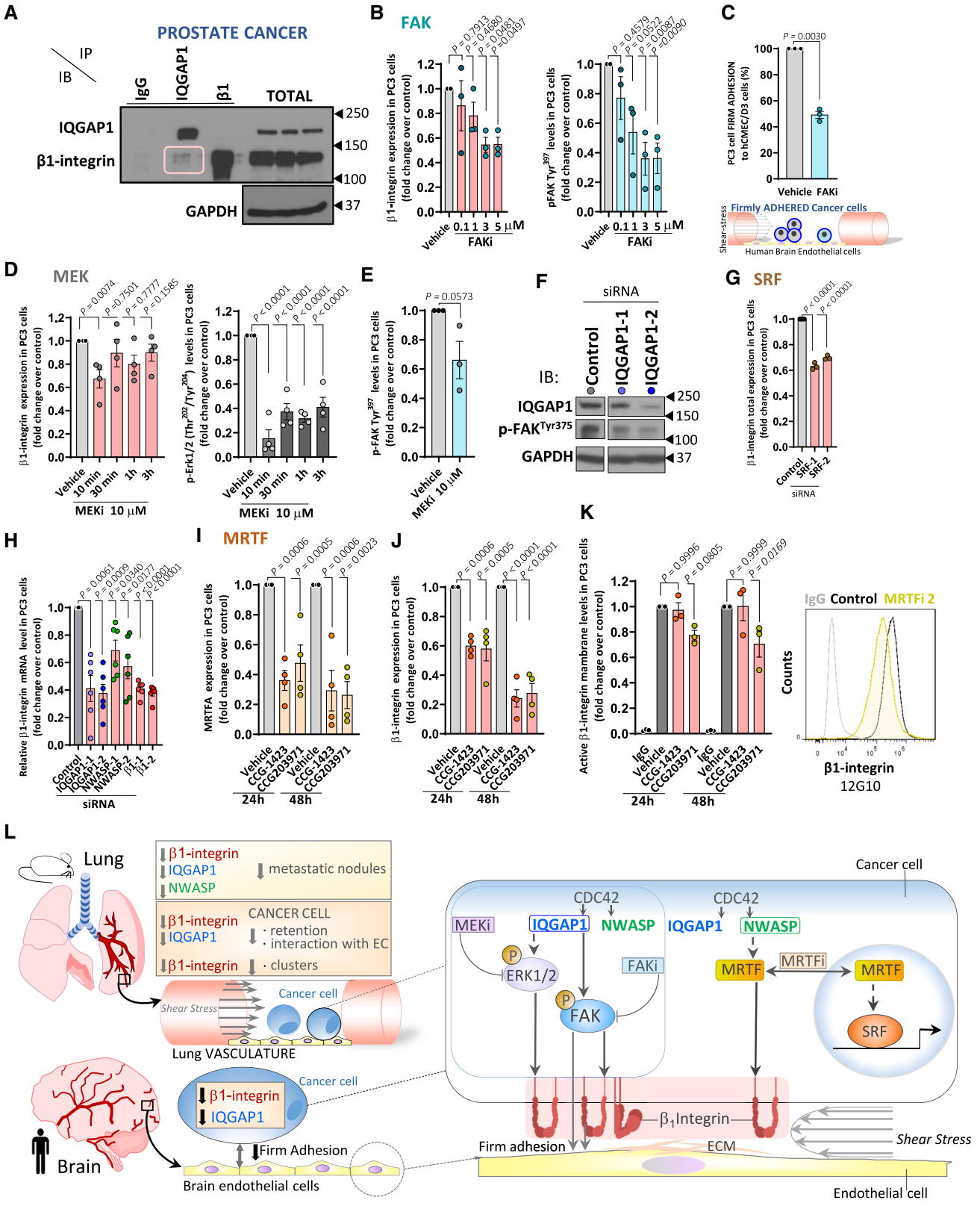

(legend on next page)

β1-integrin at the cell surface (Figure 5K). The MRTFis had no effect on IQGAP1 expression but, interestingly, reduced NWASP levels (Figure S5L), suggesting a positive feedback loop whereby NWASP acts via the MRTF-SRF complex to induce β1-integrin expression and MRTFs then activate NWASP expression.[60] Taken together, these results indicate that NWASP and IQGAP1 act downstream of Cdc42 to stimulate both ERK and FAK signaling, leading to a rapid increase in β1-integrin protein levels, and also induce β1-integrin transcription via MRTF/SRF (Figure 5L).

DISCUSSION

Cancer metastasis is responsible for most patient deaths, yet we still have limited mechanistic understanding of the process of cancer progression to metastasis. Here, we focused on critical steps of cancer metastasis formation: cancer cell adhesion to vascular ECs and cancer cell retention and survival leading to metastasis growth. We show that NWASP and IQGAP1, two Rho GTPase Cdc42 effectors, control these processes in both breast and prostate cancer cells, suggesting IQGAP1 and NWASP as potential therapeutic targets to reduce early metastatic dissemination.

Circulating cancer cell dissemination requires close contact between cancer cells and microvascular and/or capillary ECs[3,23,61] under hemodynamic shear stress[62,63] mediated by cell surface receptors such as integrins.[5] Here, we show that β1-integrin is important for cancer cell retention in lung capillaries, both in breast and prostate cancer cells, providing additional insight into how β1-integrin contributes to metastasis formation in a model of experimental metastasis. Because β1-integrin affects the steps of the metastatic cascade before intravasation and adhesion, the spontaneous metastasis model is not valid to study these early stages of metastasis formation. The use of an experimental model of metastasis is the only way to ensure that the intravascular phase of metastasis is studied.[5] Furthermore, in this model, it is unlikely that the metastases observed are predominantly due to effects on clustering due to mechanical entrapment, as we showed that β1-integrin and IQGAP1 depletion decreased the intravascular retention of cancer cells (early step of metastasis) independently from the cluster number or composition (Figures 1 and 4). Interestingly, β1-integrin plays a crucial role in the firm adhesion of breast and prostate cancer cells to brain ECs in a microfluidic model, an early step of metastasis formation that can be targeted for patient treatment. Some clinical trials with β1-integrin inhibitors have been promising in stabilizing cancers in patients,[64,65] but so far none have been approved for clinical use in cancer. Recent clinical trials with new inhibitors targeting β1-integrins and other integrins have started, and it will be interesting to know if these reduce or stabilize disease progression.[66] Previous β1-integrin clinical trials partially failed in patients with cancer due to either acquired resistance or compensatory effects that need further investigation.[66] Therefore, alternative therapeutic targets are required. To address this need, we identified the Cdc42 effectors IQGAP1 and NWASP as the major links between Cdc42, β1-integrin, and metastasis using a siRNA screening approach.

It is interesting that, of the three IQGAPs, only IQGAP1 has a reproducible effect on β1-integrin expression. This could reflect the relative expression levels of the three IQGAP1 proteins in PC3 prostate cancer cells: IQGAP3 protein was expressed as detected by immunoblotting, but we could not find a suitable antibody to detect IQGAP2 specifically. It is possible that total IQGAP3 levels are much lower than IQGAP1. Much less is known about IQGAP2 and IQGAP3 than IQGAP1, but it is interesting that IQGAP1 and IQGAP3 act similarly in cancer cells in promoting migration, invasion, and proliferation, whereas IQGAP2 is a tumor suppressor in a variety of cancer types.[44] In addition to IQGAP1 and NWASP, depletion of the Cdc42 target FMNL3 reduces β1-integrin mRNA and protein expression, although it did not affect surface levels. One possible explanation is that FMNL3 acts only via MRTF/SRF-mediated transcriptional regulation of β1-integrin and not through the rapidly acting FAK/ERK pathway. On the other hand, FMNL1 depletion increased β1-integrin mRNA, protein expression, and surface levels. It would therefore be interesting to compare the effects of FMNL1 and FMNL3 on cancer cell attachment to ECs in the future. Notably, in our original siRNA screen of Rho GTPases for PC3 cell attachment to ECs *in vitro*, RhoQ depletion enhanced PC3 adhesion.[9] FMNL3 is widely

Figure 5. IQGAP1 and NWASP regulate β1-integrin via both ERK/FAK signaling and SRF/MRTF-induced transcription

(A) β1-integrin and IQGAP1 immunoprecipitates (and IgG control) from PC3 cells were immunoblotted for IQGAP1 and β1-integrin.

(B and C) PC3 cells were treated with either vehicle or FAK inhibitor (FAKi) 4548 for 30 min at the indicated concentrations. (B) Quantification of β1-integrin expression (left) and p-FAK (Tyr^{397}) (right). Mean ± SEM; n = 3 independent experiments, one-way ANOVA test. (C) (Top) Quantification in percentage of vehicle- or FAKi (3 μM)-treated PC3 cell shear-stress-resistant adhesion to human brain ECs (hCMEC/D3). PC3 cells were fluorescently labeled and treated with FAKi for 30 min. hCMEC/D3 monolayers were exposed to 2 × 10^6 PC3 cells/mL at 0.1 dyn/cm^2 for 5 min followed by 1 dyn/cm^2 for 30 s. Data are mean ± SEM (n = 3) with 10 technical replicates each, two-tailed unpaired t test. (Bottom) Graphical representation of firm adhesion of PC3 cells to hCMEC/D3.

(D and E) PC3 cells were treated with either vehicle or MEKi U0126 at the time indicated. (D) Quantification of β1-integrin expression and p-ERK 1/2 (p-P44/42 mitogen-activated protein kinase) levels (right). Mean ± SEM; n = 4 independent experiments, one-way ANOVA test. (E) Quantification of p-FAK (Tyr^{397}) levels. Mean ± SEM; n = 3 independent experiments, two-tailed unpaired t test.

(F) Representative immunoblot from total lysates of PC3 cells transfected with either control or IQGAP1 siRNAs and probed for IQGAP1 and p-FAK (Tyr^{397}); lanes are all from the same immunoblot.

(G) Quantification of β1-integrin expression in PC3 cells transfected with either control or SRF siRNAs. Mean ± SEM; n = 3 independent experiments, one-way ANOVA test.

(H) PC3 cells were transfected with either control siRNA or with the indicated siRNAs. Quantification of relative β1-integrin mRNA levels was done by real-time qPCR. Mean ± SEM; n = 6.

(I–K) PC3 cells were treated with vehicle, MRTFi-1 (CCG-1423), or MRTFi-2 (CCG-203971) at 20 μM. Quantification of total (I) MRTF-A and (J) β1-integrin. Data are mean ± SEM (n = 4). (K) (Left) Quantification of active β1-integrin by flow cytometry. (Right) Representative flow cytometry histograms. Data are mean ± SEM (n = 3).

(G–K) One-way ANOVA.

(L) Graphical summary of IQGAP1 and NWASP regulation of β1-integrin to mediate cancer cell attachment to ECs, dissemination, and metastasis formation.

expressed, and its expression has been reported to be upregulated in nasopharyngeal carcinoma (NPC) and to contribute to epithelial-mesenchymal transition in NPC-derived cell lines.[67] On the other hand, FMNL1 is normally most highly expressed in hematopoietic cells but is upregulated in a range of epithelial cancers.[68] Interestingly, FMNL1 depletion in MDA-MB-231 cells strongly reduced cell migration,[69] and thus it would be interesting to explore whether this effect involves upregulated β1-integrin expression. FMNL2 and FMNL3 stimulate lamellipodial protrusion and migration in melanoma cells and fibroblasts,[70] and FMNL3 is also required for filopodial assembly in osteosarcoma cells.[71] Whether the effect of FMNL3 depletion in reducing β1-integrin contributes to either of these responses remains to be established, but integrins including β1-integrin are located at the tips of filopodia, and β1-integrin is located at filopodium-like protrusions in extravasated cancer cells in the lung *in vivo*.[72]

IQGAP1 and NWASP silencing decrease β1-integrin integrin expression; however, NWASP consistently has a weaker effect in reducing β1-integrin than IQGAP1, which could explain why it does not decrease cancer cell retention in the lung. Nevertheless, NWASP significantly reduces cancer firm adhesion to ECs and metastasis formation and growth, which is likely to be through an additional mechanism, for example, via its effects on matrix remodeling and invadopodia.[73,74] IQGAP1 not only reduces cancer cell adhesion, retention, and metastasis formation but also significantly reduces interaction with the vasculature *in vivo*, suggesting that it could be an important player in an early step of cancer metastasis formation, when the cancer cells are still in the blood circulation and can thus be targeted to prevent metastatic progression.

Our observation that IQGAP1 depletion decreases FAK phosphorylation may explain the downstream β1-integrin reduction. Consistent with this model, a small-molecule FAKi reduces cancer cell adhesion to human brain ECs under flow *in vitro*. FAK is frequently upregulated in human cancers, contributes to cancer progression in animal models, and is considered a good target for cancer treatment.[48,75] Indeed, several combination clinical trials with FAKis are ongoing.[75] FAKis therefore represent a promising pharmacological tool to prevent cancer cell adhesion to the endothelium during metastatic dissemination.

In summary, we have delineated a pathway linking Cdc42, via its targets IQGAP1 and NWASP, to β1-integrin-mediated cancer cell attachment to ECs, retention in the lungs, and metastatic nodule formation. Furthermore, we propose a mechanism whereby these Cdc42 effectors contribute to cancer cell adhesion to ECs through both acute and long-term effects on β1-integrin expression. First, they activate ERK/FAK signaling, leading to a rapid increase in β1-integrin protein levels, and second, they increase β1-integrin transcription via the MRTF/SRF transcription factor complex (model in Figure S5K). Depletion of IQGAP1 reduces cancer cell retention in the lungs, which ultimately decreases the number and size of metastatic foci in the lungs. This implies that targeting components of this Cdc42/IQGAP1/β1-integrin pathway could be used as a treatment to reduce metastases in human patients with cancer.

Limitation of the study

Preclinical models of the early steps of breast and prostate cancer metastasizing to the brain and lung are limited. Because we were interested in studying the effects of NWASP/IQGAP1/β1-integrin on early steps of the metastatic cascade, we used of an experimental model of metastasis that allows the study of the intravascular phase of metastasis that the spontaneous metastasis model does not offer except with big limitations, such as the low amount of cells, and very complex approaches like the lung or cranial window that require a high number of animals. We overcome this using human brain ECs in an *in-vivo*-like microfluidic system.

IQGAP1 is known to interact with FAK and ERK, both of which are required to maintain β1-integrin protein levels. Cdc42 increases β1-integrin transcription,[9] and here, we find that IQGAP1 and NWASP also mediate a longer-term increase in β1-integrin mRNA through the MRTF/SRF transcription factor. It is not yet clear whether the acute decrease in β1-integrin levels observed in FAKi- and ERKi-treated cells is directly linked to IQGAP1 or NWASP signaling; this could be tested, for example, by expressing IQGAP1 mutants that cannot associate with FAK or ERK and determining whether they can no longer alter active surface levels of β1-integrin. In addition, we have not shown whether the reported interaction between IQGAP1 and NWASP induced by growth factors[43] underlies their contributions to β1-integrin expression or cancer cell:EC interaction. This would involve mapping their interaction sites and testing relevant mutants in our assays. Despite these limitations, our results and other reports clearly point to the interaction of cancer cells with ECs as an important step for cancer cell retention at metastatic sites such as the lung in mouse models and that targeting this step of cancer progression in patients could help to reduce the metastatic spread of epithelial tumors. The use of patient-derived cancer cells grown in patient-derived xenograft *in vivo* models, another human organ-specific vasculature *in vitro* (i.e., lung), and emerging technologies like single-cell -omics (transcriptomic and proteomic) to investigate the role of IQGAP1 and NWASP in breast and prostate cancer metastasis formation will allow us to further unravel their mechanism of action to find novel target for clinical treatments.

STAR★METHODS

Detailed methods are provided in the online version of this paper and include the following:

- KEY RESOURCES TABLE
- RESOURCES AVAILABILITY
  - Lead contact
  - Materials availability
  - Data and code availability
- EXPERIMENTAL MODEL AND STUDY PARTICIPANT DETAILS
  - Experimental design
  - Mouse studies, power analysis and randomization
  - Cell culture
  - Cancer cell treatments: β1-integrin, FAK and MEK inhibition
  - Cell transfection
- METHOD DETAILS
  - Cell staining and detachment

- *Ex vivo* whole lung imaging and confocal microscopy analysis
- Experimental lung metastasis assay and MRI scans
- Flow-based adhesion assay
- Surface biotinylation assay
- Immunoprecipitation and immunoblotting
- Flow cytometry
- Real-time qPCR
- Immunostaining

- QUANTIFICATION AND STATISTICAL ANALYSIS

SUPPLEMENTAL INFORMATION

Supplemental information can be found online at https://doi.org/10.1016/j.celrep.2024.113989.

ACKNOWLEDGMENTS

We thank Magali Soyer for the ImageJ macro border, Paul Kinchesh for developing MRI scans, Stuart Gilchrist for developing the robot carriage system, and Ana L Gomes and Sean Smart for the MRI scans. We thank Magali Williamson, Mirella Georgouli, Eva Crosas Molist, Caterina Giacomini, Raquel Haga, and Francesco Romeo for technical advice and discussions. This work was funded by a Cancer Research UK grant (C6620/A15961) (A.J.R., C.C., R.G., and N.R.), the University of Bristol School of Cellular and Molecular Medicine (A.J.R. and C.C.), a Cancer Research UK Oxford Center DPhil Prize Studentship (BBRTJW00) (S.L.), the European Union's Horizon 2020 research and innovation programme under the Marie Skłodowska-Curie grant agreement (no. 655817) MSCA-IF-2014 (S.T.M. and A.R.), a Cancer Research UK grant A1731 (R.M.), and the Biotechnology and Biological Sciences Research Council (grant no. BB/K009184/1) (I.A.R.).

AUTHOR CONTRIBUTIONS

Conceptualization, A.J.R., C.C., and N.R.; funding acquisition, A.J.R. and R.M.; investigation, C.C., S.L., S.T.M., N.R., and R.G.; methodology, C.C., S.L., N.R., and S.T.M.; resources, I.A.R.; supervision, A.J.R. and R.M.; visualization, C.C. and S.L.; writing – original draft, C.C. and A.J.R.; writing – review & editing, C.C., S.L., R.M., N.R., S.T.M., and A.J.R. Specifics: C.C. designed and performed the experiments, analyzed and interpreted the data, prepared the figures, and wrote the original manuscript. S.L. co-designed the *in vivo* experiments, developed *in vivo* methodology, and co-designed and performed *in vivo* and *ex vivo* experiments. S.T.M., R.G., and N.R. performed and/or analyzed the siRNA screening in Figures 3A, 3E, and S3A–S3E. I.A.R. provided the hCMEC/D3 cell line and reagents/microscope facility for preliminary flow-based adhesion experiments. R.M. supervised the *in vivo* experiments. A.J.R. conceived and supervised the study and co-wrote the manuscript. All the authors read, reviewed, and edited the manuscript.

DECLARATION OF INTERESTS

The authors declare no competing interests.

Received: August 13, 2023
Revised: February 1, 2024
Accepted: March 7, 2024

REFERENCES

1. Lambert, A.W., Pattabiraman, D.R., and Weinberg, R.A. (2017). Emerging Biological Principles of Metastasis. Cell *168*, 670–691. https://doi.org/10.1016/j.cell.2016.11.037.
2. Follain, G., Herrmann, D., Harlepp, S., Hyenne, V., Osmani, N., Warren, S.C., Timpson, P., and Goetz, J.G. (2020). Fluids and their mechanics in tumour transit: shaping metastasis. Nat. Rev. Cancer *20*, 107–124. https://doi.org/10.1038/s41568-019-0221-x.
3. Massagué, J., and Obenauf, A.C. (2016). Metastatic colonization by circulating tumour cells. Nature *529*, 298–306. https://doi.org/10.1038/nature17038.
4. Reymond, N., d'Água, B.B., and Ridley, A.J. (2013). Crossing the endothelial barrier during metastasis. Nat. Rev. Cancer *13*, 858–870. https://doi.org/10.1038/nrc3628.
5. Hamidi, H., and Ivaska, J. (2018). Every step of the way: integrins in cancer progression and metastasis. Nat. Rev. Cancer *18*, 533–548. https://doi.org/10.1038/s41568-018-0038-z.
6. Cooper, J., and Giancotti, F.G. (2019). Integrin Signaling in Cancer: Mechanotransduction, Stemness, Epithelial Plasticity, and Therapeutic Resistance. Cancer Cell *35*, 347–367. https://doi.org/10.1016/j.ccell.2019.01.007.
7. Desgrosellier, J.S., and Cheresh, D.A. (2010). Integrins in cancer: biological implications and therapeutic opportunities. Nat. Rev. Cancer *10*, 9–22. https://doi.org/10.1038/nrc2748.
8. Sökeland, G., and Schumacher, U. (2019). The functional role of integrins during intra- and extravasation within the metastatic cascade. Mol. Cancer *18*, 12. https://doi.org/10.1186/s12943-018-0937-3.
9. Reymond, N., Im, J.H., Garg, R., Vega, F.M., Borda d'Agua, B., Riou, P., Cox, S., Valderrama, F., Muschel, R.J., and Ridley, A.J. (2012). Cdc42 promotes transendothelial migration of cancer cells through β1 integrin. J. Cell Biol. *199*, 653–668. https://doi.org/10.1083/jcb.201205169.
10. White, D.E., Kurpios, N.A., Zuo, D., Hassell, J.A., Blaess, S., Mueller, U., and Muller, W.J. (2004). Targeted disruption of beta1-integrin in a transgenic mouse model of human breast cancer reveals an essential role in mammary tumor induction. Cancer Cell *6*, 159–170. https://doi.org/10.1016/j.ccr.2004.06.025.
11. Shibue, T., Brooks, M.W., and Weinberg, R.A. (2013). An integrin-linked machinery of cytoskeletal regulation that enables experimental tumor initiation and metastatic colonization. Cancer Cell *24*, 481–498. https://doi.org/10.1016/j.ccr.2013.08.012.
12. Huck, L., Pontier, S.M., Zuo, D.M., and Muller, W.J. (2010). β1-integrin is dispensable for the induction of ErbB2 mammary tumors but plays a critical role in the metastatic phase of tumor progression. Proc. Natl. Acad. Sci. USA *107*, 15559–15564. https://doi.org/10.1073/pnas.1003034107.
13. Er, E.E., Valiente, M., Ganesh, K., Zou, Y., Agrawal, S., Hu, J., Griscom, B., Rosenblum, M., Boire, A., Brogi, E., et al. (2018). Pericyte-like spreading by disseminated cancer cells activates YAP and MRTF for metastatic colonization. Nat. Cell Biol. *20*, 966–978. https://doi.org/10.1038/s41556-018-0138-8.
14. Hodge, R.G., and Ridley, A.J. (2016). Regulating Rho GTPases and their regulators. Nat. Rev. Mol. Cell Biol. *17*, 496–510. https://doi.org/10.1038/nrm.2016.67.
15. Bishop, A.L., and Hall, A. (2000). Rho GTPases and their effector proteins. Biochem. J. *348*, 241–255.
16. Kühn, S., and Geyer, M. (2014). Formins as effector proteins of Rho GTPases. Small GTPases *5*, e29513. https://doi.org/10.4161/sgtp.29513.
17. Hedman, A.C., Smith, J.M., and Sacks, D.B. (2015). The biology of IQGAP proteins: beyond the cytoskeleton. EMBO Rep. *16*, 427–446. https://doi.org/10.15252/embr.201439834.
18. Murphy, N.P., Mott, H.R., and Owen, D. (2021). Progress in the therapeutic inhibition of Cdc42 signalling. Biochem. Soc. Trans. *49*, 1443–1456. https://doi.org/10.1042/BST20210112.
19. Lucotti, S., Cerutti, C., Soyer, M., Gil-Bernabé, A.M., Gomes, A.L., Allen, P.D., Smart, S., Markelc, B., Watson, K., Armstrong, P.C., et al. (2019). Aspirin blocks formation of metastatic intravascular niches by inhibiting platelet-derived COX-1/thromboxane A2. J. Clin. Invest. *129*, 1845–1862. https://doi.org/10.1172/JCI121985.
20. Yu, M., Bardia, A., Wittner, B.S., Stott, S.L., Smas, M.E., Ting, D.T., Isakoff, S.J., Ciciliano, J.C., Wells, M.N., Shah, A.M., et al. (2013). Circulating

breast tumor cells exhibit dynamic changes in epithelial and mesenchymal composition. Science *339*, 580–584. https://doi.org/10.1126/science.1228522.

21. Aceto, N., Bardia, A., Miyamoto, D.T., Donaldson, M.C., Wittner, B.S., Spencer, J.A., Yu, M., Pely, A., Engstrom, A., Zhu, H., et al. (2014). Circulating tumor cell clusters are oligoclonal precursors of breast cancer metastasis. Cell *158*, 1110–1122. https://doi.org/10.1016/j.cell.2014.07.013.
22. Leong, H.S., Robertson, A.E., Stoletov, K., Leith, S.J., Chin, C.A., Chien, A.E., Hague, M.N., Ablack, A., Carmine-Simmen, K., McPherson, V.A., et al. (2014). Invadopodia are required for cancer cell extravasation and are a therapeutic target for metastasis. Cell Rep. *8*, 1558–1570. https://doi.org/10.1016/j.celrep.2014.07.050.
23. Valiente, M., Ahluwalia, M.S., Boire, A., Brastianos, P.K., Goldberg, S.B., Lee, E.Q., Le Rhun, E., Preusser, M., Winkler, F., and Soffietti, R. (2018). The Evolving Landscape of Brain Metastasis. Trends Cancer *4*, 176–196. https://doi.org/10.1016/j.trecan.2018.01.003.
24. Laschinger, M., and Engelhardt, B. (2000). Interaction of α4-integrin with VCAM-1 is involved in adhesion of encephalitogenic T cell blasts to brain endothelium but not in their transendothelial migration in vitro. J. Neuroimmunol. *102*, 32–43. https://doi.org/10.1016/s0165-5728(99)00156-3.
25. García-Martín, A.B., Zwicky, P., Gruber, T., Matti, C., Moalli, F., Stein, J.V., Francisco, D., Enzmann, G., Levesque, M.P., Hewer, E., and Lyck, R. (2019). VLA-4 mediated adhesion of melanoma cells on the blood-brain barrier is the critical cue for melanoma cell intercalation and barrier disruption. J. Cereb. Blood Flow Metab. *39*, 1995–2010. https://doi.org/10.1177/0271678X18775887.
26. Taddei, I., Faraldo, M.M., Teulière, J., Deugnier, M.A., Thiery, J.P., and Glukhova, M.A. (2003). Integrins in mammary gland development and differentiation of mammary epithelium. J. Mammary Gland Biol. Neoplasia *8*, 383–394. https://doi.org/10.1023/B:JOMG.0000017426.74915.b9.
27. Dehghani, M., Kianpour, S., Zangeneh, A., and Mostafavi-Pour, Z. (2014). CXCL12 modulates prostate cancer cell adhesion by altering the levels or activities of β1-containing integrins. Int. J. Cell Biol. *2014*, 981750. https://doi.org/10.1155/2014/981750.
28. Haidari, M., Zhang, W., Caivano, A., Chen, Z., Ganjehei, L., Mortazavi, A., Stroud, C., Woodside, D.G., Willerson, J.T., and Dixon, R.A.F. (2012). Integrin α2β1 mediates tyrosine phosphorylation of vascular endothelial cadherin induced by invasive breast cancer cells. J. Biol. Chem. *287*, 32981–32992. https://doi.org/10.1074/jbc.M112.395905.
29. Humphries, J.D., Byron, A., and Humphries, M.J. (2006). Integrin ligands at a glance. J. Cell Sci. *119*, 3901–3903. https://doi.org/10.1242/jcs.03098.
30. Barbazán, J., Alonso-Alconada, L., Elkhatib, N., Geraldo, S., Gurchenkov, V., Glentis, A., van Niel, G., Palmulli, R., Fernández, B., Viaño, P., et al. (2017). Liver metastasis is facilitated by the adherence of circulating tumor cells to vascular fibronectin deposits. Cancer Res. *77*, 3431–3441. https://doi.org/10.1158/0008-5472.CAN-16-1917.
31. Hebert, J.D., Myers, S.A., Naba, A., Abbruzzese, G., Lamar, J.M., Carr, S.A., and Hynes, R.O. (2020). Proteomic Profiling of the ECM of xenograft breast cancer metastases in different organs reveals distinct metastatic niches. Cancer Res. *80*, 1475–1485. https://doi.org/10.1158/0008-5472.CAN-19-2961.
32. Uhlen, M., Zhang, C., Lee, S., Sjöstedt, E., Fagerberg, L., Bidkhori, G., Benfeitas, R., Arif, M., Liu, Z., Edfors, F., et al. (2017). A pathology atlas of the human cancer transcriptome. Science *357*, eaan2507. https://doi.org/10.1126/science.aan2507.
33. Uhlén, M., Fagerberg, L., Hallström, B.M., Lindskog, C., Oksvold, P., Mardinoglu, A., Sivertsson, Å., Kampf, C., Sjöstedt, E., Asplund, A., et al. (2015). Proteomics. Tissue-based map of the human proteome. Science *347*, 1260419. https://doi.org/10.1126/science.1260419.
34. Bartha, Á., and Győrffy, B. (2021). TNMplot.com: A Web Tool for the Comparison of Gene Expression in Normal, Tumor and Metastatic Tissues. Int. J. Mol. Sci. *22*, 2622. https://doi.org/10.3390/ijms22052622.
35. Cortazar, A.R., Torrano, V., Martín-Martín, N., Caro-Maldonado, A., Camacho, L., Hermanova, I., Guruceaga, E., Lorenzo-Martín, L.F., Caloto, R., Gomis, R.R., et al. (2018). CANCERTOOL: A Visualization and representation interface to exploit cancer datasets. Cancer Res. *78*, 6320–6328. https://doi.org/10.1158/0008-5472.CAN-18-1669.
36. Thul, P.J., Åkesson, L., Wiking, M., Mahdessian, D., Geladaki, A., Ait Blal, H., Alm, T., Asplund, A., Björk, L., Breckels, L.M., et al. (2017). A subcellular map of the human proteome. Science *356*, eaal3321. https://doi.org/10.1126/science.aal3321.
37. Győrffy, B. (2021). Survival analysis across the entire transcriptome identifies biomarkers with the highest prognostic power in breast cancer. Comput. Struct. Biotechnol. J. *19*, 4101–4109. https://doi.org/10.1016/j.csbj.2021.07.014.
38. Ősz, Á., Lánczky, A., and Győrffy, B. (2021). Survival analysis in breast cancer using proteomic data from four independent datasets. Sci. Rep. *11*, 16787. https://doi.org/10.1038/s41598-021-96340-5.
39. Tang, W., Zhou, M., Dorsey, T.H., Prieto, D.A., Wang, X.W., Ruppin, E., Veenstra, T.D., and Ambs, S. (2018). Integrated proteotranscriptomics of breast cancer reveals globally increased protein-mRNA concordance associated with subtypes and survival. Genome Med. *10*, 94. https://doi.org/10.1186/s13073-018-0602-x.
40. King, S.J., Worth, D.C., Scales, T.M.E., Monypenny, J., Jones, G.E., and Parsons, M. (2011). beta1 integrins regulate fibroblast chemotaxis through control of N-WASP stability. EMBO J. *30*, 1705–1718. https://doi.org/10.1038/emboj.2011.82.
41. Zaidel-Bar, R., Itzkovitz, S., Ma'ayan, A., Iyengar, R., and Geiger, B. (2007). Functional atlas of the integrin adhesome. Nat. Cell Biol. *9*, 858–867. https://doi.org/10.1038/ncb0807-858.
42. Jacquemet, G., Morgan, M.R., Byron, A., Humphries, J.D., Choi, C.K., Chen, C.S., Caswell, P.T., and Humphries, M.J. (2013). Rac1 is deactivated at integrin activation sites through an IQGAP1-filamin-A-RacGAP1 pathway. J. Cell Sci. *126*, 4121–4135. https://doi.org/10.1242/jcs.121988.
43. Benseñor, L.B., Kan, H.M., Wang, N., Wallrabe, H., Davidson, L.A., Cai, Y., Schafer, D.A., and Bloom, G.S. (2007). IQGAP1 regulates cell motility by linking growth factor signaling to actin assembly. J. Cell Sci. *120*, 658–669. https://doi.org/10.1242/jcs.03376.
44. Smith, J.M., Hedman, A.C., and Sacks, D.B. (2015). IQGAPs choreograph cellular signaling from the membrane to the nucleus. Trends Cell Biol. *25*, 171–184. https://doi.org/10.1016/j.tcb.2014.12.005.
45. Velasco-Velázquez, M.A., Salinas-Jazmín, N., Mendoza-Patiño, N., and Mandoki, J.J. (2008). Reduced paxillin expression contributes to the antimetastatic effect of 4-hydroxycoumarin on B16-F10 melanoma cells. Cancer Cell Int. *8*, 8. https://doi.org/10.1186/1475-2867-8-8.
46. Horton, E.R., Humphries, J.D., Stutchbury, B., Jacquemet, G., Ballestrem, C., Barry, S.T., and Humphries, M.J. (2016). Modulation of FAK and Src adhesion signaling occurs independently of adhesion complex composition. J. Cell Biol. *212*, 349–364. https://doi.org/10.1083/jcb.201508080.
47. Lorusso, G., Wyss, C.B., Kuonen, F., Vannini, N., Billottet, C., Duffey, N., Pineau, R., Lan, Q., Wirapati, P., Barras, D., et al. (2022). Connexins orchestrate progression of breast cancer metastasis to the brain by promoting FAK activation. Sci. Transl. Med. *14*, eaax8933. https://doi.org/10.1126/scitranslmed.aax8933.
48. Sulzmaier, F.J., Jean, C., and Schlaepfer, D.D. (2014). FAK in cancer: mechanistic findings and clinical applications. Nat. Rev. Cancer *14*, 598–610. https://doi.org/10.1038/nrc3792.
49. Bardwell, A.J., Lagunes, L., Zebarjedi, R., and Bardwell, L. (2017). The WW domain of the scaffolding protein IQGAP1 is neither necessary nor sufficient for binding to the MAPKs ERK1 and ERK2. J. Biol. Chem. *292*, 8750–8761. https://doi.org/10.1074/jbc.M116.767087.
50. Roy, M., Li, Z., and Sacks, D.B. (2005). IQGAP1 is a scaffold for mitogen-activated protein kinase signaling. Mol. Cell Biol. *25*, 7940–7952. https://doi.org/10.1128/MCB.25.18.7940-7952.2005.

51. Zhao, Y., and Adjei, A.A. (2014). The clinical development of MEK inhibitors. Nat. Rev. Clin. Oncol. *11*, 385–400. https://doi.org/10.1038/nrclinonc.2014.83.

52. Carmon, K.S., Gong, X., Yi, J., Thomas, A., and Liu, Q. (2014). RSPO-LGR4 functions via IQGAP1 to potentiate Wnt signaling. Proc. Natl. Acad. Sci. USA *111*, E1221–E1229. https://doi.org/10.1073/pnas.1323106111.

53. Di Modugno, F., Spada, S., Palermo, B., Visca, P., Iapicca, P., Di Carlo, A., Antoniani, B., Sperduti, I., Di Benedetto, A., Terrenato, I., et al. (2018). hMENA isoforms impact NSCLC patient outcome through fibronectin/β1 integrin axis. Oncogene *37*, 5605–5617. https://doi.org/10.1038/s41388-018-0364-3.

54. Gau, D., and Roy, P. (2018). SRF'ing and SAP'ing - the role of MRTF proteins in cell migration. J. Cell Sci. *131*, jcs218222. https://doi.org/10.1242/jcs.218222.

55. Diring, J., Mouilleron, S., McDonald, N.Q., and Treisman, R. (2019). RPEL-family rhoGAPs link Rac/Cdc42 GTP loading to G-actin availability. Nat. Cell Biol. *21*, 845–855. https://doi.org/10.1038/s41556-019-0337-y.

56. Vartiainen, M.K., Guettler, S., Larijani, B., and Treisman, R. (2007). Nuclear actin regulates dynamic subcellular localization and activity of the SRF cofactor MAL. Science *316*, 1749–1752. https://doi.org/10.1126/science.1141084.

57. Evelyn, C.R., Wade, S.M., Wang, Q., Wu, M., Iñiguez-Lluhí, J.A., Merajver, S.D., and Neubig, R.R. (2007). CCG-1423: a small-molecule inhibitor of RhoA transcriptional signaling. Mol. Cancer Ther. *6*, 2249–2260. https://doi.org/10.1158/1535-7163.MCT-06-0782.

58. Hayashi, K., Watanabe, B., Nakagawa, Y., Minami, S., and Morita, T. (2014). RPEL proteins are the molecular targets for CCG-1423, an inhibitor of Rho signaling. PLoS One *9*, e89016. https://doi.org/10.1371/journal.pone.0089016.

59. Bell, J.L., Haak, A.J., Wade, S.M., Kirchhoff, P.D., Neubig, R.R., and Larsen, S.D. (2013). Optimization of novel nipecotic bis(amide) inhibitors of the Rho/MKL1/SRF transcriptional pathway as potential anti-metastasis agents. Bioorg. Med. Chem. Lett. *23*, 3826–3832. https://doi.org/10.1016/j.bmcl.2013.04.080.

60. Olson, E.N., and Nordheim, A. (2010). Linking actin dynamics and gene transcription to drive cellular motile functions. Nat. Rev. Mol. Cell Biol. *11*, 353–365. https://doi.org/10.1038/nrm2890.

61. Kienast, Y., von Baumgarten, L., Fuhrmann, M., Klinkert, W.E.F., Goldbrunner, R., Herms, J., and Winkler, F. (2010). Real-time imaging reveals the single steps of brain metastasis formation. Nat. Med. *16*, 116–122. https://doi.org/10.1038/nm.2072.

62. Peralta, M., Osmani, N., and Goetz, J.G. (2022). Circulating tumor cells: Towards mechanical phenotyping of metastasis. iScience *25*, 103969. https://doi.org/10.1016/j.isci.2022.103969.

63. Wirtz, D., Konstantopoulos, K., and Searson, P.C. (2011). The physics of cancer: the role of physical interactions and mechanical forces in metastasis. Nat. Rev. Cancer *11*, 512–522. https://doi.org/10.1038/nrc3080.

64. Park, C.C., Zhang, H.J., Yao, E.S., Park, C.J., and Bissell, M.J. (2008). Beta1 integrin inhibition dramatically enhances radiotherapy efficacy in human breast cancer xenografts. Cancer Res. *68*, 4398–4405. https://doi.org/10.1158/0008-5472.CAN-07-6390.

65. Barkan, D., and Chambers, A.F. (2011). β1-integrin: a potential therapeutic target in the battle against cancer recurrence. Clin. Cancer Res. *17*, 7219–7223. https://doi.org/10.1158/1078-0432.CCR-11-0642.

66. Slack, R.J., Macdonald, S.J.F., Roper, J.A., Jenkins, R.G., and Hatley, R.J.D. (2022). Emerging therapeutic opportunities for integrin inhibitors. Nat. Rev. Drug Discov. *21*, 60–78. https://doi.org/10.1038/s41573-021-00284-4.

67. Wu, Y., Shen, Z., Wang, K., Ha, Y., Lei, H., Jia, Y., Ding, R., Wu, D., Gan, S., Li, R., et al. (2017). High FMNL3 expression promotes nasopharyngeal carcinoma cell metastasis: role in TGF-β1-induced epithelia-to-mesenchymal transition. Sci. Rep. *7*, 42507. https://doi.org/10.1038/srep42507.

68. Gardberg, M., Heuser, V.D., Iljin, K., Kampf, C., Uhlen, M., and Carpén, O. (2014). Characterization of Leukocyte Formin FMNL1 Expression in Human Tissues. J. Histochem. Cytochem. *62*, 460–470. https://doi.org/10.1369/0022155414532293.

69. Miller, E.W., and Blystone, S.D. (2019). The carboxy-terminus of the formin FMNL1 bundles actin to potentiate adenocarcinoma migration. J. Cell. Biochem. *120*, 14383–14404. https://doi.org/10.1002/jcb.28694.

70. Kage, F., Winterhoff, M., Dimchev, V., Mueller, J., Thalheim, T., Freise, A., Brühmann, S., Kollasser, J., Block, J., Dimchev, G., et al. (2017). FMNL formins boost lamellipodial force generation. Nat. Commun. *8*, 14832. https://doi.org/10.1038/ncomms14832.

71. Young, L.E., Latario, C.J., and Higgs, H.N. (2018). Roles for Ena/VASP proteins in FMNL3-mediated filopodial assembly. J. Cell Sci. *131*, jcs220814. https://doi.org/10.1242/jcs.220814.

72. Shibue, T., Brooks, M.W., Inan, M.F., Reinhardt, F., and Weinberg, R.A. (2012). The outgrowth of micrometastases is enabled by the formation of filopodium-like protrusions. Cancer Discov. *2*, 706–721. https://doi.org/10.1158/2159-8290.CD-11-0239.

73. Juin, A., Spence, H.J., Martin, K.J., McGhee, E., Neilson, M., Cutiongco, M.F.A., Gadegaard, N., Mackay, G., Fort, L., Lilla, S., et al. (2019). N-WASP Control of LPAR1 trafficking establishes response to self-generated LPA gradients to promote pancreatic cancer cell metastasis. Dev. Cell *51*, 431–445.e7. https://doi.org/10.1016/j.devcel.2019.09.018.

74. Murphy, D.A., and Courtneidge, S.A. (2011). The 'ins' and 'outs' of podosomes and invadopodia: characteristics, formation and function. Nat. Rev. Mol. Cell Biol. *12*, 413–426. https://doi.org/10.1038/nrm3141.

75. Dawson, J.C., Serrels, A., Stupack, D.G., Schlaepfer, D.D., and Frame, M.C. (2021). Targeting FAK in anticancer combination therapies. Nat. Rev. Cancer *21*, 313–324. https://doi.org/10.1038/s41568-021-00340-6.

76. Wilkinson, S., Paterson, H.F., and Marshall, C.J. (2005). Cdc42-MRCK and Rho-ROCK signalling cooperate in myosin phosphorylation and cell invasion. Nat. Cell Biol. *7*, 255–261. https://doi.org/10.1038/ncb1230.

77. Yushkevich, P.A., Piven, J., Hazlett, H.C., Smith, R.G., Ho, S., Gee, J.C., and Gerig, G. (2006). User-guided 3D active contour segmentation of anatomical structures: significantly improved efficiency and reliability. Neuroimage *31*, 1116–1128. https://doi.org/10.1016/j.neuroimage.2006.01.015.

78. Cerutti, C., Edwards, L.J., de Vries, H.E., Sharrack, B., Male, D.K., and Romero, I.A. (2017). MiR-126 and miR-126* regulate shear-resistant firm leukocyte adhesion to human brain endothelium. Sci. Rep. *7*, 45284. https://doi.org/10.1038/srep45284.

79. Cerutti, C., Soblechero-Martin, P., Wu, D., Lopez-Ramirez, M.A., de Vries, H., Sharrack, B., Male, D.K., and Romero, I.A. (2016). MicroRNA-155 contributes to shear-resistant leukocyte adhesion to human brain endothelium in vitro. Fluids Barriers CNS *13*, 8. https://doi.org/10.1186/s12987-016-0032-3.

80. Coisne, C., Lyck, R., and Engelhardt, B. (2013). Live cell imaging techniques to study T cell trafficking across the blood-brain barrier in vitro and in vivo. Fluids Barriers CNS *10*, 7. https://doi.org/10.1186/2045-8118-10-7.

81. Cerutti, C., and Ridley, A.J. (2021). Analyzing the Roles of Rho GTPases in Cancer Cell Adhesion to Endothelial Cells Under Flow Conditions. Methods Mol. Biol. *2294*, 93–109. https://doi.org/10.1007/978-1-0716-1350-4_7.

STAR★METHODS

KEY RESOURCES TABLE

REAGENT or RESOURCE	SOURCE	IDENTIFIER
Antibodies		
β1-INTEGRIN (CD29)	BD Biosciences	Mouse-610467; RRID: AB_2128060
β1-INTEGRIN (CD29) D2E5	Cell Signaling	Rabbit-4706; RRID: AB_823544
β1-INTEGRIN (CD29) 12G10	Abcam	Mouse-ab30394; RRID: AB_775726
β1-INTEGRIN (CD29) B3B11	Merck Millipore	Mouse-MAB2251; RRID: AB_94609
β1-INTEGRIN (CD29) P5D2	Abcam	Mouse-ab24693; RRID: AB_448230
β1-INTEGRIN (CD29) 4B7	Merck Millipore	Mouse-CP26; RRID: AB_212819
FMNL1	Atlas Antibodies	Rabbit-HPA028288; RRID: AB_10612110
FMNL2/3	Abcam	Mouse-ab57963; RRID: AB_941625
CDC49d	Biolegend	Brilliant Violet CD49d 304321; RRID: AB_2563971
Cdc42 B-8	Santa Cruz	Mouse-sc-8401; RRID: AB_627233
PARD3	Abcam	Rabbit-ab64646; RRID: AB_1603911
PAK4	Cell Signaling	Rabbit-3242; RRID: AB_2158622
PKCζ	Insight Technology	N/A
MRCKα	C Marshall Lab (London, UK)	Rabbit (Wilkinson et al.[76])
MRCKβ	C Marshall Lab (London, UK)	Rabbit (Wilkinson et al.[76])
Wave1	Merck Millipore	Mouse-05-618; RRID: AB_309847
IQGAP1	Invitrogen	Mouse-33-8900
IQGAP1	Cell Signaling	Rabbit-2293; RRID: AB_2125903
IQGAP2	Merck Millipore	Mouse-050-505; RRID: AB_309768
IQGAP3	Sigma-Aldrich	Rabbit-SAB1401987; RRID: AB_10608125
NWASP	Cell Signaling	Rabbit-4848; RRID: AB_10694415
PAXILLIN D9G12	Cell Signaling	Rabbit-12065; RRID: AB_2797814
MAPK (Erk1/2)	Cell Signaling	Rabbit-9102; RRID: AB_330744
P-MAPK (Erk1/2)(Thr201/Tyr204)	Cell Signaling	Rabbit-9101; RRID: AB_331646
FAK	Cell Signaling	Rabbit-3285; RRID: AB_2269034
P-FAK (Tyr397)	Cell Signaling	Rabbit-8556; RRID: AB_10891442
P-FAK (Tyr397)	BD Biosciences	Mouse-611722; RRID: AB_399198
SRF	Cell Signaling	Rabbit-5147; RRID: AB_10694554
FIBRONECTIN	Abcam	Mouse-ab23750; RRID: AB_447655
LAMININ	Abcam	Rabbit-ab11575; RRID: AB_298179
GAPDH	Merck Millipore	Mouse-CB1001; RRID: AB_2107426
β-tubulin	Sigma-Aldrich	Mouse-T6199; RRID: AB_477583
PE anti-mouse CD31 (PeCAM1)	Biolegend	160204; RRID: AB_2860750
Goat anti-Mouse IgG (H + L), Superclonal™ Recombinant Secondary Antibody, Alexa Fluor™ 488	Thermo Fisher Scientific	A28175; RRID: AB_2536161
Goat anti-Rabbit IgG (H + L) Highly Cross-Adsorbed Secondary Antibody, Alexa Fluor™ 546	Thermo Fisher Scientific	A-11035; RRID: AB_2534093
ITGA1 α1/CD49a-PeVio770	Miltenyi	REAfinity™130-119-409; RRID: AB_2733240
ITGA2 α2/CD49b-FITC	Miltenyi	REAfinity™130-100-335; RRID: AB_2658459
ITGA3 α3/CD49c-Vioblue	Miltenyi	REAfinity™130-105-404; RRID: AB_2658485
ITGA4 α4/CD49d-PeVio615	Miltenyi	REAfinity™130-123-046; RRID: AB_2811444
ITGA5 α5/CD49e-APC-Vio770	Miltenyi	REAfinity™130-129-856; RRID: AB_2922155

(*Continued on next page*)

Continued

REAGENT or RESOURCE	SOURCE	IDENTIFIER
ITGA6 α6/CD49f-PE	Miltenyi	REAfinity™130-127-248; RRID: AB_2921801
Chemicals, peptides, and recombinant proteins		
Fibronectin	Calbiochem, Merck Millipore	341635-5mg
Collagen from calf skin	Sigma-Aldrich	c-8919
β1-integrin blocking monoclonal antibody (mAb)	kind gift from Prof Nancy Hogg, CRUK LRI, London	N/A
FAK inhibitor 4548	AstraZeneca	AZ13256675
MAP kinase U0126	Tocris	11–445
MRTF inhibitor CCG-1423	Selleckchem	57719
MRTF inhibitor CCG-203971	Tocris	5277
Oligofectamine	Invitrogen	12252–011
EGM2 bulletKit medium	Lonza	cc-3162
Cell dissociation solution non-enzimatic 1x	Sigma Merck Millipore	C5789-100mL
Sodium pyruvate	Hyclone	SH30239.01
CellTracker™ Green CMFDA Dye	Thermo Fisher Scientific	C7025
Protease Inhibitor Cocktail II complete EDTA free	Roche	11873580001
Phosfatase Inhibitor cocktail IV	Calbiochem	524628
Hoechst 33342	Thermo Fisher Scientific	H3570
Phoshatase Inhibitor Cocktail set II	Calbiochem	524636
EGTA	Sigma-Aldrich	E3889
Sepharose Protein G	Thermo Fisher Scientific	1856205
Trizol	Ambion Life Technologies	1559–026
Brilliant III Ultra-Fast SYBR Green real-time qPCR Master Mix	Agilent Technologies	600886–51
Critical commercial assays		
Ibidi® μ-Slides VI0.4	Ibidi® GmbH	80606–90
Immunoprecipitation Kit Dynabeads Protein G	Novex Life Technologies	10003D
Experimental models: Cell lines		
Pooled primary human umbilical vein endothelial cells (HUVECs)	Lonza	Catalog #: C2519A
PC3	gift from Magali Williamson (King's College London)	N/A
MDA-MB-231	ATCC	HTB-26™
hCMEC/D3	Provided by Prof Romero	N/A
Jurkat T cells	ATCC	TIB-152™
Experimental models: Organisms/strains		
Chase SCID® CB17/Icr-Prkdcscid/IcrlcoCrl mice	Charles River	236
Oligonucleotides		
Cdc42 siRNA	Sigma	GAUUACGACCGCUGAGUUA
β1-INTEGRIN-1 siRNA	Sigma	GAACAGAUCUGAUGAAUGA
β1-INTEGRIN-2 siRNA	Sigma	CAAGAGAGCUGAAGACUAU
FMNL1-POOL siRNA	Sigma	GAGAAGGGGUUAAUCCGUA GAAUUGGGCCCAGGAGUGA GCCAAGCCAUUGAGGCGUA AGGCGUACCUGGACAAUAU
FMNL2-POOL siRNA	Sigma	GAACCUACCUCCUGACAAA UAAGAGAACUGGAAAUUUC UAACAGACAUGUAUAUGAG AAUUAGGCCUGGACGAAUA

(*Continued on next page*)

Continued

REAGENT or RESOURCE	SOURCE	IDENTIFIER
FMNL3-POOL siRNA	Sigma	GCGAGGAGGUCACGAAAUC UAAAGCUGCUGCGGCAAUA UGUCAGCCAUUCGAAUUAA CAGCGUCGAUGUCAUUUGG
mDIA2-POOL siRNA	Sigma	CUGCACACCUAUCGUAUUU GCACAGUACUUGCUUGACA GUAUGCAGCUCAUCAAUGC GUAGACAUUUGCAUAGAUC
RasGRF2-POOL siRNA	Sigma	CUGCACACCUAUCGUAUUU GCACAGUACUUGCUUGACA CAACAGAGGUGAACAUUUG GAAGGAACACCAAACUUUA
Cdc42BPA-POOL siRNA	Sigma	CCAUAUAACUUGUGUAAAC GGAAACAAAUGGUUAGAAA GCGCAAGACUCACCAGUUU GAAGAUAGAUUGCCUGAAG
Cdc42BPB-POOL siRNA	Sigma	GAAGUGGGUUGGGAUUCUA GAAGAAUACUGAACGAAUU GAGAAACACGGAAAUAUUA CGAGAAGACUUUGAAAUAA
MRCKα-1- INDIVIDUAL siRNA	Dharmacon	GGAAACAAAUGGUUAGAAA
MRCKα-2-INDIVIDUAL siRNA	Dharmacon	GCGCAAGACUCACCAGUUU
MRCKβ-1-INDIVIDUAL siRNA	Dharmacon	GAAGAAUACUGAACGAAUU
MRCKβ-2-INDIVIDUAL siRNA	Dharmacon	CGAGAAGACUUUGAAAUAA
Par3-1 siRNA	Dharmacon	AAGCAUGGAUUUAGGUAUA
Par3-2 siRNA	Dharmacon	AAACAGCGUUGGAUGAUAG
ParD6G-2 (#2) siRNA	Dharmacon	UCAUAAGCCUGGGAAGUUU
ParD6G-1 (#3) siRNA	Dharmacon	GCAAGGCGGUUUCUAGUGC
PAK4-1 (#5) siRNA	Dharmacon	GGGUGAAGCUGUCAGACUU
PAK4-2 (#7) siRNA	Dharmacon	CCAUGAAGAUGAUUCGGGA
PKCζ-1 (#10) siRNA	Dharmacon	GAACGAGGACCGACCUUUU
PKCζ-2 (#11) siRNA	Dharmacon	GACCAAAUUUACGCCAUGA
PKCτ-1 siRNA	Dharmacon	N/A
PKCτ-2 siRNA siRNA	Dharmacon	N/A
Wave1-1 siRNA	Dharmacon	AAACAAGACCUCAGACAUA
Wave1-2 siRNA	Dharmacon	UUACACAGCUUGAUCCAAA
Wave2-1 siRNA	Dharmacon	UCAACAAUCUUACCCCUUA
Wave2-2 siRNA	Dharmacon	GCAAGUAGCUAUCCGCCAC
IQGAP1-1 (#1) siRNA	Sigma	GGAAAGCUCUGGCAAUUUA
IQGAP1-2 (#3) siRNA	Sigma	GAACGUGGCUUAUGAGUAC
IQGAP2-1 (#1) siRNA	Sigma	GAAGUUUGCUUAGUUGAAG
IQGAP2-2 (#2) siRNA	Sigma	GAACAAGUCCACUAAAUUU
IQGAP2-3 (#3) siRNA	Sigma	GCAAUAGGCUUAAACAAUC
IQGAP2-4 (#4) siRNA	Sigma	CAAAAGAGCUCAAAUCUGA
IQGAP3-1 (#2) siRNA	Sigma	CAAUGAGGCUCUGGACAAA
IQGAP3-2 (#3) siRNA	Sigma	CAAGAUGACUACAGGAUAU
NWASP-1 (#2) siRNA	Sigma	CAGCAGUGGUGCAGUUAUA
NWASP-2 (#3) siRNA	Sigma	GGUGUUGCUUGUCUUGUUA
PAXILLIN-1 siRNA	Sigma	UGGCUUCGCUGUCGGAUUU
PAXILLIN-2 siRNA	Sigma	GAACGACAAGCCUUACUGU
PAXILLIN-3 siRNA	Sigma	GGACGUGGCACCCUGAACA

(*Continued on next page*)

Continued

REAGENT or RESOURCE	SOURCE	IDENTIFIER
PAXILLIN-4 siRNA	Sigma	GCAGCAACCUUUCUGAACU
SRF-1 siRNA	Sigma	GGACUGUGCUGAAGAGUAC
SRF-2 siRNA	Sigma	GCACCAGUGUCUGCUAGUG
CONTROL siRNA	Sigma	UUCUCCGAACGUGUCACGU
Hs_GAPDH_1_SG (qPCR)	QIAGEN #QT00079247	N/A
IQGAP1 FW (qPCR)	IDT Integrated DNA technology	GCATGCTGCTTCCAATAAGATGT
IQGAP1 RV (qPCR)	IDT Integrated DNA technology	AAACCGTCTGAATTTCTGGTAGGA
FW3_WASL (qPCR)	SIGMA	TGTGGGAACAAGAGCTATAC
RV3_WASL (qPCR)	SIGMA	TTCTCAGATTTCCTTTGTCG
β1-integrin FW (qPCR)	IDT Integrated DNA technology	AGGTGGTTTCGATGCCATCAT
β1-integrin RV (qPCR)	IDT Integrated DNA technology	AAGTGAAACCCGGCATCTGTG
Hs_GAPDH_1_SG (qPCR)	QIAGEN #QT00079247	N/A
Software and algorithms		
GraphPad Prism	GraphPad	https://www.graphpad.com
Zen microscopy software	ZEISS	https://www.zeiss.com/microscopy/en/products/software/zeiss-zen.html
Image Pro Plus	MEDIA Cybernetics	https://my.mediacy.com/
Lasx	Leica	https://www.leica-microsystems.com/products/microscope-software/p/leica-las-x-ls/
Imaris	Oxford Instruments	https://imaris.oxinst.com/
ImageJ	NIH	https://imagej.nih.gov/ij/download.html
FlowJo	Tree Star	https://www.flowjo.com/
QuantStudioTM real-time	ThermoFisher	https://www.thermofisher.com/it/en/home/global/forms/life-science/quantstudio-6-7-flex-software.html
ITK-SNAP	University of Pennsylvania	http://www.itksnap.org/pmwiki/pmwiki.php

RESOURCES AVAILABILITY

Lead contact

Further information and requests for resources and reagents should be directed to and will be fulfilled by the lead contact, Anne Ridley (anne.ridley@bristol.ac.uk).

Materials availability

This study did not generate new unique reagents.

Data and code availability

- All data are available in the main text or the supplementary materials. Original western blot images are in the supplemental material. Blot and imaging data reported in this paper will be shared by the lead contact upon request.
- This paper does not report original code.
- Any additional information required to reanalyze the data reported in this paper is available from the lead contact upon request.

EXPERIMENTAL MODEL AND STUDY PARTICIPANT DETAILS

Experimental design

The study was designed to (1) test whether β1-integrin inhibition in prostate and breast cancer cell lines could reduce their interaction with human primary ECs, human brain ECs *in vitro* and in the mouse lung *in vivo,* to study whether cell interaction correlated with retention in the lung and subsequent metastatic nodules formation. (2) To identify which of the known Cdc42 downstream effectors contributes to β1-integrin expression in human cancer cells, how these effectors signal to alter β1-integrin expression *in vitro*, and whether they contribute to EC interaction, lung retention and metastatic nodule formation *in vivo*.

Mouse studies, power analysis and randomization

Fox Chase SCID CB17/Icr-Prkdc^{scid}/IcrlcoCrl mice (Charles River UK Ltd) were maintained under specific-pathogen-free conditions and were provided with food and water *ad libitum*, in accordance with UK Home Office regulations (The Home Office Animals Scientific Procedures Act, 1986). Female mice between 6 and 10 weeks of age were used for experiments. All animal work was conducted according to UK Home Office regulations and local ethics approval at the University of Oxford under project licence 30/3413.

Sample size was calculated through power analysis of previous data.[19] At least 3 biological replicates/mice were included in each experiment to have an 80% power ($1 - \beta$) to reject the null hypothesis at the 5% level of significance. Mice were randomly allocated to different experimental groups and distributed across multiple cages with more than one group per cage. Whenever possible, investigators were blinded to allocation during outcome assessment.

Cell culture

Human PC3 prostate cancer cells were a gift from Magali Williamson (King's College London). They were grown in RPMI supplemented with 10% FCS, 100 μg/mL streptomycin, and 100 U/ml penicillin. Human MDA-MB-231 breast cancer cells were grown in DMEM supplemented with 10% FCS, 1% pyruvate, 100 μg/mL streptomycin, and 100 U/ml penicillin. PC3 and MDA-MB-231 cells were authenticated by Eurofins-Genomics. Jurkat T cells were grown in suspension in RPMI 1640 W/GLUTAMAX I medium (Gibco-Invitrogen, Paisley, UK) with 10% FCS, 100 μg/mL streptomycin and 100 U/ml penicillin. Pooled primary human umbilical vein endothelial cells (HUVECs) were purchased from Lonza and maintained in EGM2 complete medium (Lonza) on dishes coated with 10 μg/mL fibronectin (Calbiochem, MerckMillipore) and used within 1–3 passages. The human cerebral microvascular endothelial (hCMEC/D3) cell line[75] was cultured in endothelial cell basal medium-2 (EBM2) medium (Lonza) and supplemented with the following components (Lonza): 0.025% (v/v) rhEGF, 0.025% (v/v) VEGF, 0.025% (v/v) IGF, 0.1% (v/v) rhFGF, 0.1% (v/v) gentamycin, 0.1% (v/v) ascorbic acid, 0.04% (v/v) hydrocortisone and 2.5% (v/v) fetal bovine serum (FBS), hereafter referred to as endothelial complete medium. hCMEC/D3 cells were grown to confluence (~1×10^5 cells/cm^2) on tissue culture flasks coated with collagen from calf skin (Sigma-Aldrich). All cells were cultured at 37°C, 5% CO_2.

Cancer cell treatments: β1-integrin, FAK and MEK inhibition

β1-integrin blocking monoclonal antibody (mAb) (a kind gift from Prof Nancy Hogg, Cancer Research UK London Research Institute, London), FAK inhibitor 4548 AZ13256675 (AstraZeneca), MAP kinase U0126 (Tocris), MRTF inhibitors CCG-1423 (Selleckchem) and CCG-203971 (Tocris) inhibitors were used to treat cancer cells at the concentrations and time-points indicated. DMSO was used as vehicle control for all treatments.

Cell transfection

PC3 and MDA-MB-231 cells were grown to ~30% confluence and transfected with siRNA oligos (50 nM) (key resources table) in Optimem-I (Gibco) using Oligofectamine (Invitrogen) or transfected by nucleofection (Lonza) for 6 h following the manufacturer's instructions. Following transfection, medium was replaced with growth medium. Unless otherwise indicated, cells were used for assays after 72 h.

METHOD DETAILS

Cell staining and detachment

Exponentially growing PC3 and MDA-MB-231 cells were stained with 12.5 μM CellTracker Green CMFDA dye (Thermo Fisher Scientific) and, where indicated, with Hoechst 33342 (Invitrogen) following the manufacturer's instructions. Cells were detached from culture plates with non-enzymatic cell dissociation solution (Sigma-Aldrich) and used for functional assays.

Ex vivo whole lung imaging and confocal microscopy analysis

Whole lung imaging was performed as previously described.[19] Briefly, PC3 and MDA-MB-231 (5×10^5) cells were injected IV into the tail vein of SCID mice. After 6 and 24 h, mice were terminally anesthetized with pentobarbital (70 mg/kg, i.p.). Lungs were then artificially ventilated through a tracheotomy. To visualize lung ECs, anti-CD31-PE antibody (50 mg/kg; 102408, BioLegend) was injected into the vena cava followed by ligation and left to circulate for 5 min before exsanguination. Lungs were perfused with

Krebs-Ringer buffer (KRB) through the pulmonary artery and placed in a custom-made imaging chamber.[19] Lungs were inflated with 0.5 mL of air prior to imaging.

Tile scans (10x) and *Z*-stacks (20-100x, 15–40 slices at 1- to 2-μm intervals) of whole lungs were acquired with an inverted confocal microscope (LSM-880, Zeiss), equipped with a Plan-Apochromat 20×/0.8 M27 objective. Hoechst/CMAC (excitation, 405 nm; emission, 410–513 nm), GFP/Alexa Fluor 488/CMFDA (excitation, 488 nm; emission, 490–653 nm), PE/CMRA (excitation, 543 nm; emission, 548–692 nm) scans were acquired sequentially to minimize bleed-through of emitted light. Cancer cell interaction with the lung endothelium was analyzed by 3D reconstruction of cancer cells and vessel surface with Imaris software (versions 8.2 and 9, Bitplane).

Experimental lung metastasis assay and MRI scans

Prostate PC3 and breast MDA-MB-231 (5×10^5) cancer cells were detached from culture plates with non-enzymatic cell dissociation solution (Sigma-Aldrich), passed through insulin syringe with needle gradually smaller (28G, 30G, 33G) and injected IV into SCID mice. All the animal injected reached the end date (6 weeks) in good health and with no signs of sickness or distress. After 6 weeks, lungs were perfused-isolated as described above. After clearance of blood, lungs were immersed in 10% neutral buffered formalin (Sigma-Aldrich) and fixed for at least 48 h. Lungs were embedded in 4% agarose and metastatic lung nodules were assessed by MRI scanning as previously described.[19] MRI Images were segmented and the volume of metastatic nodules was quantified by ITK-SNAP software (version 3.6.0).[77]

Flow-based adhesion assay

A flow-based adhesion assay with time-lapse live imaging[78,79] was used, HUVECs or hCMEC/D3 cells were grown to confluence in Ibidi μ-Slides VI$^{0.4}$ (Ibidi GmbH, Martinstreid, Germany) and washes with complete medium performed before the flow adhesion assay. The μ-Slide was positioned on the stage of an inverted time-lapse Nikon Eclipse TE2000-E microscope (Nikon Plan Fluor 10×/0.30 Ph1 DL objective) equipped with a Hamamatsu ORCA-ER digital camera or a Leica DMi8 microscope (HC PL FLUOTAR 10x/0.32 and 10x0.3 NA PH1) with a Hamamatsu Flash 4 V2 digital camera both with an environmentally controlled chamber (37°C, 5% CO_2). CMFDA-labelled-PC3 cells (2×10^6 cells/ml), Jurkat T cells (1.5×10^6 cells/ml) or MDA-MB-231 cells (1×10^6 cells/ml) were flowed in EC medium (pulled via a 5-mL Hamilton glass syringe coupled to a high precision pump, Harvard) through the μ-Slide channel at 0.1 dyn/cm^2 (PC3 and MDA-MB-231) or 0.5 dyn/cm^2 (Jurkat) for 5 min. The flow was then increased to 1 dyn/cm^2 (venular vessel wall shear stress[80]) for 30 s to remove cells that were not firmly attached to the EC. Cell-EC interactions were recorded in bright field and FITC channels (excitation, 495 nm; emission, 521 nm) at 12 frames/min (Nikon) or at 4 frames/sec (Leica).[81] The Videos were manually analyzed counting firmly adhered cells on fluorescence images using ImageJ software. Firm cancer cell adhesion was quantified from images of 10 different fields of view (1204.4 × 1615.9 μm; area = 1.95 mm^2) along the μ-Slide channel at the end of the assay, per technical replicate.

Surface biotinylation assay

Cancer cells were washed three times in ice-cold PBS and surface-labelled at 4°C with 0.3 mg/mL NHS-LC-biotin (Thermo Scientific) in PBS for 30 min. Labeled cells were washed four times in ice-cold PBS, and excess biotin was removed by incubation with RPMI containing 10% FCS for 20 min at 4°C. After three PBS washes, cells were lysed in 50 mM Tris pH 8, 150 mM NaCl, 5 mM EDTA, 1% NP-40, 25 mM NaF, 2 mM Na_3VO_4, phosphatase inhibitor cocktail (Calbiochem) and protease inhibitor cocktail (Roche). Lysates were sonicated, clarified by centrifugation at 16,000g for 10 min and incubated with streptavidin-agarose beads (Thermo Scientific) for 2 h at 4°C. Beads were washed four times with lysis buffer, and the proteins were eluted with NuPAGE LDS Sample Buffer (Invitrogen) containing 5% β-mercaptoethanol (Sigma-Aldrich). Samples were analyzed by immunoblotting.

Immunoprecipitation and immunoblotting

Cancer cells were lysed in IP lysis buffer (1% Triton X-100, 20 mM Tris pH 8, 130 mM NaCl, 1 mM DTT, supplemented with protease inhibitor cocktail complete (Roche) and PhosphoStop (Roche)). After clarifying the samples, lysates were incubated (4°C, 3 h) with magnetic Dynabeads or agarose beads previously incubated with the antibody (4°C, 1 h) (Life Technologies). The immunoprecipitates were washed with IP lysis buffer, and the proteins were eluted with NuPAGE LDS Sample Buffer (Invitrogen) containing 5% β-mercaptoethanol (Sigma-Aldrich).

Lysates were resolved in 8% SDS-polyacrylamide gels and transferred to nitrocellulose or PVDF (0.45 μm, Immobilon) membranes. Membranes were blocked using 5% (w/v) dried milk powder dissolved in Tris-buffered saline with 0.1% Tween 20 (TBS-T) and incubated with primary antibodies (key resources table) for 16–18 h at 4°C. Membranes were washed 3 times with TBS-T and incubated for 1 h at room temperature with appropriated HRP-labelled secondary antibodies (GE Healthcare). Enhanced chemiluminescence (ECL, GE Healthcare) was used for detection with films (Fujifilm). Bands were quantified using ImageJ 1.50i.

Flow cytometry

Cancer cells were detached with non-enzymatic dissociation buffer (Merck Millipore), washed once with FACS buffer (PBS without Ca^{2+} and Mg^{2+}, 1% BSA, 2 mM EDTA, 0.1% (w/v) NaN_3) and after FcR blocking, incubated for 1 h with primary antibody (key resources table). Cells were washed twice with FACS buffer (300*g*, 4°C, 5 min) then incubated with FITC-conjugated goat anti-mouse

secondary antibody (Life Technologies) for 1 h at 4°C in the dark. Cells were washed twice and immediately analyzed on a BD FACS CANTO II or Acea NovoCyte flow cytometer and results analyzed using FlowJo software (Tree Star, version 7.6.5).

Real-time qPCR

RNA was isolated with TRIzol Reagent (Invitrogen) following the manufacturer's protocol. qPCR was carried out using Brilliant III Ultra-Fast SYBR Green QRT-PCR Master Mix (Agilent Technologies). Each condition was carried out in technical triplicate. GAPDH was used as a reference gene (internal control) (key resources table). Assays were carried out using the Viia7 Real-Time system (Thermo Fisher Scientific) following the manufacturer's instructions for amplification cycles. The raw data were analyzed using QuantStudio real-time software. Quantification of the amplified product was determined by comparing the number of amplification cycles (Ct) after which the fluorescent signal crossed a threshold level. The following formula was applied to quantify the results: 2-ΔΔCT = [(Ct gene of interest – Ct internal control) sample A – (Ct gene of interest – Ct internal control) sample B)], $2-\Delta\Delta Ct$ (delta-delta Ct) method and normalized against GAPDH, used as internal control.

Immunostaining

Cells were fixed for 10 min with 4% paraformaldehyde (Sigma-Aldrich), washed 3 times, permeabilized with 0.2% Triton X-100 in PBS at 4°C for 5 min (this was omitted for membrane protein quantification) and then incubated with blocking solution (3% bovine serum albumin (BSA) and 0.05% Tween 20) for 30 min. Primary antibodies (key resources table) in blocking solution were incubated for 16–18 h at 4°C, followed by the secondary antibodies (Goat Alexa Fluor 488 or 546 IgG) combined with DAPI and phalloidin for 1 h in the dark. Cells were washed and mounted for imaging. Pictures were acquired with a LSM510 inverted confocal microscope (Zeiss) using a 63x (1.4 NA) objective with Zen software (Zeiss).

QUANTIFICATION AND STATISTICAL ANALYSIS

Statistical analyses were performed using Prism v.7.0 (GraphPad Software). Data were analyzed using an unpaired *t* test (2-tailed with paired or unpaired adjustment, two groups), Mann Whitney test or 1-way ANOVA with test indicated in the figure legend for each panel (more than two groups).

Cell Reports, Volume *43*

Supplemental information

IQGAP1 and NWASP promote human cancer cell dissemination and metastasis by regulating β1-integrin via FAK and MRTF/SRF

Camilla Cerutti, Serena Lucotti, Sofia T. Menendez, Nicolas Reymond, Ritu Garg, Ignacio A. Romero, Ruth Muschel, and Anne J. Ridley

Supplemental figures

Fig. S1. β1-integrin contributes to cancer cell retention and nodule formation in the lung.

(A-C) β1-integrin expression in cancer cells. PC3 (prostate) and MD-MB-231 (breast) cancer cells were transfected with either control- or β1 integrin siRNA and analyzed after 72 h. (**A)** β1-integrin siRNA decreases β1-integrin protein expression determined by western blotting. (**B)** β1-integrin siRNA decreases surface levels of active β1-integrin (for 12G10 and B3B11 antibody clones), determined by flow cytometry with representative histograms, and (**C**) by biotinylation assay. (**A** to **C** *n*=5, 5). (**D**) Rendering (Imaris software) of confocal z-stacks of single (cyan) and grouped (white) cancer cells in the lung vasculature (CD31PE-red); Scale bar, 50 µm. (E) Confocal z-stack rendering of single and grouped cancer cell nuclei (Hoechst 33342-blue). Scale bars: main panels, 30 µm; enlarged inserts, 10 µm. (**F**) Cancer cell nuclei versus cell volume quantification for PC3 cells. Cancer cell volume (average vol/nuclei for PC3 cells = 14825.26 μm^3 (range = 5206-31200), for MDA-MB-231 cells= 8495.667 μm^3 (range = 5337-11850). (**G**) Number of MDA-MB-231 cancer cell groups per lung (*n*=5, 5 mouse left lungs) and (**H**) Number of MDA-MB-231 cancer cells per group per lung (*n*=5, 5 mice). (**I**) Number of cell protrusions per MDA-MB-231 cancer cell per lung (*n*=5, 5 mice) and (**J)** Percentage of MDA-MB-231 cancer cell surface directly interacting with vasculature surface (*n*=5, 5 mice; 65 and 67 cells). (**K**) Confocal z-stack Imaris rendering of MDA-MB-231 cancer cells (cyan) in the lung vasculature (CD31-PE, red); Scale bar, 10 µm. (**L**) Confocal z-stack Imaris rendering of CMFDA-green PC3 cells grouped (TOP) or single (MIDDLE) and MDA-MB-231 cells (BOTTOM) in the lung vasculature (CD31-PE, red), showing in the portion of cancer cell interacting (blue) with the vasculature inner surface, and cross-sections of cancer cell/vasculature interaction (TOP and MIDDLE right). Scale bars: 30 µm, enlargement (TOP) 25 µm, enlargement (MIDDLE) and cross-sections, 10 µm. (**M**) Quantification of single cancer cell shape in the lung vasculature using confocal z-stacks at high magnification (x63, x100): PC3 cells (*n*=6, 6 mice; 152 and 266 single cells), MDA-MB-231 cells (*n*=5, 5 mice; 303 and 227 single cells). (**N**) Quantification of single cancer cell volume in the lung vasculature using confocal z-stacks (x20); PC3 cells (*n*=6, 6 mice; 173 and 236 single cells), MDA-MB-231 cells (*n*=5, 5 mice; 295 and 224 single cells). (**O**) Representative images of perfused and fixed lungs isolated 6 weeks after tail vein injection with control- or β1-integrin-depleted PC3 cells. Data are mean ± s.e.m. Statistical analysis of biological replicates by two-tailed paired *t-test* (**A** to **C**)**,** unpaired Mann-Whitney test (**G** to **I**), One-way ANOVA with Tukey`s multiple comparison test (**J, O**).

Figure S1

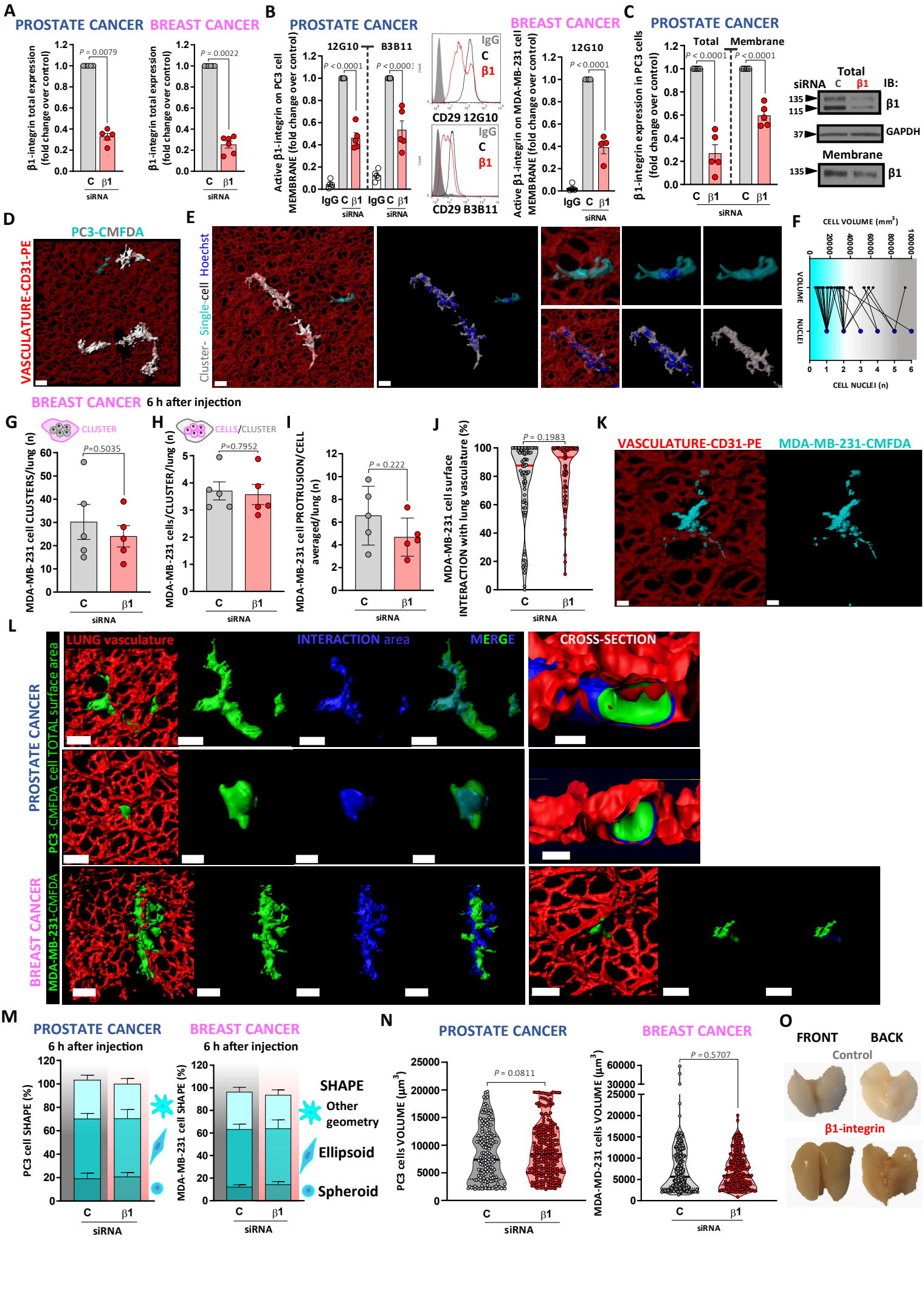
A
PROSTATE CANCER
BREAST CANCER
β1-integrin total expression (fold change over control)
P = 0.0079
P = 0.0022
C β1
siRNA
B
PROSTATE CANCER
Active β1-integrin on PC3 cell MEMBRANE (fold change over control)
12G10
B3B11
P < 0.0001
IgG C β1
siRNA
IgG
C
β1
CD29 12G10
CD29 B3B11
BREAST CANCER
Active β1-integrin on MDA-MB-231 cell MEMBRANE (fold change over control)
C
PROSTATE CANCER
β1-integrin expression in PC3 cells (fold change over control)
Total
Membrane
P < 0.0001
siRNA C β1 IB:
135
115
β1
37
GAPDH
Membrane
D
PC3-CMFDA
VASCULATURE-CD31-PE
E
Cluster- Single-cell Hoechst
F
CELL VOLUME (mm3)
VOLUME
NUCLEI
CELL NUCLEI (n)
BREAST CANCER 6 h after injection
G
CLUSTER
MDA-MB-231 cell CLUSTERS/lung (n)
P=0.5035
H
CELLS/CLUSTER
MDA-MB-231 cells/CLUSTER/lung (n)
P=0.7952
I
MDA-MB-231 cell PROTRUSION/CELL averaged/lung (n)
P = 0.222
J
MDA-MB-231 cell surface INTERACTION with lung vasculature (%)
P = 0.1983
K
VASCULATURE-CD31-PE
MDA-MB-231-CMFDA
L
LUNG vasculature
INTERACTION area
MERGE
CROSS-SECTION
PROSTATE CANCER
PC3-CMFDA cell TOTAL surface area
BREAST CANCER
MDA-MB-231-CMFDA
M
PROSTATE CANCER
6 h after injection
BREAST CANCER
6 h after injection
PC3 cell SHAPE (%)
MDA-MB-231 cell SHAPE (%)
SHAPE
Other geometry
Ellipsoid
Spheroid
N
PROSTATE CANCER
BREAST CANCER
PC3 cells VOLUME (μm3)
MDA-MD-231 cells VOLUME (μm3)
P = 0.0811
P = 0.5707
O
FRONT
BACK
Control
β1-integrin

Fig. S2. β1-integrin contributes to shear-stress resistant cancer cell adhesion to endothelial cells *in vitro.*

(A) Flow cytometry gating strategy. **(B** and **C)** β1-integrin blocking antibody reduces Jurkat T cell firm adhesion to hCMEC/D3 cells. Jurkat T cells were fluorescently labelled, incubated with blocking β1-integrin antibody, vehicle (control) or IgG for 20 min. hCMEC/D3 monolayers were exposed to $1.5x10^6$ Jurkat T cells/ml at 0.5 dyn/cm^2 for 5 min followed by 1 dyn/cm^2 for 30 sec. (**B**) Representative images of firmly adherent Jurkat T cells treated with β1-integrin blocking antibody versus control and (**C**) quantification (*n*=3), ANOVA. (**D**) β1-integrin siRNA nucleofection efficiency determined by western blotting in PC3 cells used for adhesion flow assay. (**E**) Representative flow cytometry histograms for CD49d (α4 integrin, α-chain of VLA-4) expression in PC3, MDA-MB-231 and Jurkat T cells. (**F**) Representative confocal fluorescence images of human ECs cultured on collagen (nuclei, DAPI-blue and F-actin, phalloidin-red), HUVEC (TOP) and hCMEC/D3 cells (BOTTOM), showing secretion of extracellular matrix components, fibronectin (green) and laminin (green). Scale bar, 50 μm.

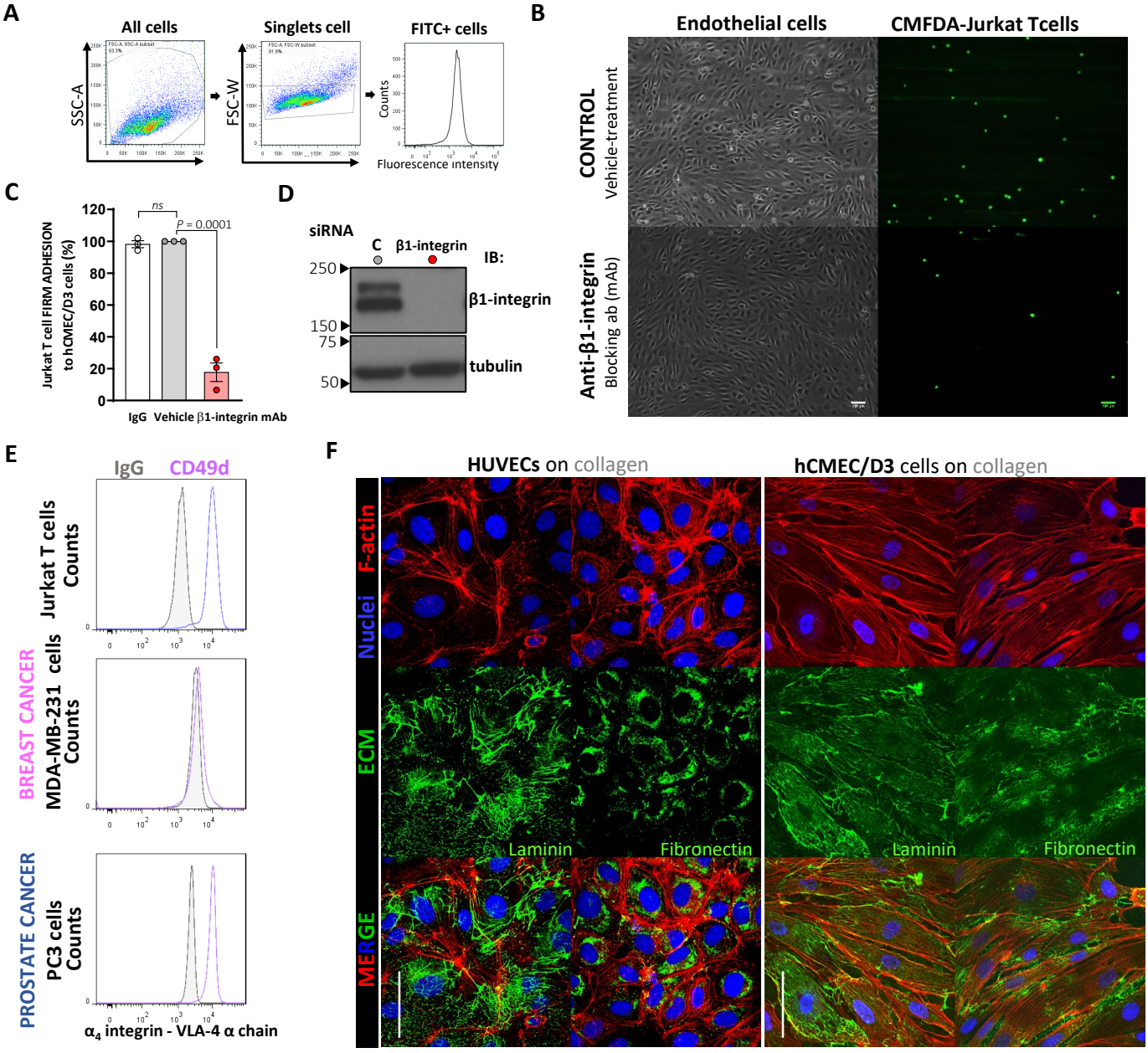
A
All cells
Singlets cell
FITC+ cells
SSC-A
FSC-W
Counts
Fluorescence intensity
B
Endothelial cells
CMFDA-Jurkat Tcells
CONTROL
Vehicle-treatment
Anti-β1-integrin
Blocking ab (mAb)
C
Jurkat T cell FIRM ADHESION to hCMEC/D3 cells (%)
ns
P = 0.0001
IgG
Vehicle
β1-integrin mAb
D
siRNA
C
β1-integrin
IB:
250
150
75
50
β1-integrin
tubulin
E
IgG
CD49d
Jurkat T cells Counts
BREAST CANCER
MDA-MB-231 cells Counts
PROSTATE CANCER
PC3 cells Counts
α4 integrin - VLA-4 α chain
F
HUVECs on collagen
hCMEC/D3 cells on collagen
F-actin
Nuclei
ECM
Laminin
Fibronectin
MERGE

Fig. S3. Cdc42 targets IQGAP1 and NWASP contribute to cancer adhesion retention and metastatic nodule formation *in vivo*.

(**A** to **E**) Representative immunoblots of PC3 cells transfected with the indicated siRNAs to quantify for β1-integrin protein levels. (**F** to **H**) Time course of PC3 cells transfected with IQGAP1, IQGAP3 or control siRNAs. (**F**) Representative immunoblot, (**G**) Quantification of IQGAP3 and (**H**) Quantification of total β1-integrin. (**I**) Representative biotinylation assay immunoblots for (top) total and (bottom) membrane levels of β1-integrin in PC3 cells transfected with the indicated siRNAs. (**J** to **L**). PC3 cells transfected with a combination of NWASP and IQGAP1 siRNAs. (**J**) Quantification of IQGAP-1 and NWASP expression and (**K)** total active β1-integrin from western blots. (**L**) Active β1-integrin expression at the cell surface; (left) quantification and (right) representative flow cytometry histograms. Representative immunoblots of (**M**) PC3 and (**N**) MDAMB231 cells transfected with the indicated siRNAs probed for NWASP and IQGAP1 expression used to quantify β1-integrin alpha chains partners. Quantification of α1/CD49a, α2/CD49b α3/CD49c, α4/CD49d, α5/CD49e, α6/CD49f membrane expression by FACS in (**O**) PC3 and (**P**) MDAMB231 cells. Mean ± s.e.m.; n=3 or 4, one-way ANOVA.

Figure S3

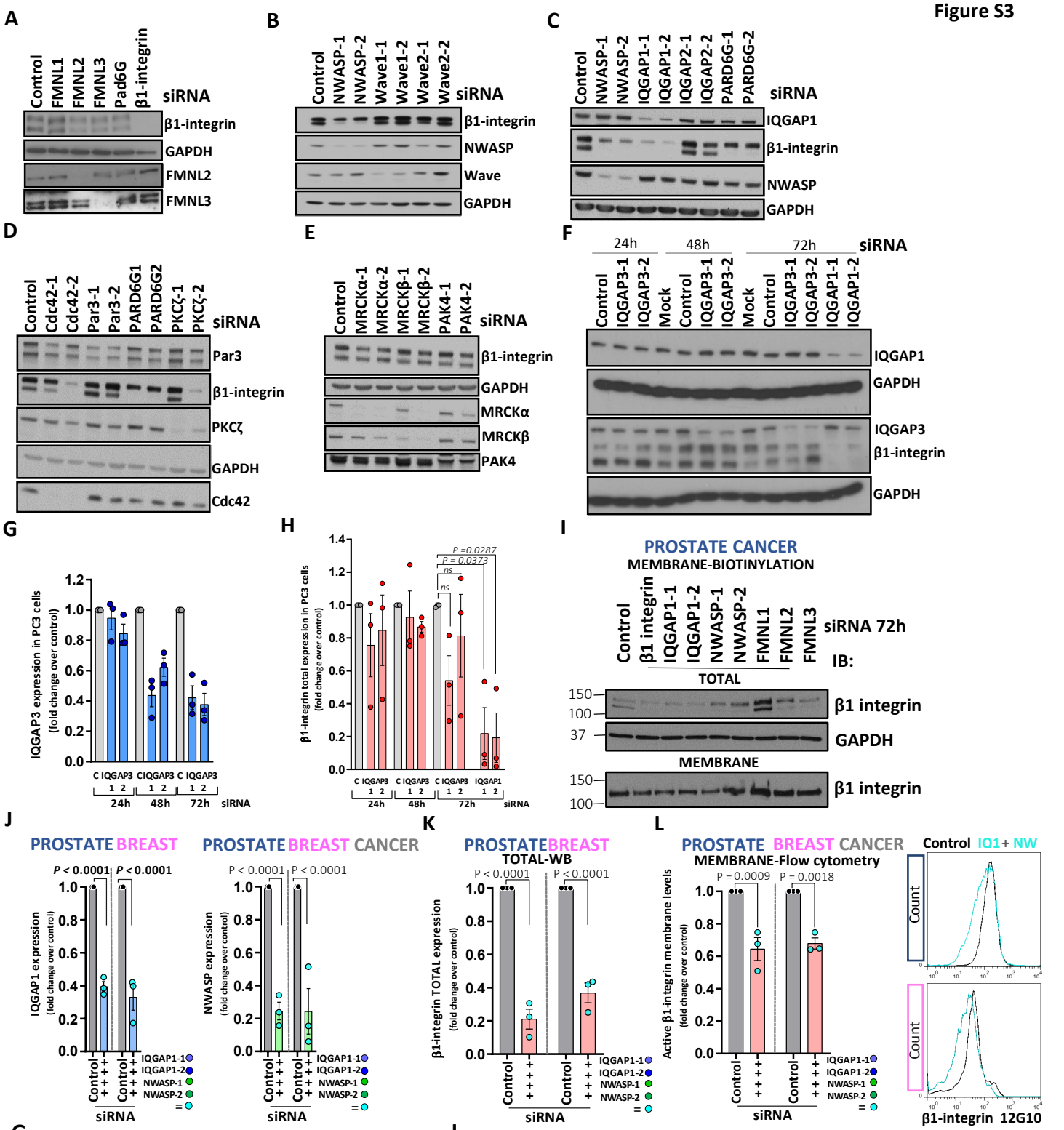
A
Control
FMNL1
FMNL2
FMNL3
Pad6G
β1-integrin
siRNA
β1-integrin
GAPDH
FMNL2
FMNL3
B
Control
NWASP-1
NWASP-2
Wave1-1
Wave1-2
Wave2-1
Wave2-2
siRNA
β1-integrin
NWASP
Wave
GAPDH
C
Control
NWASP-1
NWASP-2
IQGAP1-1
IQGAP1-2
IQGAP2-1
IQGAP2-2
PARD6G-1
PARD6G-2
siRNA
IQGAP1
β1-integrin
NWASP
GAPDH
D
Control
Cdc42-1
Cdc42-2
Par3-1
Par3-2
PARD6G1
PARD6G2
PKCζ-1
PKCζ-2
siRNA
Par3
β1-integrin
PKCζ
GAPDH
Cdc42
E
Control
MRCKα-1
MRCKα-2
MRCKβ-1
MRCKβ-2
PAK4-1
PAK4-2
siRNA
β1-integrin
GAPDH
MRCKα
MRCKβ
PAK4
F
24h
48h
72h
siRNA
Control
IQGAP3-1
IQGAP3-2
Mock
Control
IQGAP3-1
IQGAP3-2
Mock
Control
IQGAP3-1
IQGAP3-2
IQGAP1-1
IQGAP1-2
IQGAP1
GAPDH
IQGAP3
β1-integrin
GAPDH
G
IQGAP3 expression in PC3 cells
(fold change over control)
1.2
1.0
0.8
0.6
0.4
0.2
0.0
C IQGAP3 C IQGAP3 C IQGAP3
1 2 1 2 1 2
24h 48h 72h siRNA
H
β1-integrin total expression in PC3 cells
(fold change over control)
P =0.0287
P = 0.0373
ns
ns
1.4
1.2
1.0
0.8
0.6
0.4
0.2
0.0
C IQGAP3 C IQGAP3 C IQGAP3 IQGAP1
1 2 1 2 1 2 1 2
24h 48h 72h siRNA
I
PROSTATE CANCER
MEMBRANE-BIOTINYLATION
Control
β1 integrin
IQGAP1-1
IQGAP1-2
NWASP-1
NWASP-2
FMNL1
FMNL2
FMNL3
siRNA 72h
IB:
TOTAL
150
100
37
β1 integrin
GAPDH
MEMBRANE
150
100
β1 integrin
J
PROSTATE BREAST
PROSTATE BREAST CANCER
IQGAP1 expression
(fold change over control)
P < 0.0001
P < 0.0001
P < 0.0001
P < 0.0001
1.0
0.8
0.6
0.4
0.2
0.0
Control
Control
IQGAP1-1
IQGAP1-2
NWASP-1
NWASP-2
siRNA
NWASP expression
(fold change over control)
K
PROSTATE BREAST
TOTAL-WB
β1-integrin TOTAL expression
(fold change over control)
P < 0.0001
P < 0.0001
L
PROSTATE BREAST CANCER
MEMBRANE-Flow cytometry
Active β1-integrin membrane levels
(fold change over control)
P = 0.0009
P = 0.0018
Control IQ1+ NW
Count
Count
β1-integrin 12G10
G
PROSTATE CANCER
Control
Control
IQGAP1-1
IQGAP1-2
NWASP-1
NWASP-2
siRNA 72h
IB:
250
75
37
IQGAP1
NWASP
GAPDH
H
α integrin membrane expression in PC3 cells
(fold change over control)
14
7
2.0
1.5
1.0
0.5
0.0
IgG
Control
IQGAP1-1
IQGAP1-2
NWASP-1
NWASP-2
α1-CD49a
α2-CD49b
α3-CD49c
α4-CD49d
α5-CD49e
α6-CD49f
I
BREAST CANCER
Control
Control
IQGAP1-1
IQGAP1-2
NWASP-1
NWASP-2
siRNA 72h
IB:
250
75
37
IQGAP1
NWASP
GAPDH
J
α integrin membrane expression in MDA-MB-231 cells
(fold change over control)
3.0
2.5
2.0
1.5
1.0
0.5
0.0
IgG
Control
IQGAP1-1
IQGAP1-2
NWASP-1
NWASP-2
α1-CD49a
α2-CD49b
α3-CD49c
α4-CD49d
α5-CD49e
α6-CD49f

Fig. S4. IQGAP1 and NWASP contribute to cancer cell adhesion to endothelial cells, retention in the vasculature and metastatic nodule formation.

(A) A Representative immunoblot of lysates from PC3 prostate cancer cells transfected by nucleofection with the indicated siRNAs, analyzed after 72 h. (**B**) Quantification in percentage of IQGAP1- and NWASP-depleted PC3 cell shear-stress resistant adhesion to human brain ECs (hCMEC/D3). PC3 cells were fluorescently labelled, harvested and transfected with either IQGAP1, NWASP or control siRNA. hCMEC/D3 monolayers were exposed to $2x10^6$ PC3 cells/ml at 0.1 dyn/cm^2 for 5 min followed by 1 dyn/cm^2 for 30 sec. Data are mean ±s.e.m. (*n*=3), One-way ANOVA. (**C**) Quantification and representative immunoblots of IQGAP1 expression in lysates of PC3 (*n*=5) and MDA-MB-231 (*n*=3) cells transfected with control or IQGAP1-1 siRNAs, analyzed after 72 h. Two-tailed unpaired *t-test.* (**D**) Immunoblots of NWASP expression in PC3 cells transfected with control or NWASP-2 siRNAs, analyzed after 72 h. *n*=3; bands shown are from the same blot. **(E**) Number of siRNA-transfected PC3 cells disseminated in the mouse lung (left lobe) vasculature. *n*=3, two-tailed unpaired *t-test.* **(F**) Confocal z-stack rendering of CMFDA-labelled PC3 cells (green) in the lung vasculature (CD31-PE, red), interacting with ECs (blue). Scale bars, 30 µm. (**G-Q**) PC3 transfected with IQGAP1-1 siRNA. (**G**) Quantification of grouped in cluster and single PC3 cells in the left lung vasculature, control, *n*=384 cells from 4 mice; IQGAP1, *n*=684 cells, 6 mice. (**H)** Number of groups per lung and (**I)** number of cells per group, mean per lung (control n=4, IQGAP1 n=5). (**J**) Volume and (**K**) shape of PC3 cells retained in the lung vasculature (control n=4 lungs, 108 cells, IQGAP1 n=5 lungs, 277 cells). (**L**) Quantification of grouped and single MDA-MB-231 cells in the lung vasculature. (**M)** Number of groups per lung and (**N)** number of cells per group, mean per lung (control n=4, IQGAP1 n=5). (**O**) Volume and (**P**) shape of MDA-MB-231 cells in the lung vasculature (control n=4 lungs, 108 cells, IQGAP1 n=5 lungs, 277 cells). (**Q**) Representative pictures of isolated, perfused and fixed lungs prior to embedding for MRI scan. (**R**) IQGAP1 and NWASP protein expression-based Kaplan-Meier survival analysis plots from the public database dataset (www.kmplot.com). Survival over time (150 months, 12.5 years) of the patients with high (red), and low (black) protein expression (n=65), HR represent the magnitude of the difference between the two curves in the Kaplan–Meier plot, logrank test between the distribution over time of the high and low protein expression patient groups was used and is expressed in p-value, where $p<0.05$ is considered significant. Graphs (**B-P**), mean ± s.e.m.

Figure S4

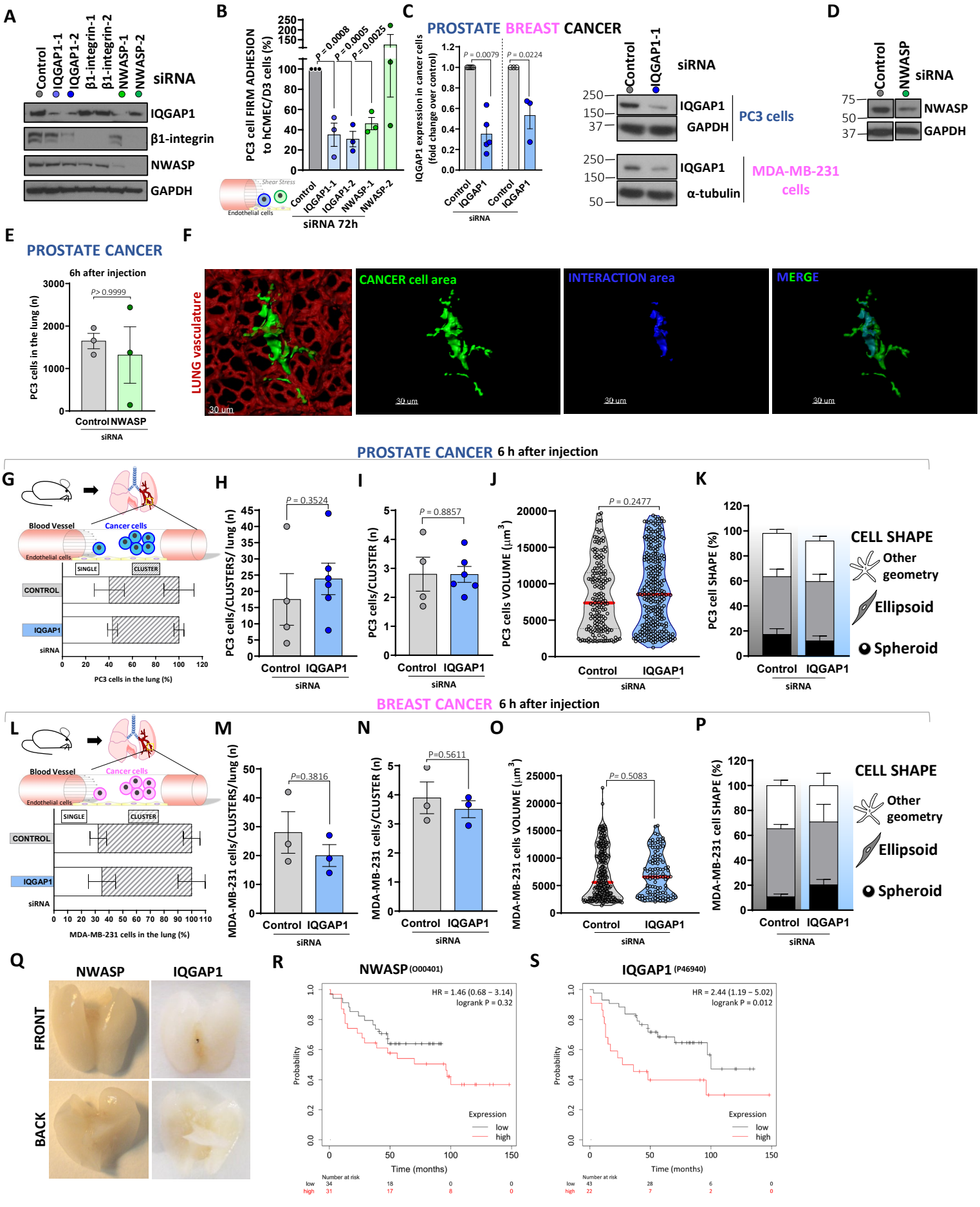
A
Control
IQGAP1-1
IQGAP1-2
β1-integrin-1
β1-integrin-2
NWASP-1
NWASP-2
siRNA
IQGAP1
β1-integrin
NWASP
GAPDH
B
PC3 cell FIRM ADHESION to hCMEC/D3 cells (%)
P = 0.0008
P = 0.0005
P = 0.0025
Shear Stress
Endothelial cells
Control
IQGAP1-1
IQGAP1-2
NWASP-1
NWASP-2
siRNA 72h
C
PROSTATE BREAST CANCER
IQGAP1 expression in cancer cells (fold change over control)
P = 0.0079
P = 0.0224
Control
IQGAP1
siRNA
Control
IQGAP1-1
siRNA
IQGAP1
GAPDH
PC3 cells
IQGAP1
α-tubulin
MDA-MB-231 cells
D
Control
NWASP
siRNA
NWASP
GAPDH
E
PROSTATE CANCER
6h after injection
PC3 cells in the lung (n)
P> 0.9999
Control NWASP
siRNA
F
LUNG vasculature
CANCER cell area
INTERACTION area
MERGE
30 um
PROSTATE CANCER 6 h after injection
G
Blood Vessel
Cancer cells
Endothelial cells
SINGLE
CLUSTER
CONTROL
IQGAP1
siRNA
PC3 cells in the lung (%)
H
PC3 cells/CLUSTERS/ lung (n)
P = 0.3524
Control IQGAP1
siRNA
I
PC3 cells/CLUSTER (n)
P = 0.8857
Control IQGAP1
siRNA
J
PC3 cells VOLUME (μm3)
P = 0.2477
Control IQGAP1
siRNA
K
PC3 cell SHAPE (%)
CELL SHAPE
Other geometry
Ellipsoid
Spheroid
Control IQGAP1
siRNA
BREAST CANCER 6 h after injection
L
Blood Vessel
Cancer cells
Endothelial cells
SINGLE
CLUSTER
CONTROL
IQGAP1
siRNA
MDA-MB-231 cells in the lung (%)
M
MDA-MB-231 cells/CLUSTERS/lung (n)
P=0.3816
Control IQGAP1
siRNA
N
MDA-MB-231 cells/CLUSTER (n)
P=0.5611
Control IQGAP1
siRNA
O
MDA-MB-231 cells VOLUME (μm3)
P= 0.5083
Control IQGAP1
siRNA
P
MDA-MB-231 cell SHAPE (%)
CELL SHAPE
Other geometry
Ellipsoid
Spheroid
Control IQGAP1
siRNA
Q
NWASP
IQGAP1
FRONT
BACK
R
NWASP (O00401)
HR = 1.46 (0.68 – 3.14)
logrank P = 0.32
Probability
Expression
low
high
Time (months)
Number at risk
low 34 18 0 0
high 31 17 8 0
S
IQGAP1 (P46940)
HR = 2.44 (1.19 – 5.02)
logrank P = 0.012
Probability
Expression
low
high
Time (months)
Number at risk
low 43 28 6 0
high 22 7 2 0

Fig. S5. IQGAP1 and NWASP regulate β1-integrin via both FAK/ERK signaling and transcription by SRF/MRTF.

(A) MDA-MB-231 cell lysates were immunoprecipitated with the indicated antibodies followed by immunoblotting for IQGAP1 and β1-integrin. (**B**) PC3 cell lysates were immunoprecipitated with the indicated antibodies followed by immunoblotting for IQGAP1 and paxillin. (**C**) Flow cytometry gating strategy. (**D**) Representative flow cytometry histogram of active β1-integrin levels on PC3 cells treated with vehicle or 3 μM FAKi (AZ13256675) for 30 min. MDAMB231 cells were treated with either vehicle or FAK inhibitor (FAKi) 4548 for 30 min at the indicated concentrations. (**E**) Quantification of β1-integrin expression and (**F**) p-FAK (Tyr397). Mean ± s.e.m.; n=3 independent experiments, one-way ANOVA test. (**G**) Quantification of shear-stress resistant adhesion of vehicle or FAKi (3 μM) treated MDAMB231 cells to human brain ECs (hCMEC/D3). MDAMB231 cells were fluorescently CMFDA-labelled and treated with FAKi for 30 min. hCMEC/D3 monolayers were exposed to 2x106 MDAMB231 cells/ml at 0.1dyn/cm2 for 5 min followed by 1 dyn/cm2 872 for 30 sec. Data are mean ±s.e.m. (n=3) with 10-15 technical each, two-tailed unpaired t-test. (**H**, **I)** PC3 cells were transfected with the indicated siRNAs and analyzed 72 h later. Quantification of (**H**) β1-integrin and (**I**) paxillin by immunoblotting. Data are mean ± s.e.m. (*n*=3), one-way ANOVA test. (**J**) PC3 cells were transfected with either control siRNA or with the indicated siRNAs. Quantification of relative mRNA levels by qRT-PCR of IQGAP1 and NWASP. Mean ± s.e.m. (*n*=5), one-way ANOVA. (**K**) Representative immunoblots from total cell lysates of PC3 cells transfected with indicated siRNAs and probed for SRF levels. (**L**) PC3 cells were treated with either vehicle, MRTF inhibitor-1 (CCG-1423) or MRTF inhibitor-2 (CCG-203971) at 20 μM for 24 or 48 h. Quantification of total NWASP protein expression in cell lysates. Mean ± s.e.m. (*n*=3), one-way ANOVA.

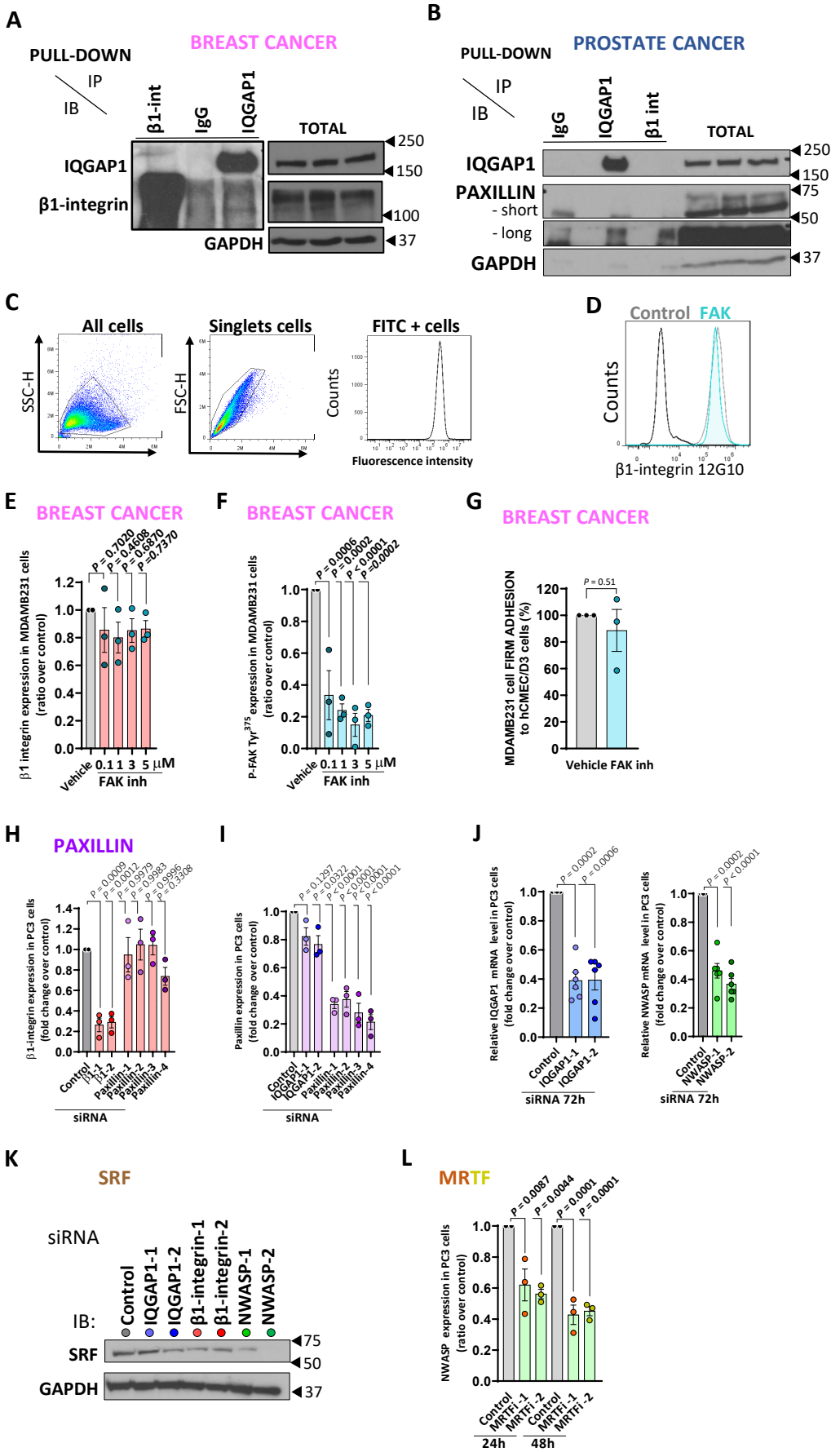
A
BREAST CANCER
PULL-DOWN
IP
IB
β1-int
IgG
IQGAP1
TOTAL
IQGAP1
β1-integrin
GAPDH
250
150
100
37
B
PROSTATE CANCER
PULL-DOWN
IP
IB
IgG
IQGAP1
β1 int
TOTAL
IQGAP1
PAXILLIN
- short
- long
GAPDH
250
150
75
50
37
C
All cells
Singlets cells
FITC + cells
SSC-H
FSC-H
Counts
Fluorescence intensity
D
Control FAK
Counts
β1-integrin 12G10
E
BREAST CANCER
β1 integrin expression in MDAMB231 cells (ratio over control)
P = 0.7020
P = 0.4608
P = 0.6870
P =0.7370
Vehicle
0.1
1
3
5 μM
FAK inh
F
BREAST CANCER
P-FAK Tyr397 expression in MDAMB231 cells (ratio over control)
P = 0.0006
P = 0.0002
P < 0.0001
P =0.0002
Vehicle
0.1
1
3
5 μM
FAK inh
G
BREAST CANCER
MDAMB231 cell FIRM ADHESION to hCMEC/D3 cells (%)
P = 0.51
Vehicle
FAK inh
H
PAXILLIN
β1-integrin expression in PC3 cells (fold change over control)
P = 0.0009
P = 0.0012
P = 0.9979
P = 0.9983
P = 0.9996
P = 0.3308
Control
β1-1
β1-2
Paxillin-1
Paxillin-2
Paxillin-3
Paxillin-4
siRNA
I
Paxillin expression in PC3 cells (fold change over control)
P = 0.1297
P = 0.0322
P < 0.0001
P < 0.0001
P < 0.0001
P < 0.0001
Control
IQGAP1-1
IQGAP1-2
Paxillin-1
Paxillin-2
Paxillin-3
Paxillin-4
siRNA
J
Relative IQGAP1 mRNA level in PC3 cells (fold change over control)
P = 0.0002
P = 0.0006
Control
IQGAP1-1
IQGAP1-2
siRNA 72h
Relative NWASP mRNA level in PC3 cells (fold change over control)
P = 0.0002
P < 0.0001
Control
NWASP-1
NWASP-2
siRNA 72h
K
SRF
siRNA
Control
IQGAP1-1
IQGAP1-2
β1-integrin-1
β1-integrin-2
NWASP-1
NWASP-2
IB:
SRF
GAPDH
75
50
37
L
MRTF
NWASP expression in PC3 cells (ratio over control)
P = 0.0087
P = 0.0044
P = 0.0001
P = 0.0001
Control
MRTFi-1
MRTFi-2
Control
MRTFi-1
MRTFi-2
24h
48h

Uncropped left lobe lung tilescans (1x) from ZEN (Zeiss) saved in TIF

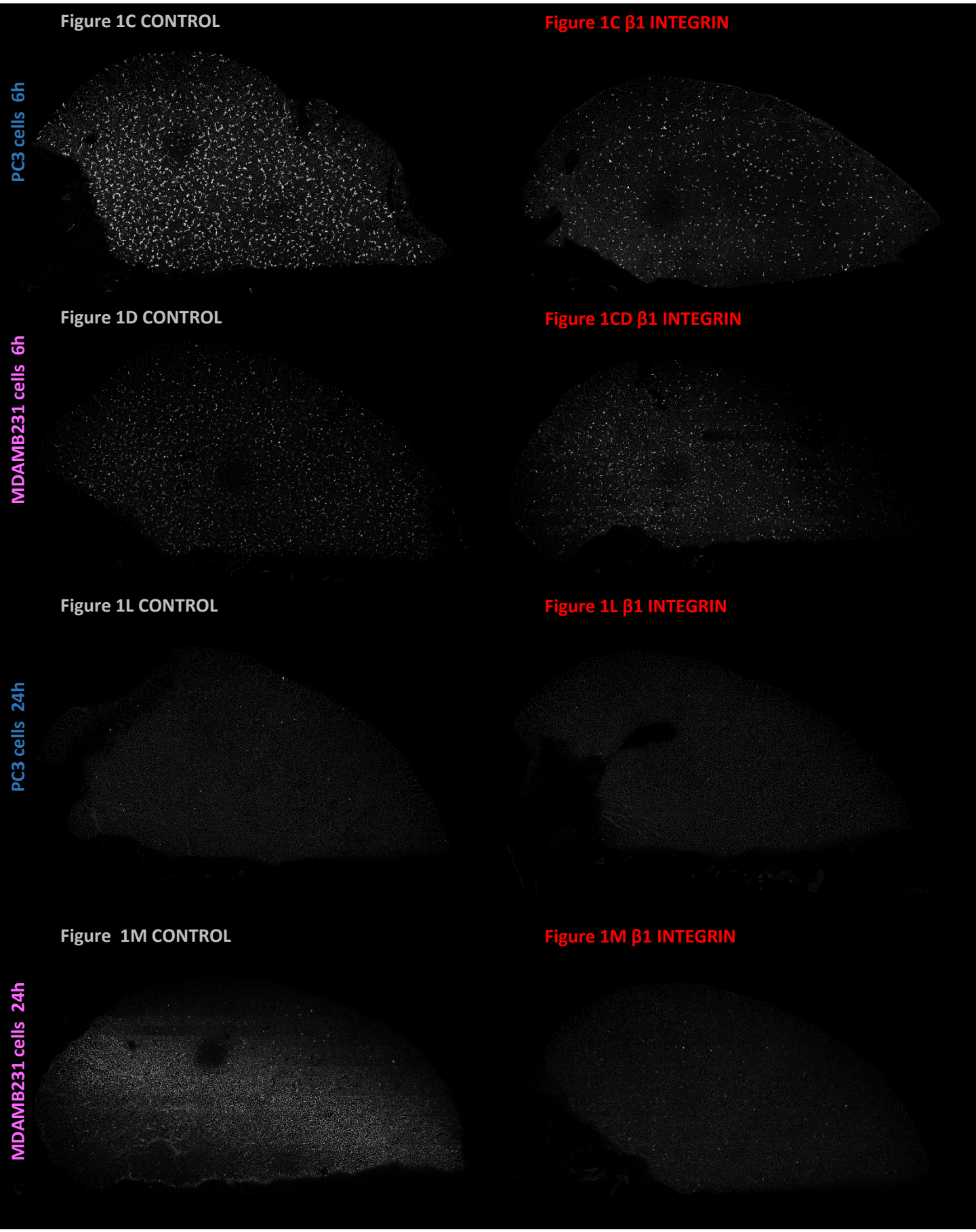

Figure S1 C (short)

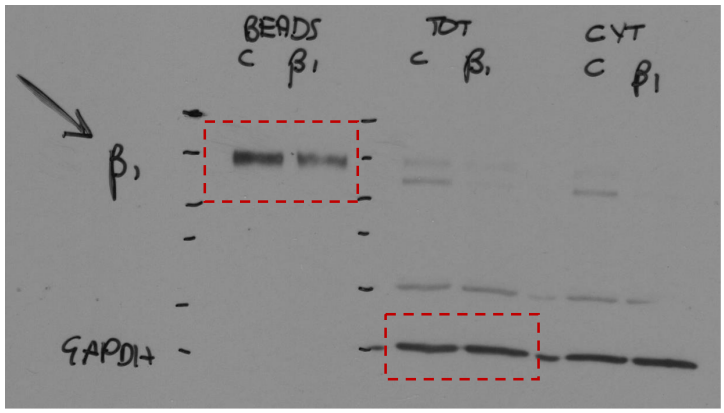

Figure S1 C (long)

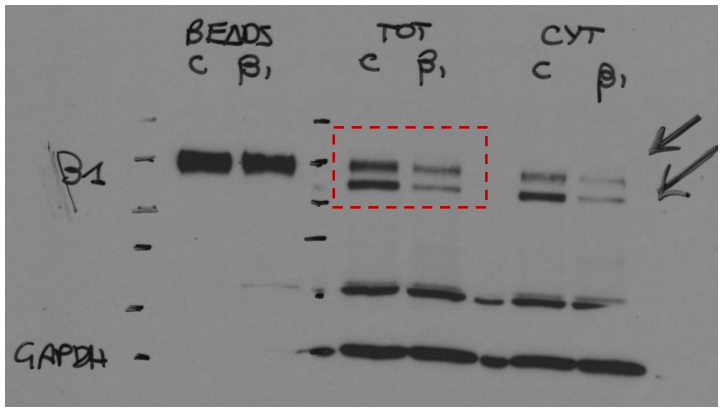

Figure S1 O

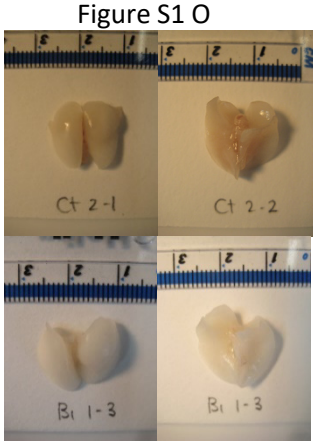

Figure S2 D (long)

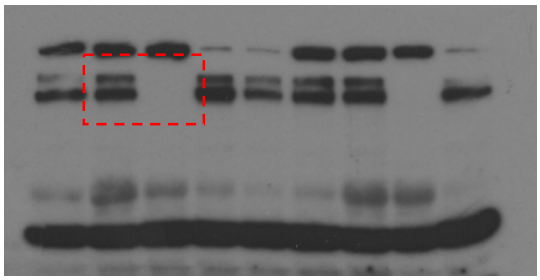

Figure S2 D (short)

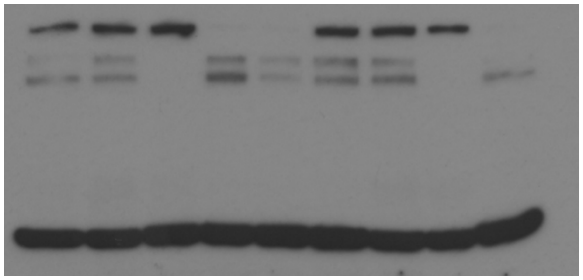

Figure S2 D

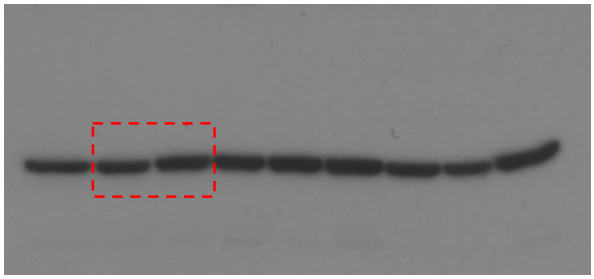

Figure 3 D (short)

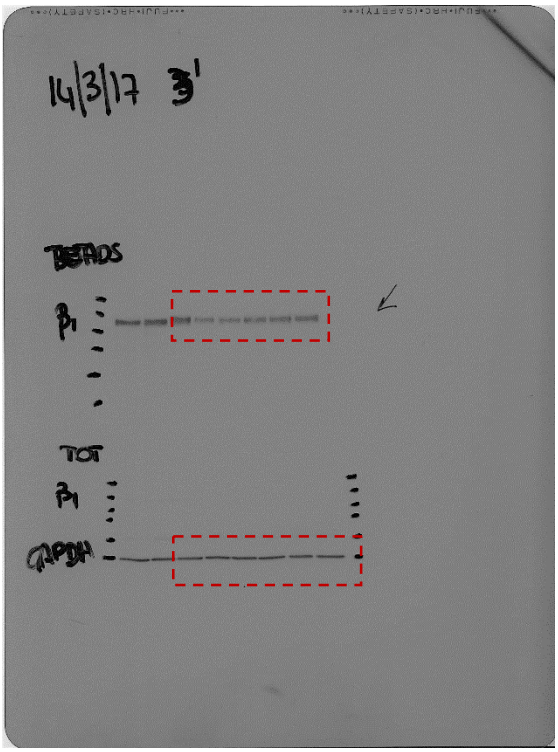

Figure 3 D (LONG)

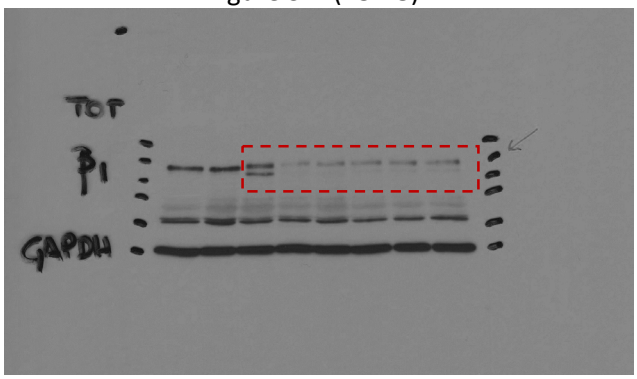

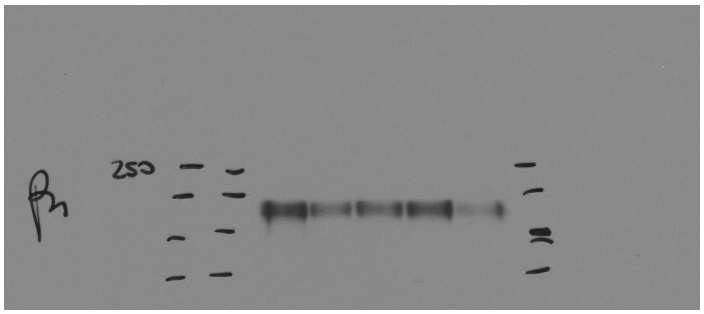

Figure 3 F

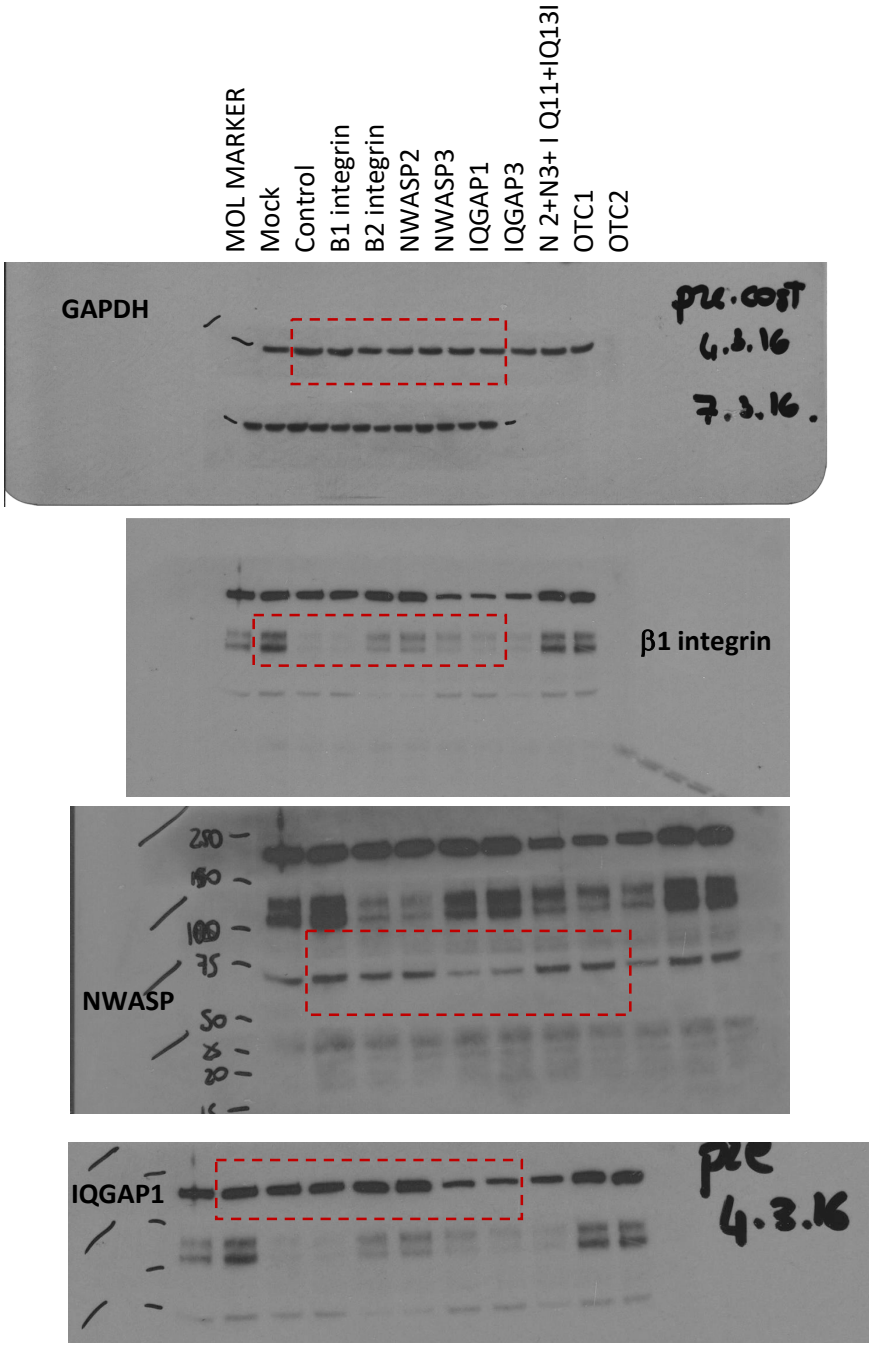
MOL MARKER
Mock
Control
B1 integrin
B2 integrin
NWASP2
NWASP3
IQGAP1
IQGAP3
N 2+N3+ I Q11+IQ13I
OTC1
OTC2
GAPDH
β1 integrin
NWASP
IQGAP1

Figure 3 H

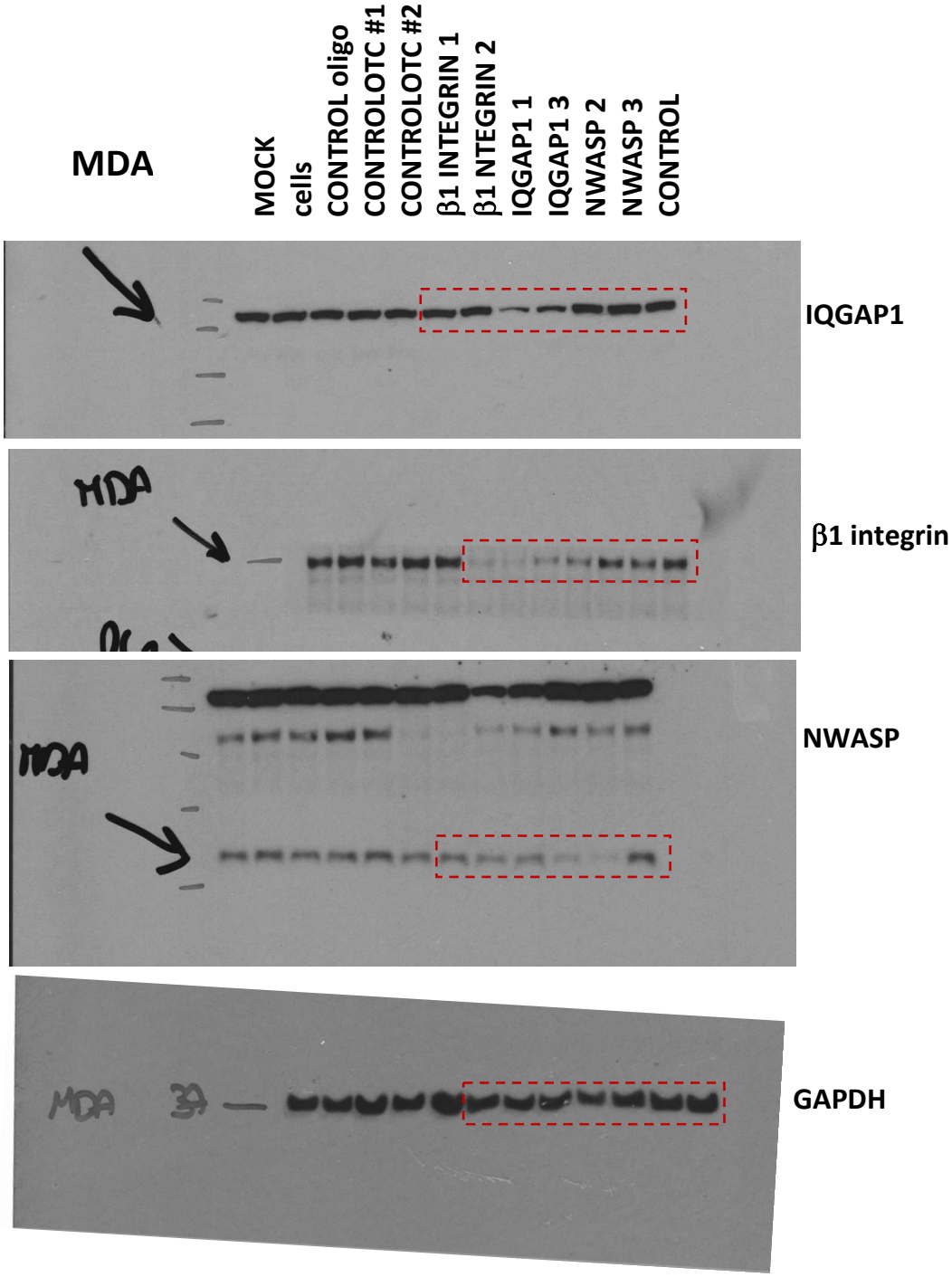
MDA
MOCK
cells
CONTROL oligo
CONTROLOTC #1
CONTROLOTC #2
β1 INTEGRIN 1
β1 NTEGRIN 2
IQGAP1 1
IQGAP1 3
NWASP 2
NWASP 3
CONTROL
IQGAP1
β1 integrin
NWASP
GAPDH

Figure S3 A

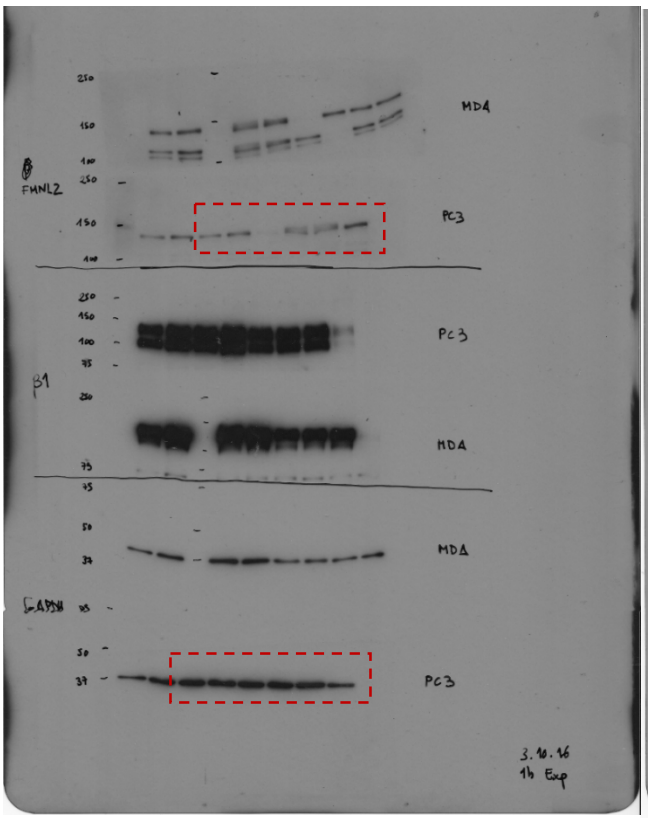

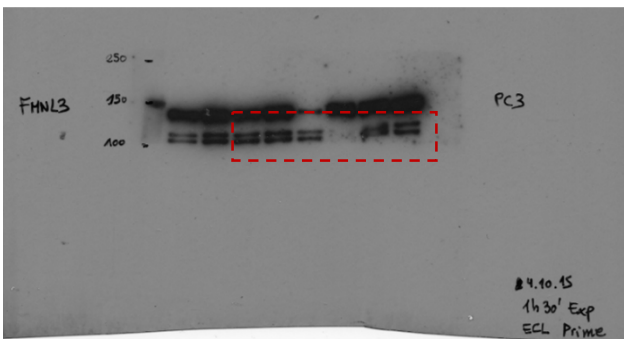

Figure S3 A

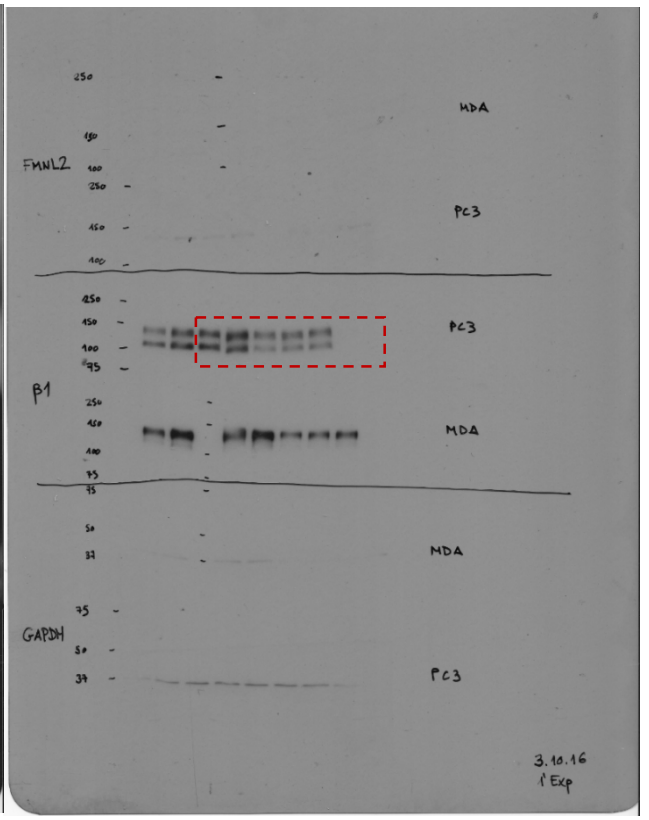

Figure S3 C-E

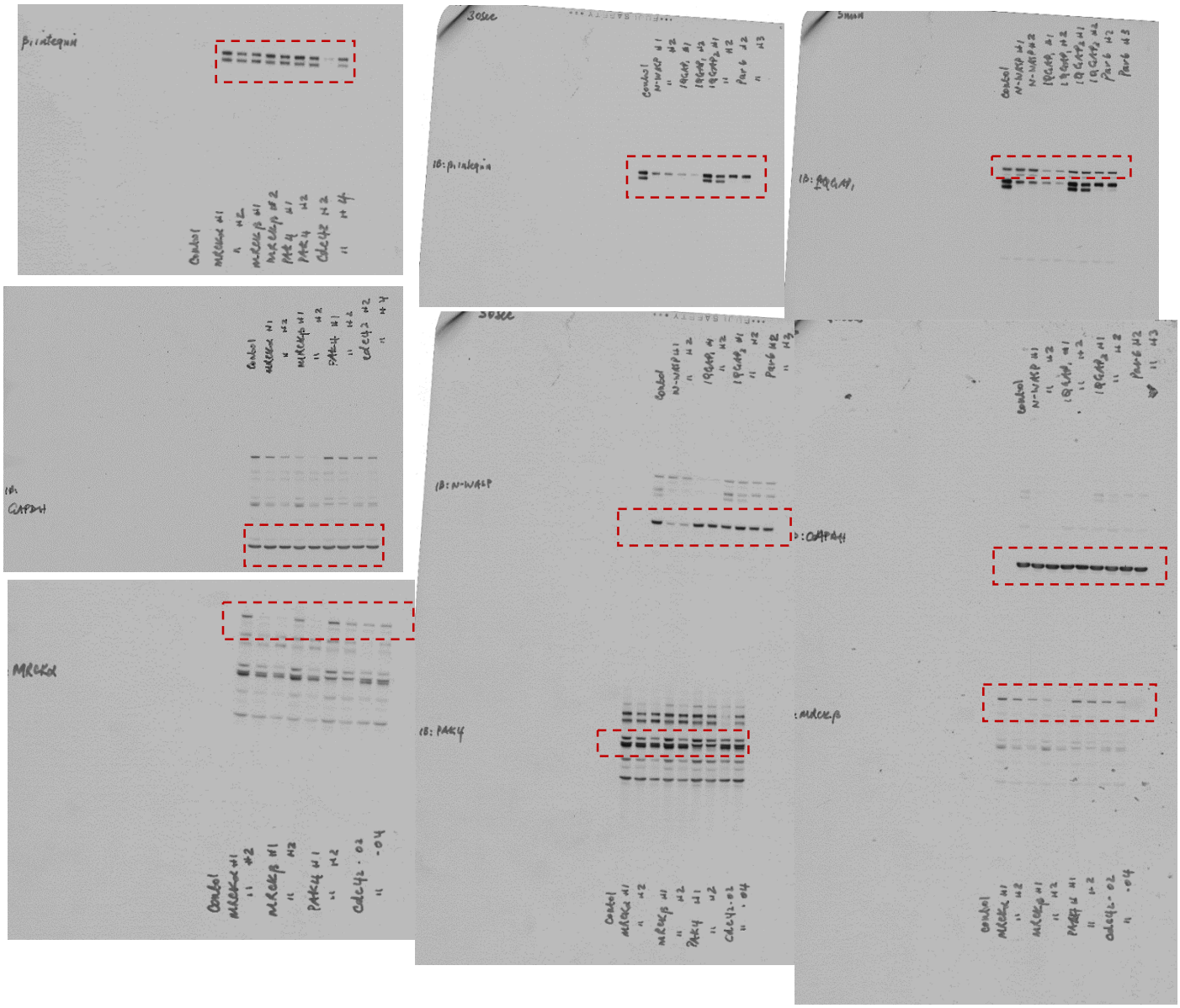
β1integrin
IB: β1integrin
IB: N-WASP
IB: PAK4
IB: GAPDH
IB: MRCKα
IB: MRCKβ
Control
MRCKα #1
MRCKβ #1
MRCKβ #2
PAK4 #1
PAK4 #2
Cdc42 #2
Par6 #2
Par6 #3

Supplementary information-Data file uncropped

Figure S3 D

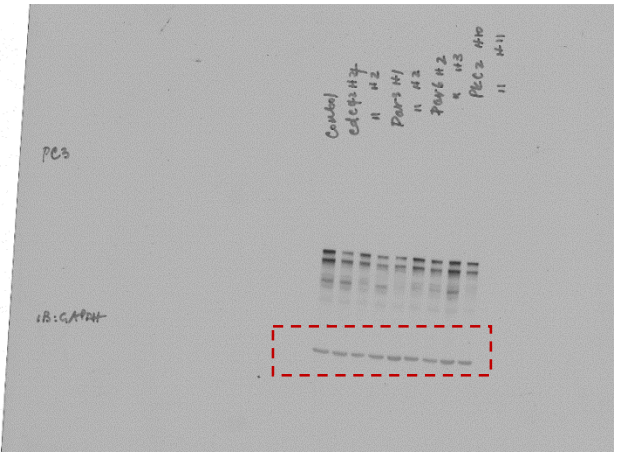

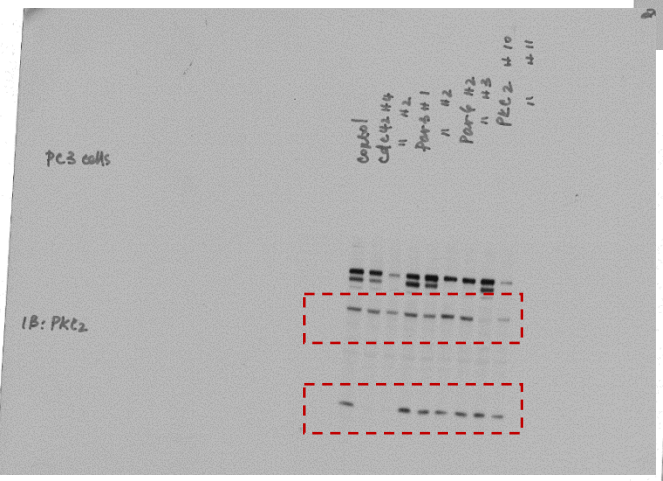

Figure S3 D

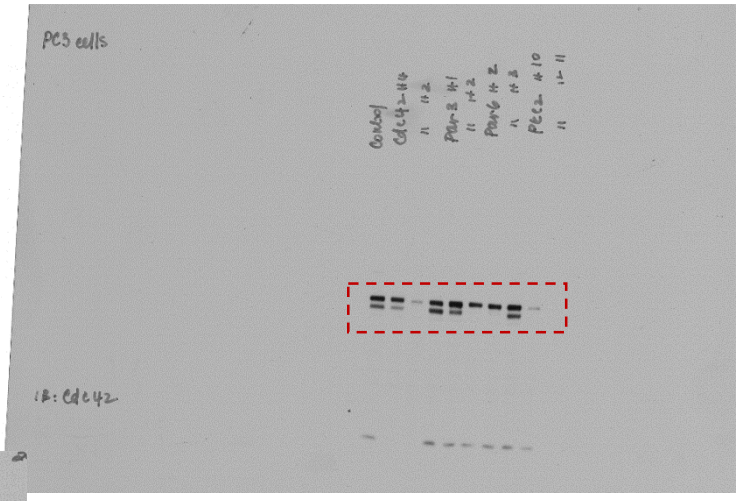

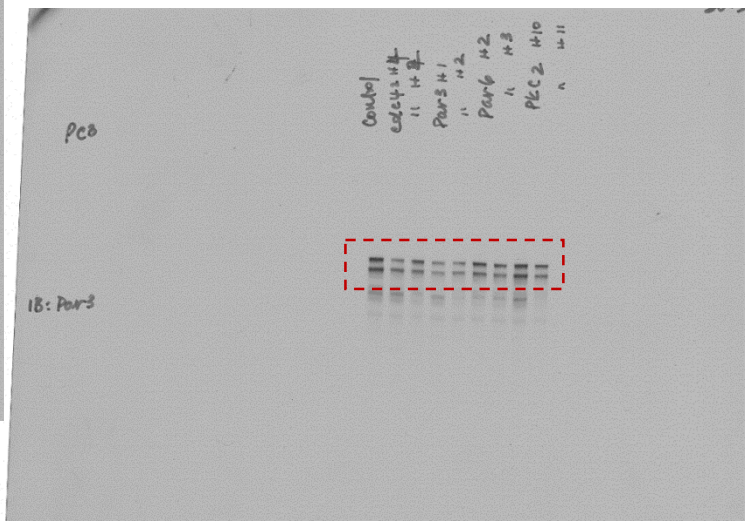

Figure S3 F

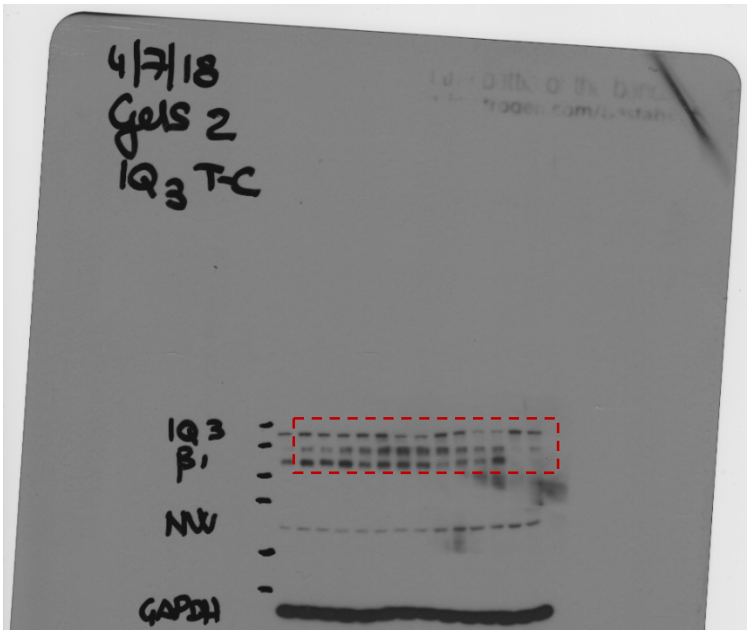

Figure S3 F

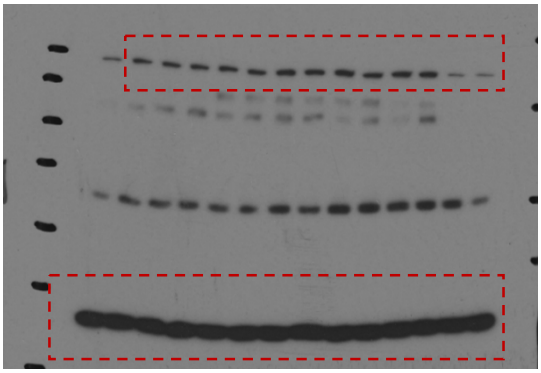

Figure S3 F

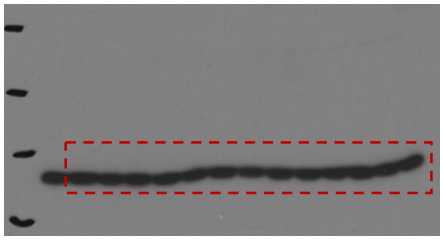

Figure S3 F Short

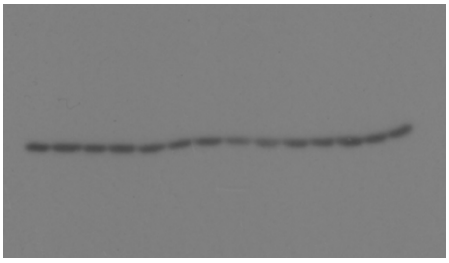

Figure S3 I

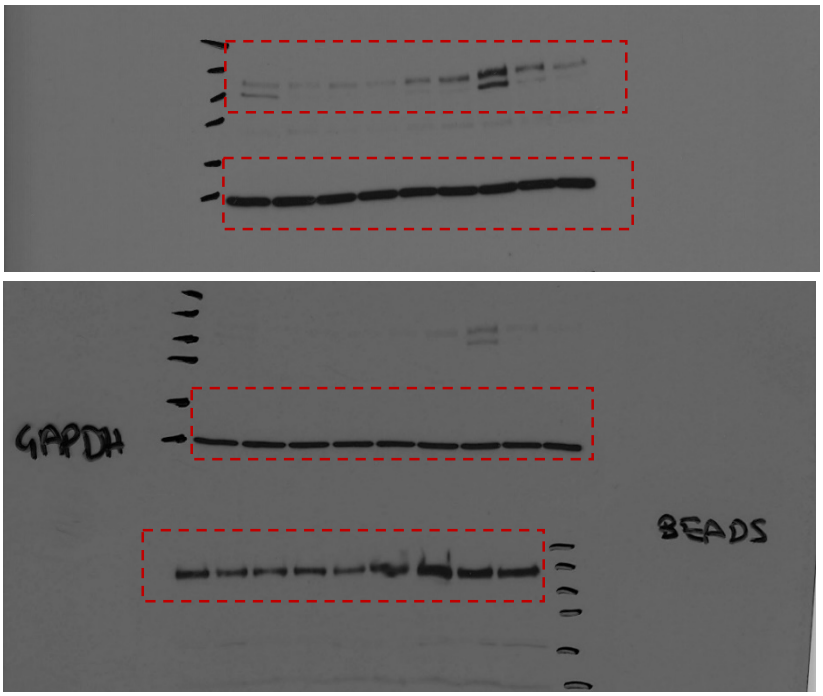

Uncropped left lobe lung tilescans (1x) from ZEN (Zeiss) saved in TIF

Figure 4A CONTROL

Figure 4A IQGAP1

PC3 cells 6h

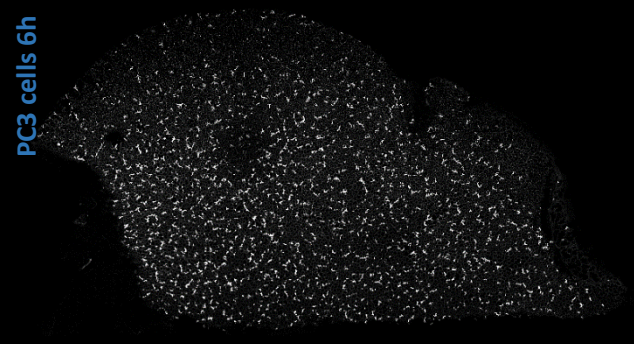

Figure 4B CONTROL

Figure 4B IQGAP1

MDAMB231 cells 6h

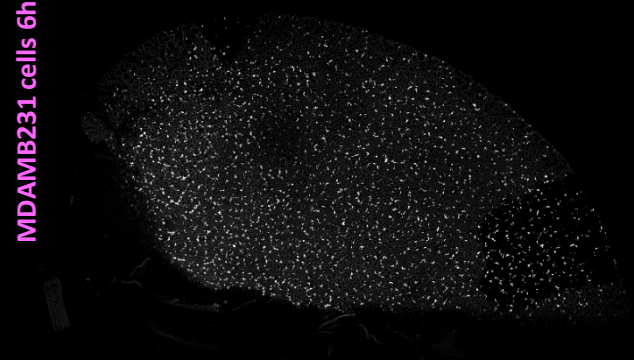

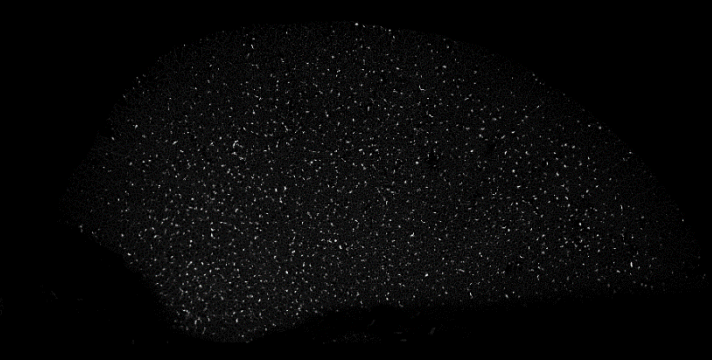

Figure 4H CONTROL

Figure 4H IQGAP1

PC3 cells 24h

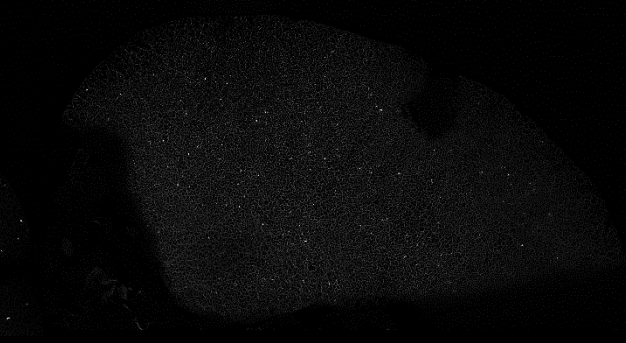

Figure 4I CONTROL

Figure 4I IQGAP1

MDAMB231 cells 24h

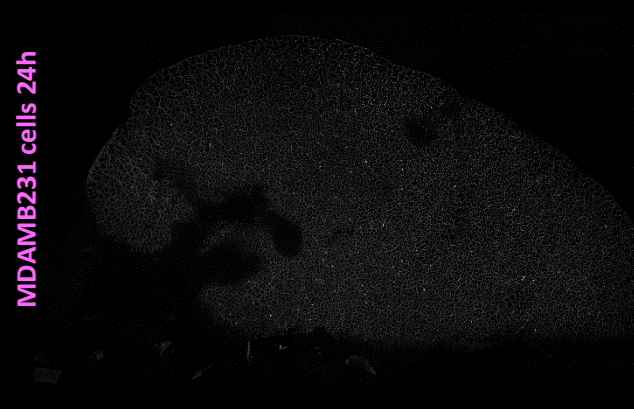

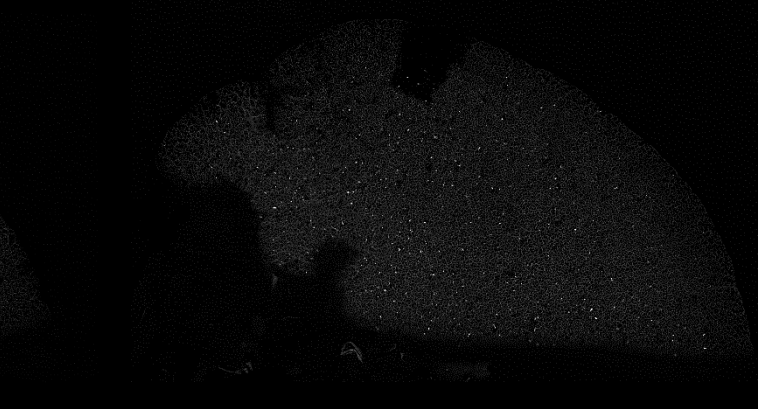

Figure S4 A

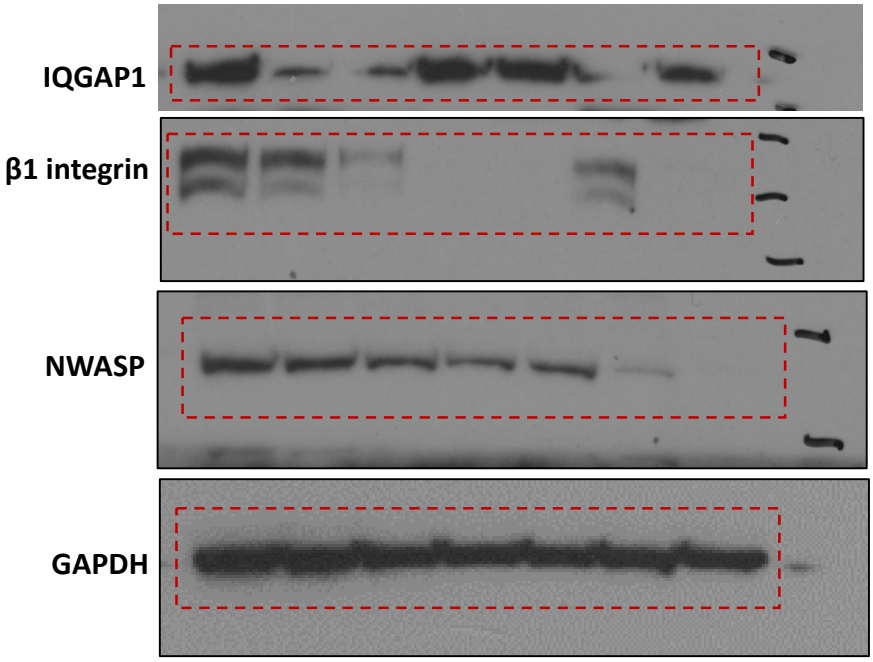

Figure S4 C

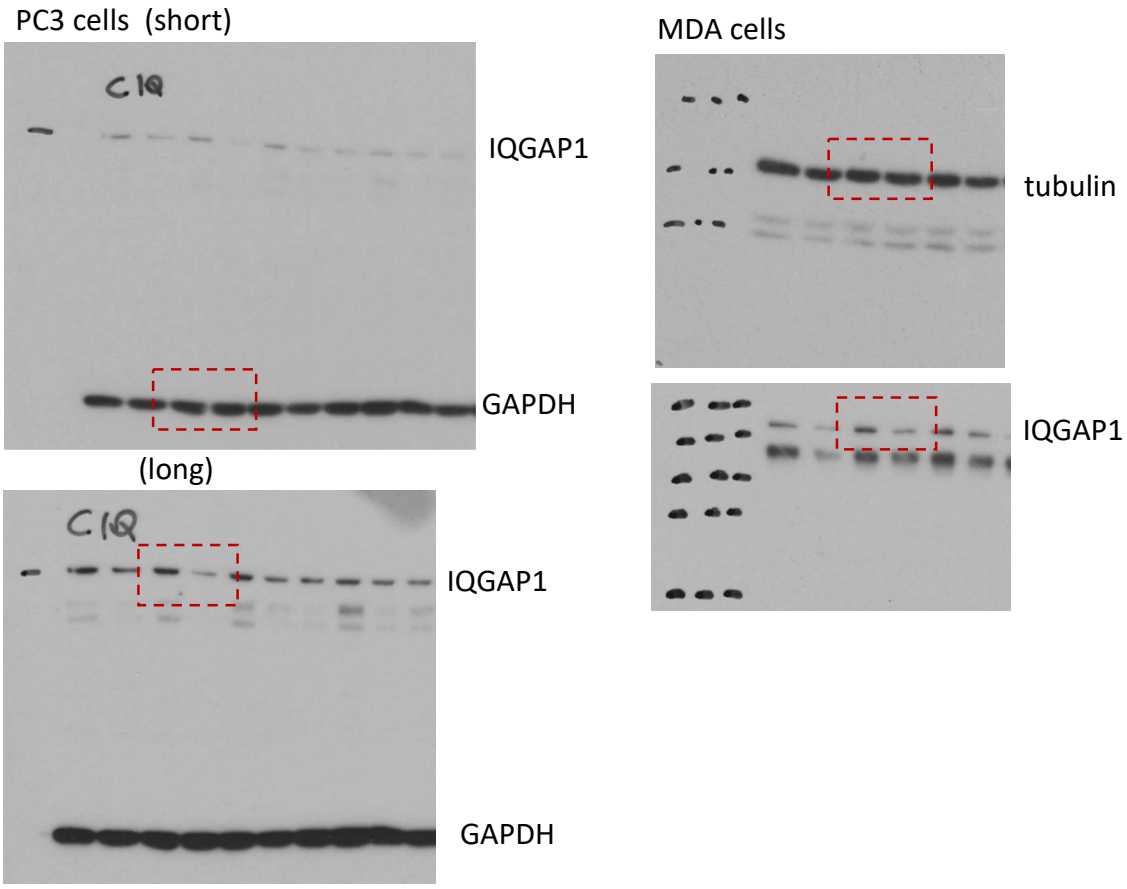

Figure S4 D

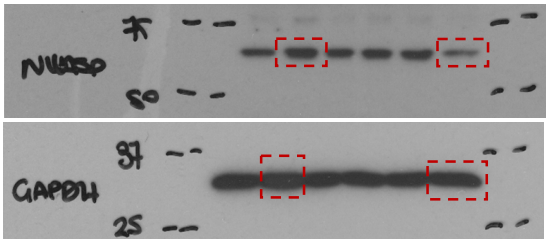

Figure S4 Q

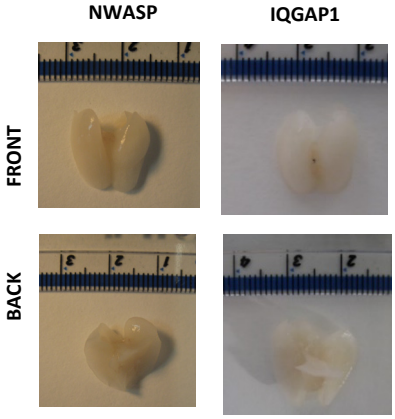

Supplementary information-Data file uncropped

PROSTATE CANCER

Figure 5A (short)

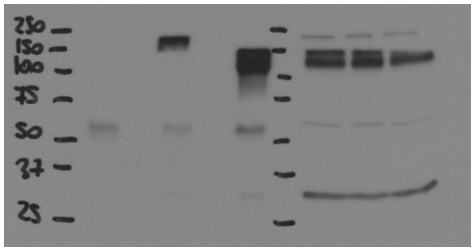

Figure 5A (long)

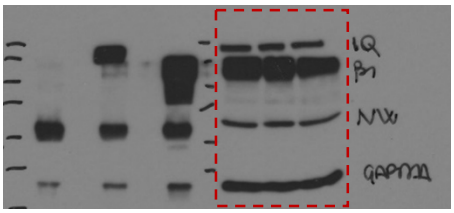

Figure 5A (long) rexposed separating the membranes

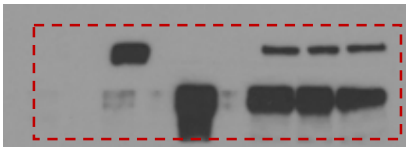

BREAST CANCER

Figure S5 A (short)

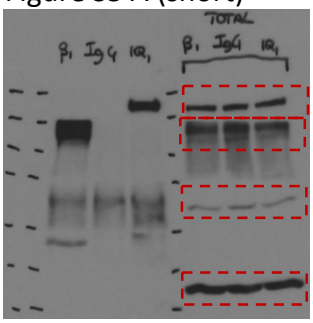

Figure S5 A (long)

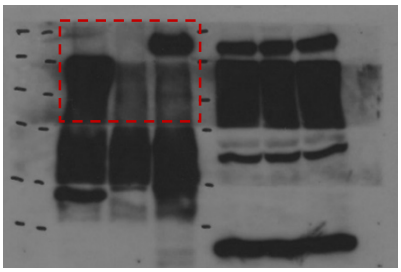

PROSTATE CANCER

Figure S5 A (short)

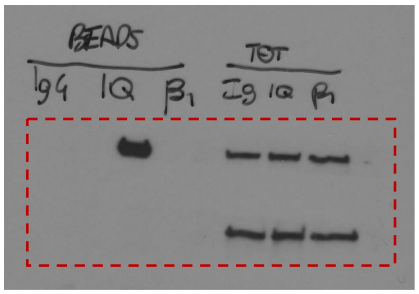

Figure S5 A(long)

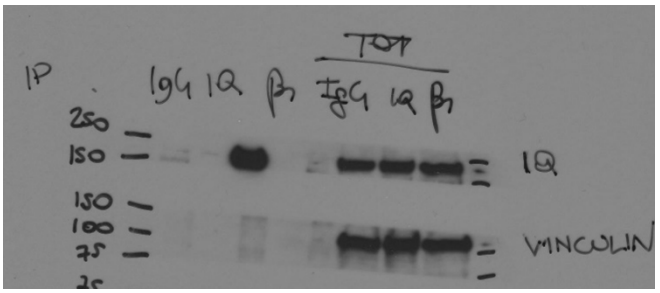

Figure S5 H